Title
Bacterial cytological profiling : : a shortcut for determining mechanism of action of antibacterial molecules

Permalink
https://escholarship.org/uc/item/01f8x90t

Author
Nonejuie, Poochit

Publication Date
2014

Peer reviewed|Thesis/dissertation

UNIVERSITY OF CALIFORNIA, SAN DIEGO

Bacterial cytological profiling: a shortcut for determining mechanism of action of antibacterial molecules

A dissertation submitted in partial satisfaction of the requirements for the degree

Doctor of Philosophy

in

Biology

by

Poochit Nonejuie

Committee in charge:

Professor Joe Pogliano, Chair
Professor Michael Burkart
Professor Arshad Desai
Professor Jeff Hasty
Professor Kit Pogliano

2014

The Dissertation of Poochit Nonejuie is approved, and it is acceptable in quality and form

for publication on microfilm and electronically:

_____

_____

_____

_____

_____

Chair

University of California, San Diego

2014

iii

DEDICATION

I dedicate my dissertation to my mother, Sunee Nonejuie, and my family that let me chase my dream and do what I love, and always support me in every way.

EPIGRAPH

"This experiment is very easy and will be done in 2 weeks" – Joe Pogliano

TABLE OF CONTENTS

LIST OF FIGURES

LIST OF TABLES

ACKNOWLEDGEMENTS

I would like to sincerely thank Joe Pogliano for being a superb graduate advisor. Working with him is my greatest pleasure. He is undoubtedly the best mentor one could ask for. He always encouraged me to try many different interesting projects, purely for scientific interests and sometimes just for fun. All these exciting experiences opened up my mind to different aspects of science and reminded me the fun of science.

I would also like to thank all the members of both Pogliano labs. They are very supportive and help me get through rough times. Thanks for understanding and being patient whenever they are trying to communicate with me in English. Living as an international student would be very tough without their supports and loves. I love you guys. Thanks so much. I would like to specially thank Alan Derman who is my first mentor during my rotation in the lab. He always called himself "pseudo-PI with an A-parking permit" and I think it is definitely true (UCSD should open this position in the future). Without Alan, we, everyone in Pogliano labs, will have a very difficult time working in the lab. I can ask him everything (preferably scientific questions) and he always came up with elaborate long answers that amazed me every time. Thank you so much, Alan.

I really appreciate my thesis committee for their time. They are very supportive and gave me very useful suggestions on my work. Also, I would like to thank all my past and present collaborators. They are very enthusiastic about science and really take me to the whole different world of science. I learned a lot from working with them. Thanks so much.

Last but not least, I would like to thank all the friendships from Thai community here in San Diego. We have been through a lot together, in both good and bad times. Thanks for all your supports and fun stuffs we did together. It is my honor to know you guys and I will never forget our friendships. Love you all.

Chapter 2, in full, is a reprint of the material as it appears in *Proceedings of the National Academy of Sciences* 2013 Vol.110(40). Poochit Nonejuie, Michael Burkart, Kit Pogliano, and Joe Pogliano. "Bacterial Cytological Profiling Rapidly Identifies the Cellular Pathways Targeted by Antibacterial Molecules." *Proceedings of the National Academy of Sciences* 110, no. 40 (2013): 16169–16174.   I was a primary author, conducted all the experiments and made all of the figures.

Chapter 3, in full, is a reprint of the material as it appears in *Antimicrobial Agents and Chemotherapy* 2013 Vol.57(8). George Sakoulas, Poochit Nonejuie, Victor Nizet, Joseph Pogliano, Nancy Crum-Cianflone, and Fadi Haddad. "Treatment of High-Level Gentamicin-Resistant Enterococcus Faecalis Endocarditis with Daptomycin Plus Ceftaroline." *Antimicrobial Agents and Chemotherapy* 57, no. 8 (2013): 4042-4045. I was a secondary author and performed the fluorescence microscopy and images analysis displayed in FIG 2.

Chapter 4, in part, is being prepared for submission for publication of the material. Poochit Nonejuie, Chiara Ricci-Tam, Joe Pogliano "Roles of polymyxin B in

bacterial membrane fluidity". I was a primary author and performed all of the fluorescence microscopy and images analysis.

Chapter 5, in full, is a reprint of the material as it appears in *Journal of Bacteriology* 2012 Vol.194(10). Alan I. Derman, Poochit Nonejuie, Brittany C. Michel, Bao D. Truong, Akina Fujioka, Marcella L. Erb, and Joe Pogliano. "Alp7R Regulates Expression of the Actin-like Protein Alp7A in Bacillus Subtilis." *Journal of Bacteriology* 194, no. 10 (2012): 2715–2724. I was a secondary author. I constructed some *Δalp7R* bacteria strain variants, performed part of plasmid stability assays and fluorescence microscopy, and western blot experiments.

VITA

2006   Bachelor of Science, Biochemistry, Chulalongkorn University

2014   Doctor of Philosophy, Biology, University of California, San Diego

Publications

Sakoulas, George, Warren Rose, Poochit Nonejuie, Joshua Olson, Joseph Pogliano, Romney Humphries, and Victor Nizet. "Ceftaroline Restores Daptomycin Activity Against Daptomycin Nonsusceptible Vancomycin Resistant Enterococcus Faecium." *Antimicrobial Agents and Chemotherapy*, 2013, ACC 02274-13.

Sakoulas, George, Cheryl Y Okumura, Wdee Thienphrapa, Joshua Olson, Poochit Nonejuie, Quang Dam, Abhay Dhand, et al. "Nafcillin Enhances Innate Immune-Mediated Killing of Methicillin-Resistant Staphylococcus Aureus." *Journal of Molecular Medicine* 92, no. 2 (2014): 139–149.

Nonejuie, Poochit, Michael Burkart, Kit Pogliano, and Joe Pogliano. "Bacterial Cytological Profiling Rapidly Identifies the Cellular Pathways Targeted by Antibacterial Molecules." *Proceedings of the National Academy of Sciences* 110, no. 40 (2013): 16169–16174.

Sakoulas, G., P. Nonejuie, V. Nizet, J. Pogliano, N. Crum-Cianflone, and F. Haddad. "Treatment of High-Level Gentamicin-Resistant Enterococcus Faecalis Endocarditis with Daptomycin plus Ceftaroline." *Antimicrobial Agents and Chemotherapy* 57, no. 8 (May 20, 2013): 4042–4045.

Werth, BJ, C Vidaillac, KP Murray, KL Newton, G Sakoulas, P Nonejuie, J Pogliano, and MJ Rybak. "Novel Combinations of Vancomycin plus Ceftaroline or Oxacillin against Methicillin-Resistant Vancomycin-Intermediate Staphylococcus Aureus (VISA) and Heterogeneous VISA." *Antimicrobial Agents and Chemotherapy* 57, no. 5 (2013): 2376–2379.

Derman, A. I., P. Nonejuie, B. C. Michel, B. D. Truong, A. Fujioka, M. L. Erb, and J. Pogliano. "Alp7R Regulates Expression of the Actin-Like Protein Alp7A in Bacillus Subtilis." *Journal of Bacteriology* 194, no. 10 (March 16, 2012): 2715–2724.

ABSTRACT OF THE DISSERTATION

Bacterial cytological profiling: a shortcut for determining mechanism of action of antibacterial molecules

by

Poochit Nonejuie

Doctor of Philosophy in Biology

University of California, San Diego, 2014

Professor Joe Pogliano, Chair

After the golden era of antibiotic discovery, we have been falling behind in stocking up our arsenal to fight against bacterial pathogens. If this trend continues, we will eventually return to the pre-antibiotic era and millions of lives will be at risk. An alarming increase in the rate of multidrug resistant pathogens and the lack of new antibiotics are a nightmare combination that we have to conquer in order to alleviate the current dire situation and regain control over pathogens. In order to do so, in previous years scientists developed many advanced tools to search for new antibiotics. However, there is no simple way to rapidly determine the mechanism of action (MOA) of antibiotics, information which is necessary to push an antibiotic through the discovery

pipeline. Here, I will present evidence to show that bacterial cytological profiling (BCP) can be used as a powerful tool in MOA studies of antibacterial molecules. BCP provides high resolution by being able to distinguish between different subgroups of compounds based on their specific activity. I also demonstrate that BCP is able to identify the MOA of an unknown compound, spirohexenolide A, as a membrane active compound that rapidly depletes the proton motive force of the bacterial membrane. Apart from BCP, I also explore additional uses of fluorescence microscopy in antibiotic studies. Fluorescently labeled antibiotics can be applied to bacterial resistance studies to provide a additional evidence about the *in vitro* resistance mechanism. Finally, BCP is used to gain insight into MOA of an existing antibiotic, polymyxin B. BCP and other cell biology data suggest that, at clinically relevant concentrations, polymyxin B acts upon LPS production. BCP provides a one step assay that can be applied in antibiotic discovery, eliminating a key bottleneck of the antibiotic discovery pipeline in how to rapidly determine the MOA of antibacterial molecules. BCP will promptly fill up our arsenal and provide us tools to prevent us from going back to the pre-antibiotic era.

Chapter 1

Introduction

Golden Age of Antibiotic Discovery

The discovery of penicillin in the 1930s is, no doubt, one of the greatest achievements of mankind and started the "golden era" of antibiotic research that last for almost 40 years. Most of the major classes of antibiotics used today were discovered during this time period including sulfonamides, β-lactam, chloramphenicols, tetracyclines, aminoglycosides, macrolides, glycopeptides, quinolones and streptogramins. New antibiotics and their derivatives were discovered and introduced to the market at the rate of 20-30 new drugs per decade (1, 2). During this era, human life span increased significantly, many uncontrollable outbreaks of infectious disease were put to stop, and certain common diseases were almost completely eradicated. Antibiotics have come to be used not only for the direct benefits human health, but also in the agricultural industry. Antibiotics have also been used to control plant diseases and as feed additives for livestock to promote increased efficiency of animal growth (3, 4).

The Decline of Antibiotic Research

During the period from the 1970s to 2000 known as the innovation gap in antibiotic discovery (5), the miracle of antibiotic discovery has faded away. The rate of new antibiotics introduced to the market was down to several new items per decade, all of which are analogues of the existing ones. This period is also called the age of medicinal chemistry that focused only on improving the existing antibiotics to fight against resistant bacteria while the main molecular scaffolds remained the same (5, 6). For example, the the quinolone based scaffold of nalidixic acid was developed into ciprofloxacin which

has higher efficiency in pathogen killing, by engineering functional groups around the quinolone core to improve cell permeability and binding to the target (5, 6). This engineering strategy worked effectively in fighting against resistant pathogens but not for long. By the 1990s, it became clear that the resistant bacteria finally outpaced the development of antibiotics (7). This spurred the scientific community to refocus on finding new classes of antibiotics to avoid millions of people being at risk of untreatable infections.

Since 2000, the antibiotic discovery situation has shown a positive trend due to the launch of five new classes of antibiotics, all of which are only effective against Gram-positive bacteria: 1) Oxazolidinone (Linezoid), 2) Lipopeptide (Daptomycin), 3) Pleuromutilin (Retapamulin), 4) Tiacumicin (Fidaxomicin), and 5) Diarylquinoline (Bedaquiline) (1, 8, 9). However, there is still an urgent need for new Gram-negative antibiotics (8, 10), which are more difficult to develop because the outer membrane provides an extra barrier to antibiotic penetration and houses multidrug-resistant pumps that can exclude antibiotics from bacterial cells (11–13). An additional problem in finding new antibiotics is the application of the Limpinski's "rule of five"(14), which describes properties of good drugs to be used in humans, on antibiotic screening in many pharmaceutical companies in the past (1). The rule of five is the guideline for a good orally active drug including; 1) no more than five hydrogen bond donors, 2) less than ten hydrogen bond acceptors, 3) less than 500 Dalton in mass, and 4) an octanol-water partition coefficient log P less than five. Following these rules will hypothetically miss potential candidates that can penetrate or permeabilize bacterial membranes (1). Nowadays, the rule of five has been improved significantly due to more advance

knowledge in high molecular weigh antibiotics and their functions on bacterial membrane. Since the extra membrane of Gram-negative bacteria also causes the penetration problem to antibiotics, high dose of antibiotics are required to combat against pathogens. This high level of antibiotics also results in higher toxicity to human cells; thus, potential lead compounds often have undesirable side effects in clinical trial leading to slower pipeline process (1).

Despite the need for new antibiotics, the research and development atmosphere in the past years has not been encouraging. Like other drugs, the whole process of antibiotic development can take up to 10-15 years. The first 3-6 years are spent on finding potential candidates or lead compounds and identifying their targets. Only if leads are identified, all efforts are put through the first phase can be called antibiotic discovery. Then, the lead compounds will go through an optimization processes, tested for efficacy, safety and toxicity in animal models. The few molecules that pass these tests are then tested in humans in FDA approved phase I, II, and III, clinical trials. Proceeding through clinical trials takes approximately 6-7 years before scaling up in the manufacturing process, adding another year or two to the pipeline (2, 15). To win approval in a clinical trial, compounds have to be proven to be as effective as current therapies. Since antibiotics such as penicillin are extraordinarily effective, the bar is set very high for approval of new drugs. In contrast, many other current medicines, such as anti-cancers are rarely as safe and effective, making approval an easier process.

How much does it cost to get one new drug on the market? It's around $800 million -$2 billion (2). At one point in time a few years ago, there were only a handful of major pharmaceutical companies that were actively pushing antibiotic development

forward compared to more than 18 companies in 1990 (9). This decrease is largely accounted for by a combination of the extreme difficulty companies have had in getting "winners" approved combined with the high cost of development. Although topselling antibiotics generate revenues of $1 billion dollars per year, economically they underperform medicines used for long-term therapies for chronic health conditions that are normally administered to patients for years or for life such as pain, diabetes, hypertension, or cancer. However, due to the emergence of antibiotic resistance, the decline in pharmaceutical antibiotic research has now reversed.

Antibiotic Resistant Bacteria

In addition to the lack of novel antibiotics, bacteria have become resistant to almost all antibiotics available in the market. Through million years of evolution, bacteria found a way to fight against antibiotics and survived. In fact, they have been living among natural antibiotic producers long before we human evolved or discovered antibiotics. Thus, it is not surprise that once we try to kill bacteria with antibiotics they become resistant in no time. The classic case of bacterial resistance is *Staphylococcus aureus*, which appeared in a series of waves (16). Shortly after the introduction of penicillin against *S. aureus*, it became resistant to penicillin and caused a pandemic across many hospitals, the resistant strain known as phage-type 80/81. This *S. aureus* strain is resistant to penicillin because of a plasmid containing penicillinase that can disarm penicillin. Wave 1 of resistance was put to an end due to the introduction of methicillin, an improved version of penicillin that is not sensitive to penicilliase. Wave 2

of resistance started by the production of an extra copy of PBP2, called PBP2a, which has very low binding affinity to methicillin. As a result, *S. aureus* became resistant to methicillin, MRSA-I. This time the bacteria used a different strategy from the first resistance. Instead of disarming the antibiotics, they produced an alternative protein that cannot be inhibited by the challenging antibiotics. The last two waves were driven by the usage of vancomycin and the presence of SCCmec gene. Vancomycin-intermediate or -resistant *S. aureus* (VISA or VRSA) became more common in the fourth wave of resistance. Moreover, resistant *S. aureus* are not restricted to hospitals anymore since the fourth wave of resistance brought resistant bacteria to the general community and is known as a community-acquired pathogen (CA-MRSA).

Human activity is one of the major contributions to the increasing number of antibiotic resistant pathogens. Mass production of antibiotics and uncontrolled applications are the most noticeable causes (3). Today, not only are most pathogenic bacteria resistant to antibiotics on the market, the old pathogens that were once eradicated or put at bay also re-emerged with potential antibiotic resistance. In the US, over two million people had hospital-acquired bacterial infections in 2000, and more than half of the cases involved antibiotic resistant bacteria (17). In 2000, the death toll in the US hit 100,000 people per year and over two millions world wide due to bacterial infections (2, 18). The mortality rate of patients infected with these multi-resistant pathogens is as high as 50%-80%. This alarming rate of infection not only affects individual patients, but also the whole community. The cost of healthcare has increased greatly in the last decade, in part due to extra costs associated with treating multidrug resistant infections and the procedures to prevent the spread of hospital-acquired infections (19). Moreover, as the

world has become smaller and every place is connected by convenient transportation, the spread of multi-drug resistant bacteria is easier than ever before (20). Altogether, there is an urgent need for novel antibiotics to curb worsening infection situations. To do so, scientists have to develop more efficient ways to search or screen for antibacterial molecules that show potential of becoming usable antibiotics.

Antibiotic screening

What defines an antibiotic? Is it anything that kills bacteria or stops bacterial growth? Practically, the answer is no. One of the most important factor that defines whether a molecule of interest is a potential antibiotic or not is the mechanism of action (MOA) of the molecule. Potential antibiotics must selectively inhibit targets found only in bacteria without interfering any eukaryotic homologs, and with no or minimum toxicity to human (1). While hundreds of proteins conserved among bacteria can be used as potential targets, there are only 6 major clinically validated targets used today including cell wall synthesis/peptidoglycan synthesis, protein synthesis, DNA replication, RNA transcription, folate synthesis, and membrane integrity (5). Knowing the target of antibacterial molecules is crucial for understanding how they kill bacteria, as well as the mechanisms by which resistance can arise (7, 8). It is relatively easy to determine if molecules exhibit antibacterial activity or not by simply performing an empirical test. However, determining MOA is very challenging and can slow down the whole antibiotic discovery pipeline (8).

There are two major types of antibiotic screening, both of which give MOA information, target-based screening and whole cell screening (15). Briefly, target-based *in vitro* screening approaches identify compounds that are active against specific bacterial proteins *in vitro*. These approaches have an advantage in that the likely targets of molecules are known from the screening, but suffer from the high possibility that many compounds obtained from the screening have no biological activity. Whole cell screening approaches, on the other hand, yield compounds with antibiotic capability, but many compounds from the screen are generally nuisance compounds that are nonspecific toxins to cell such as lipophilic or positively charged molecules.

Recently, target-based screening has been propelled by genomic and bioinformatics data. With genomic data in hand, scientists can explore bacterial genomes and find new targets (21, 22). Generally, a process starts with finding homologs of essential genes across multiple species of bacteria of interest. Candidate essential genes are confirmed by allelic replacement or deletion. Absence of growth in organisms lacking the target genes strongly suggests that the genes are essential. In contrast, they are non-essential if the organism can grow without them, thus have traditionally been ignored as uninteresting targets (15). Under- or overexpression of target genes also plays a role in target identification of antibacterial molecules. Decrease of target gene expression typically sensitizes organisms to molecules hitting that pathway, while overexpression often results in resistance (8). However, reduction of one gene can effect other genes which can give misleading results (8, 23). A classic case of target-based screening is a study done by GlaxoSmithKline (GSK) during 1995-2001 (15). They evaluated more than 300 essential genes across many bacterial species (*E. coli*, *S. aureus*,

S. pneumonia and *H. influenza*) against the SmithKline Beecham compound collections (~260,000-530,000 compounds) through the total of 70 high throughput screening (HTS). Outcomes were not impressive. Only 16 HTS gave rise to hits and a total of 5 lead targets were obtained: PDF, FabI, FabH, MetRS and PheRS. Moreover, since the screens were based on a narrow selection of bacterial species, the leads were also narrow-spectrum. Highly selective antibiotics are not always unappreciated A positive side of species-specific antibiotics is that they have fewer gastrointestinal side effects since they do not wipe out the normal flora of the human body unlike broad-spectrum antibiotics (1, 24).

Since hits from target-based screens frequently fail to exhibit biological activity,, old-fashioned empirical screens or whole cell screening is important in finding potential leads. A critical step in order to advance hits to leads is understanding the MOA of molecules (15). Generally, many different assays are needed to test if the molecule of interest inhibits any major pathways.. One of the most popular methods, also considered as the gold standard in MOA determination is the macromolecular synthesis method (MMS). MMS method uses radioactively labeled building blocks of the five major pathways to test if any of them are inhibited, including protein, RNA, DNA, lipid, or peptidoglycan synthesis (25, 26). However, this method has several drawbacks. First, molecules that immediately kill cells, such as nisin or other membrane active agents, are all grouped as non-specific inhibitors despite having a unique MOA. Second, since MMS focuses on only five major pathways, the method fails to identify the MOA for compounds with other biological targets. As mentioned earlier, finding new targets is more important than finding new molecules that inhibit the same target. Also, MMS

lacks an ability to distinguish between molecules that inhibit different steps of the same pathway since the interpretation of MMS data is based on an end-point result.

To overcome drawbacks of MMS, many alternative whole cell screening methods have been introduced and adopted (8). The –omic methods are one of the popular choices for (27) trying to understand how antibiotics work, thanks to more affordable sequencing technology and more user-friendly bioinformatics software. Briefly, standard expression patterns of known antibiotics are created, and unknown molecules expression patterns are then compared with the existing database suggesting which group of antibiotics the unknown molecules fall into (8, 27, 28). This –omic strategy can be combined with other methods, such as collections of specialized strains, hypersensitization (23, 29), overexpression (30) and stress response assays (31). All of these additional arrays are reported as useful ways to help identify the MOA of unknown molecules. Like other big-data analysis, although these methods provide a huge amount of information and clues or tendencies of likely targets of the molecules, -omic methods frequently fail to identify the exact targets of the molecules, since many different types of of inhibition can trigger the similar or overlapping cellular stress responses. Moreover, results from –omic experiments are very complicated and experts are needed to interpret the results correctly.

Isolating resistant mutants is a more conventional and simple method to identify the MOA of antibacterial molecules. To do so, organisms are grown on low level of antibacterial molecules for several generations and the resistant mutants are isolated. Simple genetic approaches can be used to identify mutations in the target genes which

provide the information of possible targets of the molecules of interest (32–35). A classic case for this method is the identification of penicillin binding protein (PBP) as a target of β-lactams. However, a common problem of this method is the presence of suppressors in organisms. Bacteria always find a way to adapt to new environments and maintain their fitness level in order to survive; thus, suppressors in genes not directly targeted by the drug can emerge to support the growth of bacteria. For example, mutations that lead to upregulation of efflux pumps can provide resistance to many antibiotics. All in all, mapping resistant mutants is very useful and simple in identifying the target of molecules only if the mutations land directly on the target gene.

Each of the above assays has its own disadvantages that can limit its utility when used alone. Thus, multiple methods are needed in order to correctly identify the MOA of molecules. Genetic methods provide very in-depth information of targets, most of the time into the amino acid residue involved in the interaction between the molecule and target. Over- or underexpression arrays approaches provide additional sets of data that strongly support the MMS technique. As mention earlier, the -omic methods provide unbiased big picture views of an organism's physiologic responses to molecules since there is no defined set of targets to be measured before hand. Running multiple types of assays requires the large amounts of compound; however, newly isolated molecules are usually available in very small amounts which prevents their being used in many of these existing methods until their production has been scaled up. Thus, to date, there is no single, simple assay to rapidly and accurately determine the MOA of a newly isolated compound.

The study of fluorescently labeled antibiotics is becoming more popular due to advances in fluorescence microscopy that allow scientists to visualize live antibiotic actions like never before. In the case of daptomycin (36), a cyclic lipopeptide produced by *Streptomyces roseosporus,* it is suggested by many lines of evidence that daptomycin inserts into the membrane and then aggregates thereby disrupting membrane fuction. and Then, the aggregated daptomycin can create holes in the membrane that lead to the leakage of ions and eventually cell death. By using fluorescently labeled daptomycin, it was shown that daptomycin colocalized with an essential cell division protein DivIVA (37). This new finding opens up a whole new hypothesis of daptomycin MOA and also other lipopeptide antibiotics. Fluorescently labeled antibiotics can provide very concrete evidence to directly support models for the MOA of molecules. Fluorescence microscopy in antibiotics study has a very high potential in the future for becoming a standard method in antibiotic study.

One of the milestones of fluorescence microscopy in drug discovery was established in 1999. Scientists used fluorescent macromolecular probes that can follow or tag different pathways in the cells to study molecules inhibiting eukaryotic cell growth (38). Later, this method, cytological profiling, had been cultivated and used as the screening method for eukaryotic drugs (39). Briefly, a fluorescence microscope was used to capture images of cells treated with different molecules and probed with pathway-specific fluorescent probes to visualize cytoskeletal proteins, motor proteins, subcellular compartments, the nucleus, and other subcellular structures. Then, collected images were analyzed based on different parameter such as probes intensity, position within the cell or

general cell morphology. Like other phenotypic profiling methods, the cytological profiling method needs a set of standard molecules of known MOA to be able to compare with unknown molecules. Overall profiles from the molecules of interest were then compared to the training set of standard compounds and scored based on an over all similarity; thus, molecules with the same or similar MOA were grouped together.

In the next several chapters I will cover the development and applications of bacterial cytological profiling (BCP) in antibiotic screening and MOA study. Chapter 2 covers the development of bacterial cytological profiling that rapidly identifies the mechanism of action of antibiotics and unknown molecules. In chapter 3, I demonstrate the use of fluorescently labeled antibiotics in the study of antibiotic resistance of the pathogen *E. faecalis*. In chapter 4, I apply fluorescence microscopy to understand the function of polymyxin B in outer membrane biosynthesis. Finally, in Chapter 6 I discuss the current usages and limitations of bacterial cytological profiling method and also its future in antibiotic discovery.

References

1. K. Lewis, Platforms for antibiotic discovery, *Nat. Rev. Drug Discov.* **12**, 371–387 (2013).

2. J. Bérdy, Thoughts and facts about antibiotics: Where we are now and where we are heading, *J. Antibiot. (Tokyo)* **65**, 385–395 (2012).

3. T. B. Stanton, A call for antibiotic alternatives research, *Trends Microbiol.* **21**, 111–113 (2013).

4. H. K. Allen, U. Y. Levine, T. Looft, M. Bandrick, T. A. Casey, Treatment, promotion, commotion: antibiotic alternatives in food-producing animals, *Trends Microbiol.* **21**, 114–119 (2013).

5. C. T. Walsh, T. A. Wencewicz, Prospects for new antibiotics: a molecule-centered perspective, *J. Antibiot. (Tokyo)* (2013)

6. M. A. Fischbach, C. T. Walsh, Antibiotics for Emerging Pathogens, *Science* **325**, 1089–1093 (2009).

7. H. Nikaido, Multidrug resistance in bacteria, *Annu. Rev. Biochem.* **78**, 119 (2009).

8. L. L. Silver, Challenges of Antibacterial Discovery, *Clin. Microbiol. Rev.* **24**, 71–109 (2011).

9. M. S. Butler, M. A. Blaskovich, M. A. Cooper, Antibiotics in the clinical pipeline in 2013, *J. Antibiot. (Tokyo)* **66**, 571–591 (2013).

10. V. Hernandez, T. Crepin, A. Palencia, S. Cusack, T. Akama, S. J. Baker, W. Bu, L. Feng, Y. R. Freund, L. Liu, M. Meewan, M. Mohan, W. Mao, F. L. Rock, H. Sexton, A. Sheoran, Y. Zhang, Y.-K. Zhang, Y. Zhou, J. A. Nieman, M. R. Anugula, E. M. Keramane, K. Savariraj, D. S. Reddy, R. Sharma, R. Subedi, R. Singh, A. O'Leary, N. L. Simon, P. L. De Marsh, S. Mushtaq, M. Warner, D. M. Livermore, M. R. K. Alley, J. J. Plattner, Discovery of a Novel Class of Boron-Based Antibacterials with Activity against Gram-Negative Bacteria, *Antimicrob. Agents Chemother.* **57**, 1394–1403 (2013).

11. A. H. Delcour, Outer membrane permeability and antibiotic resistance, *Biochim. Biophys. Acta BBA-Proteins Proteomics* **1794**, 808–816 (2009).

12. R. P. Lamers, J. F. Cavallari, L. L. Burrows, M. A. Webber, Ed. The Efflux Inhibitor Phenylalanine-Arginine Beta-Naphthylamide (PAβN) Permeabilizes the Outer Membrane of Gram-Negative Bacteria, *PLoS ONE* **8**, e60666 (2013).

13. H. Nikaido, Molecular Basis of Bacterial Outer Membrane Permeability Revisited, *Microbiol. Mol. Biol. Rev.* **67**, 593–656 (2003).

14. C. A. Lipinski, Lead- and drug-like compounds: the rule-of-five revolution, *Drug Discov. Today Technol.* **1**, 337–341 (2004).

15. D. J. Payne, M. N. Gwynn, D. J. Holmes, D. L. Pompliano, Drugs for bad bugs: confronting the challenges of antibacterial discovery, *Nat. Rev. Drug Discov.* **6**, 29–40 (2006).

16. H. F. Chambers, F. R. DeLeo, Waves of resistance: Staphylococcus aureus in the antibiotic era, *Nat. Rev. Microbiol.* **7**, 629–641 (2009).

17. W. Bereket, K. Hemalatha, B. Getenet, T. Wondwossen, A. Solomon, A. Zeynudin, S. Kannan, Update on bacterial nosocomial infections, *Eur Rev Med Pharmacol Sci* **16**, 1039–1044 (2012).

18. S. Kwon, M. L. Schweizer, E. N. Perencevich, National Institute of Allergy and Infectious Disease (NIAID) funding for studies of hospital-associated bacterial pathogens: are funds proportionate to burden of disease?, *Antimicrob Resist Infect Control* **1**, 5 (2012).

19. E. N. Perencevich, P. W. Stone, S. B. Wright, Y. Carmeli, D. N. Fisman, S. E. Cosgrove, Raising Standards While Watching the Bottom Line: Making a Business Case for Infection Control •, *Infect. Control Hosp. Epidemiol.* **28**, 1121–1133 (2007).

20. S. Le Hello, R. S. Hendriksen, B. Doublet, I. Fisher, E. M. Nielsen, J. M. Whichard, B. Bouchrif, K. Fashae, S. A. Granier, N. Jourdan-Da Silva, A. Cloeckaert, E. J. Threlfall, F. J. Angulo, F. M. Aarestrup, J. Wain, F.-X. Weill, International Spread of an Epidemic Population of Salmonella enterica Serotype Kentucky ST198 Resistant to Ciprofloxacin, *J. Infect. Dis.* **204**, 675–684 (2011).

21. R. Baltz, Renaissance in antibacterial discovery from actinomycetes, *Curr. Opin. Pharmacol.* **8**, 557–563 (2008).

22. J. W.-H. Li, J. C. Vederas, Drug Discovery and Natural Products: End of an Era or an Endless Frontier?, *Science* **325**, 161–165 (2009).

23. R. G. K. Donald, S. Skwish, R. A. Forsyth, J. W. Anderson, T. Zhong, C. Burns, S. Lee, X. Meng, L. LoCastro, L. W. Jarantow, A Staphylococcus aureus Fitness Test Platform for Mechanism-Based Profiling of Antibacterial Compounds, *Chem. Biol.* **16**, 826–836 (2009).

24. L. Dethlefsen, D. A. Relman, Incomplete recovery and individualized responses of the human distal gut microbiota to repeated antibiotic perturbation, *Proc. Natl. Acad. Sci.* **108**, 4554–4561 (2010).

25. A. Cotsonas King, L. Wu, in *Current Protocols in Pharmacology*, S. J. Enna, M. Williams, J. F. Barret, J. W. Ferkany, T. Kenakin, R. D. Porsolt, Eds. (John Wiley & Sons, Inc., Hoboken, NJ, USA, 2009).

26. L. Guan, R. M. Blumenthal, J. C. Burnham, Analysis of macromolecular biosynthesis to define the quinolone-induced postantibiotic effect in Escherichia coli., *Antimicrob. Agents Chemother.* **36**, 2118–2124 (1992).

27. T. Wecke, T. Mascher, Antibiotic research in the age of omics: from expression profiles to interspecies communication, *J. Antimicrob. Chemother.* **66**, 2689–2704 (2011).

28. S. Singh, J. Phillips, J. Wang, Highly sensitive target-based whole-cell antibacterial discovery strategy by antisense RNA silencing., *Curr. Opin. Drug Discov. Devel.* **10**, 160–166 (2007).

29. C. Freiberg, H. P. Fischer, N. A. Brunner, Discovering the mechanism of action of novel antibacterial agents through transcriptional profiling of conditional mutants, *Antimicrob. Agents Chemother.* **49**, 749–759 (2005).

30. H. H. Xu, L. Real, M. W. Bailey, An array of *Escherichia coli* clones over-expressing essential proteins: A new strategy of identifying cellular targets of potent antibacterial compounds, *Biochem. Biophys. Res. Commun.* **349**, 1250–1257 (2006).

31. J. E. Bandow, M. Hecker, Proteomic profiling of cellular stresses in Bacillus subtilis reveals cellular networks and assists in elucidating antibiotic mechanisms of action, *Syst. Biol. Approaches Infect. Dis.* , 79–101 (2007).

32. R. Hakenbeck, C. Martin, C. Dowson, T. Grebe, Penicillin-binding protein 2b of Streptococcus pneumoniae in piperacillin-resistant laboratory mutants., *J. Bacteriol.* **176**, 5574–5577 (1994).

33. N. H. Georgopapadakou, S. A. Smith, D. P. Bonner, Penicillin-binding proteins in a Staphylococcus aureus strain resistant to specific beta-lactam antibiotics., *Antimicrob. Agents Chemother.* **22**, 172–175 (1982).

34. K. Hirai, H. Aoyama, S. Suzue, T. Irikura, S. Iyobe, S. Mitsuhashi, Isolation and characterization of norfloxacin-resistant mutants of Escherichia coli K-12., *Antimicrob. Agents Chemother.* **30**, 248–253 (1986).

35. M. Bazzicalupo, B. Parisi, G. Pirali, M. Polsinelli, F. Sala, Genetic and Biochemical Characterization of a Ribosomal Mutant of Bacillus subtilis Resistant to Sporangiomycin, *Antimicrob. Agents Chemother.* **8**, 651–656 (1975).

36. L. Robbel, M. A. Marahiel, Daptomycin, a Bacterial Lipopeptide Synthesized by a Nonribosomal Machinery, *J. Biol. Chem.* **285**, 27501–27508 (2010).

37. J. Pogliano, N. Pogliano, J. A. Silverman, Daptomycin-Mediated Reorganization of Membrane Architecture Causes Mislocalization of Essential Cell Division Proteins, *J. Bacteriol.* **194**, 4494–4504 (2012).

38. T. U. Mayer, T. M. Kapoor, S. J. Haggarty, R. W. King, S. L. Schreiber, T. J. Mitchison, Small Molecule Inhibitor of Mitotic Spindle Bipolarity Identified in a Phenotype-Based Screen, *Science* **286**, 971–974 (1999).

39. T. J. Mitchison, Small-molecule screening and profiling by using automated microscopy, *Chembiochem* **6**, 33–39 (2004).

Chapter 2

Bacterial cytological profiling rapidly identifies the cellular pathways targeted by antibacterial molecule

Bacterial cytological profiling rapidly identifies the cellular pathways targeted by antibacterial molecules

Poochit Nonejuie[a], Michael Burkart[b], Kit Pogliano[a], and Joe Pogliano[a,1]

[a]Division of Biological Sciences, University of California, San Diego, CA 92093; and [b]Department of Chemistry and Biochemistry, University of California, San Diego, CA 92093

Identifying the mechanism of action for antibacterial compounds is essential for understanding how bacteria interact with one another and with other cell types and for antibiotic discovery efforts, but determining a compound's mechanism of action remains a serious challenge that limits both basic research and antibacterial discovery programs. Here, we show that bacterial cytological profiling (BCP) is a rapid and powerful approach for identifying the cellular pathway affected by antibacterial molecules. BCP can distinguish between inhibitors that affect different cellular pathways as well as different targets within the same pathway. We use BCP to demonstrate that spirohexenolide A, a spirotetronate that is active against methicillin-resistant *Staphylococcus aureus,* rapidly collapses the proton motive force. BCP offers a simple, one-step assay that can be broadly applied, solving the longstanding problem of how to rapidly determine the cellular target of thousands of compounds.

antibiotic resistance | drug screening | pharmacology | susceptibility | high throughput

Bacteria grow in complex communities where they are constantly exposed to molecules secreted by neighboring cells. Molecules that kill bacteria or strongly inhibit their growth are important evolutionary forces that determine the outcomes of bacterial interactions with each other and with host immune defenses (1–5). For example, secreted antibacterial compounds contribute to the overall composition and organization of complex microbial communities (5) while a variety of antimicrobial compounds produced by the innate immune system help to keep pathogens at bay (6). Identifying antimicrobial molecules and their cellular targets is essential for understanding how bacteria interact with one another and with other cell types (5). Knowledge of a molecule's mode of action is also important for understanding how these molecules evolve, as well as the mechanisms by which resistance can arise (7, 8). Due to the extensive use of antibiotics in the clinic, pathogenic bacteria have evolved resistance to nearly every known class of antibiotic, creating an urgent need for molecules with unique mechanisms (8, 9). Although it is relatively easy to identify molecules with antibacterial properties, determining their mechanism of action (MOA) is a notoriously difficult task that is essential for advancing hits through the discovery pipeline (8). Traditionally, a variety of assays are performed to determine whether one of five basic pathways is inhibited. These efforts typically begin with macromolecular synthesis (MMS) assays that use radioactively labeled precursors to determine whether a compound specifically inhibits protein, RNA, DNA, lipid, or peptidoglycan synthesis or whether it blocks all simultaneously (10). Although MMS is widely used throughout the pharmaceutical discovery community, it has several drawbacks. First, compounds that rapidly kill cells, such as bleach and nisin, are grouped within the sixth category of "all hitter," even though they have different mechanisms of action. Second, it can identify only a very small fraction of the total number of potential mechanisms of action. Third, in most cases, MMS assays cannot distinguish between inhibitors that effect different steps of the same pathway. Finally, MMS assays are relatively slow. Therefore,

MMS assays suffer from low resolution, low accuracy, and relatively low throughput.

To overcome the shortcomings inherent in MMS assays, several alternative methods for determining MOA have been developed (8), including isolating resistant mutants, transcriptional profiling, using a collection of strains that are sensitized to hundreds of pathways, or using species with different resistance properties (11–17). Each of these approaches is complementary to each other and has unique advantages. The genetic approach is often able to identify the molecular target of an antibiotic, the specific amino acid residues important for its interaction and the frequency with which resistance occurs. The sensitized and resistant strain methods can also identify specific cellular targets, providing much higher resolution than MMS. Transcriptional profiling offers the advantages of providing insights into the pathways that are inhibited as well as the physiological responses to antibiotic stress.

Despite many advantages, these approaches also have drawbacks that have limited their utility. The genetic approach and transcriptional profiling are relatively slow and for many antibiotics fail to correctly identify the molecular target. The sensitized and resistant-strain methods suffer from requiring a large number of specialized strains to be assayed at various concentrations of antibiotic. These methods also require substantial amounts of purified compound, yet newly isolated lead compounds are often available in very small quantities. Thus, to date, there is no single, simple assay to rapidly and accurately determine the MOA for a newly isolated compound. Here, we demonstrate that bacterial cytological profiling (BCP) can discriminate between antibacterial compounds with different MOA and accurately predict the MOA of newly isolated compounds, an approach similar to cytological profiling of eukaryotic cells (18, 19). We previously used fluorescence microscopy to discriminate between compounds that have different effects on the bacterial cell envelope (20). Here, we more broadly apply BCP to a library of antibacterial compounds that target many of the clinically relevant pathways in Gram-negative bacteria and to a molecule with an unknown MOA (Table S1).

Significance

Some bacteria have evolved resistance to nearly every known class of antibiotic, creating an urgent need for new ones that work by different mechanisms. However, there has been no simple way to determine how new antibiotics work. We have developed a unique method that provides a shortcut for understanding how antibiotics kill bacteria. This method can be used to sift through compounds to rapidly identify and characterize antibiotics that work against multidrug-resistant pathogens.
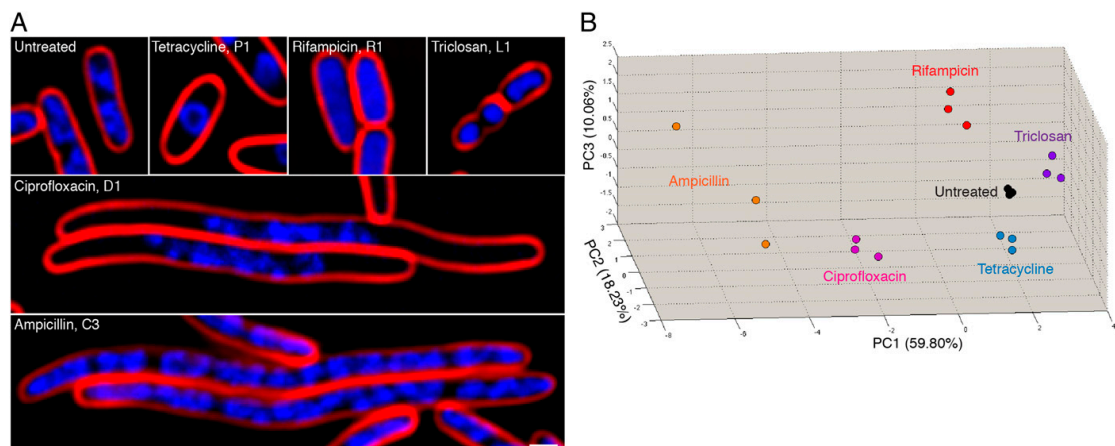

Fig. 1. Bacterial cells treated with inhibitors targeting one of five major biosynthetic pathways (DNA, protein, RNA, peptidoglycan, lipid) have unique cytological profiles. (*A*) *E. coli* cells were treated with 5x MIC of each antibiotic for 2 h and stained with FM4-64 (red) and DAPI (blue). (Scale bar, 1 μm.) (*B*) A 3D PCA graph using PC1 (59.80%), PC2 (18.23%), and PC3 (10.06%). Variables that contribute to each principal component (PC) are summarized in Fig. S1. Each antibiotic is color coded with three replicates shown. Three independent cultures of bacteria were treated with each antibiotic, and cell morphologies were measured as described in *Materials and Methods*.

Results

Categorizing Inhibitors of Five Major Biosynthetic Pathways. We first sought to determine whether BCP can distinguish between inhibitors of the five major pathways assayed by MMS (translation, transcription, DNA replication, lipid synthesis, and peptidoglycan synthesis). In Fig. 1*A*, we show cells that have been treated for 2 h with one inhibitor from each class (tetracycline, rifampicin, ciprofloxacin, triclosan, and ampicillin) at 5× the minimal inhibitory concentration (MIC). Cells in each category had strikingly different morphologies, demonstrating that compounds targeting different pathways generated unique cytological profiles. Notable among these is tetracycline, which produced toroidal chromosomes in wide cells, and rifampicin, which produced decondensed chromosomes in wide cells. To quantitatively analyze these results, we performed the experiments in triplicate, measured cell morphologies resulting from treatment with each antibiotic (Tables S2 and S3), and performed principal component analysis (PCA) to categorize cells with similar morphologies. As shown in Fig. 1*B* and Fig. S1, each of the five categories of antibiotics was quantitatively separated from each other
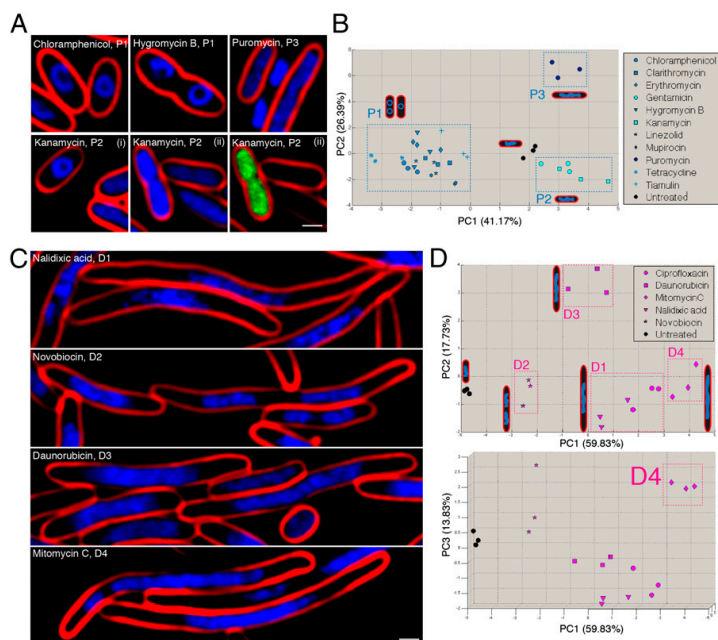
Fig. 2. Cytological profiling of translation and DNA replication inhibitors. (*A* and *B*) Images of cells treated with protein translation inhibitors (*A*) were used to construct profiles that divided them into three subclasses (P1–P3) (*B*). (*C* and *D*) DNA replication inhibitors formed four subclasses (D1–D4). Subclass D4 is distinguishable from D1 by plotting PC1 versus PC3 (*D*, *Lower* graph). The boundaries of the subgroups (boxes) were determined empirically from the training set using compounds with known mechanisms of action and the Euclidean distance cluster map shown in Figs. S2*E* and S3*D*. In all images, cell membranes are stained with FM4-64 (red), DAPI (blue), and SYTOX green (green). SYTOX green brightly stains only cells with permeabilized membranes and is absent from most images. (*A*) Kanamycin generates two types of profiles in a mixed population. Therefore, two fields are shown. *Left* shows altered DNA morphology (*i*), the *Right* two panels (*ii*) show the same field of cells with altered membrane permeability (*ii*, *Center*, FM4-64 and DAPI; *ii*, *Right*, FM4-64 and SYTOX green). (Scale bar, 1 μm.) Details of PCA graphs *B* and *D* are provided in Figs. S2 and S3, respectively.

Fig. 3. Cytological profiling of cell-wall and lipid biosynthesis inhibitors. (*A* and *C*) Bacterial cells were treated with each cell-wall synthesis inhibitor (*A*), lipid biosynthesis inhibitor (*C*), and membrane active compounds (*C*), stained with FM4-64 (red) and DAPI (blue). (Scale bars, 1 μm.) (*B*) P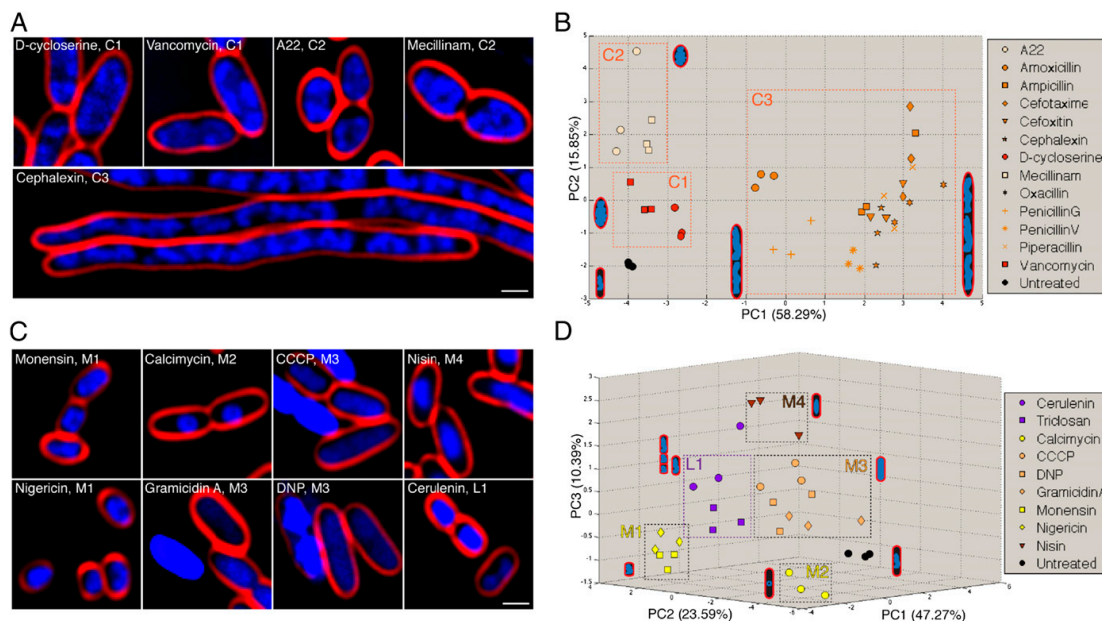CA graph showing PC1 (58.29%) and PC2 (15.85%), using unweighted variables from the cell-wall synthesis inhibitors, which form three subclasses (C1–C3). (*D*) A 3D PCA graph, PC1 (47.27%) and PC2 (23.59%) and PC3 (10.39%), using unweighted variables from membrane active compounds and lipid biosynthesis inhibitors. Variables contributing to each PC are summarized in Figs. S4 and S5. The boundaries of the subgroups (boxes) were determined empirically from the training set using compounds with known MOA and the Euclidean distance cluster map shown in Figs. S4*E* and S5*D*.

and replicates clustered closely together, demonstrating that cytological profiles for these compounds were reproducible. Thus, BCP can rapidly and quantitatively discriminate between the five major classes of antibiotics assayed by MMS.

Detection of Inhibitor Subclasses by BCP. To determine whether cytological profiles were conserved across different mechanistic classes of protein-synthesis inhibitors, we examined eleven different inhibitors belonging to eight structural classes that have a variety of biochemical effects on the ribosome. We found that we could clearly distinguish three subclasses of protein-synthesis inhibitors that have distinct biochemical mechanisms of action (Fig. 2 *A* and *B* and Fig. S2). Subclass P1 inhibitors, which are defined from the training set as box P1 in Fig. 2*B* and Fig. S2*E*, completely block peptide elongation [e.g., tetracycline (Fig. 1*A*) and chloramphenicol (Fig. 2*A*)] and produce toroid-shaped chromosomes and wide cells. Subclass P2 inhibitors, which include most of the aminoglycosides, are thought to both promote mistranslation and effect membrane permeability (21). In keeping with these two proposed MOA, each subclass P2 inhibitor produced two distinct cell populations: (*i*) those with altered chromosome morphology and (*ii*) those with altered membrane permeability (Fig. 2*A*). The one notable exception was the aminoglycoside hygromycin B, which inhibits chain elongation (22) and falls in subclass P1. The subclass P3 inhibitor puromycin causes premature chain termination and formed a distinct category on the PCA plot (Fig. 2*B*). Thus, BCP can discriminate between molecules that have a similar structure but different effects on translation. It can also cluster molecules that have different structures but the same MOA and identify individual molecules (such as the aminoglycosides) that have more than one MOA.

Inhibitors of DNA gyrase, topoisomerase II, DNA intercalating agents, and DNA cross-linking agents fall into a single

group as DNA replication inhibitors in MMS assays (10, 23, 24). To determine whether BCP could provide more detailed information on DNA synthesis inhibitors, we profiled five compounds belonging to four structural classes that interact with different cellular targets. We found that BCP could identify four subclasses that correlated with their MOA (Fig. 2 *C* and *D* and Fig. S3). Compounds that primarily target the GyrA subunit of DNA gyrase (ciprofloxacin, nalidixic acid) generated a reproducibly distinct profile (D1) from novobiocin (D2), which targets the GyrB subunit. The intercalating agent daunorubicin (D3) and the DNA cross-linker mitomycin C (D4) also formed separate subclasses. These groups have related profiles that can be distinguished by using three principal components in the analysis (e.g., D4 versus D1–D3, Fig. 2*D*, *Lower* and Fig. S3*D*).

We next profiled a variety of cell-wall synthesis inhibitors, membrane-active compounds, lipid-biosynthesis inhibitors (Fig. 3 and Figs. S4 and S5), and transcription and nucleotide-synthesis inhibitors (Fig. S6). We found that all tested antibiotics targeting different cellular pathways generated reproducibly distinct profiles. Cell-wall synthesis inhibitors fell into three different groups (Fig. 3 *A* and *B*) depending on whether they inhibit the availability of peptidoglycan precursors (C1), inhibit lateral cell-wall synthesis either by preferentially inhibiting PBP2 or by inhibiting MreB (C2), or whether they target PBP3 involved in cell division (C3).

Compounds that interfere with membrane bioenergetics (Fig. 3 *C* and *D* and Fig. S5) fell into four distinct categories based on their MOA, including the monovalent and divalent cation shuttles (M1 and M2, respectively), proton gradient dissipators (M3), and a pore-forming molecule (M4). These four categories were also distinct from inhibitors of lipid biosynthesis (L1). The profiles generated by the RNA transcription inhibitors actinomycin D and rifampicin were also distinct from other classes of antibiotics and formed two subclasses (R1 and R2, Fig. S6).
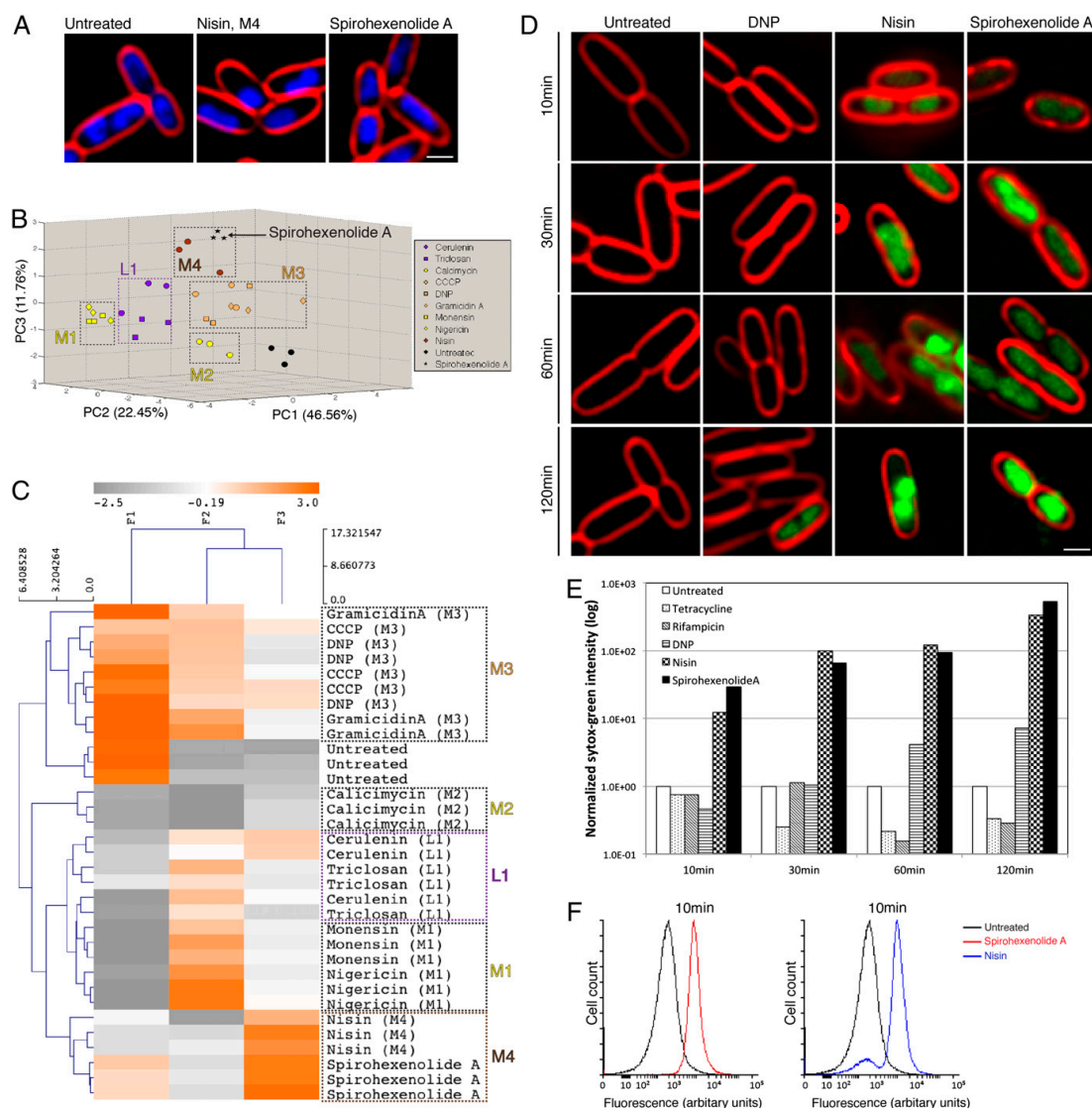
Fig. 4. Spirohexenolide A MOA determination by BCP. (*A*) Bacterial cells treated with spirohexenolide A and nisin were stained with FM 4–64 (red) and DAPI (blue). (*B* and *C*) Cells treated with spirohexenolide A clustered with nisin (M4). (*B*) A 3D PCA graph, PC1 (46.56%) and PC2 (22.45%) and PC3 (11.76%), using unweighted variables from membrane active compounds, lipid biosynthesis inhibitors, and spirohexenolide A. (*C*) Cluster map of spirohexenolide A, using PC1, PC2, and PC3 values from the PCA. (*D*) Bacterial cells treated with an energy poisoning agent DNP, a pore-forming molecule nisin, and spirohexenolide A for various times, stained with FM 4–64 (red) and SYTOX Green (green). SYTOX Green intensity was normalized to the brightest sample. (*E*) A graph of the normalized average SYTOX Green intensity per pixel of cells treated with each antibiotic for 10, 30, 60, and 120 min. Approximately 1,000 cells total were measured. (*F*) PMF assay using DiBAC4(5) stained *E. coli*. Cells were treated for 10 min with spirohexenolide A (red) or nisin (blue) and subjected to flow cytometry. A total of 10,000 cells were counted.

Our results demonstrate that all compounds that target different cellular pathways generate quantitatively distinct cytological profiles. To determine whether we could use these profiles to identify the cellular pathways targeted by a collection of antibiotics, we performed a double-blind BCP experiment. A total of 18 different known compounds were blinded and placed into three separate groups of 10, and then each group was separately profiled against *Esherichia coli*. Based solely on the cytological profile generated after drug exposure, we were able to correctly assign all 30 independently tested compounds to the correct cellular target (Table S4). This test confirmed our conclusion that bacterial cytological profiling is a rapid and powerful approach for determining the cellular pathway targeted by molecules even when their molecular identities are unknown.
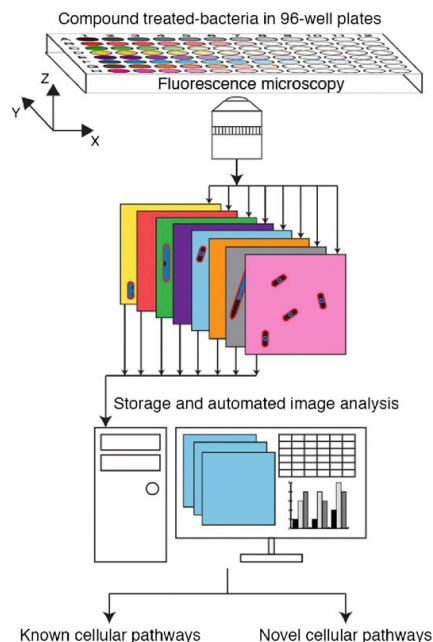
Fig. 5. Bacterial cytological profiling high-throughput screening (BCP-HTS). Bacterial cultures are grown in 96-well plates in the presence of different concentrations of antibacterial molecules. At specified time points, treated cultures are transferred to a microscopic 96-well plate, and images are collected using a fluorescence microscope. All stored images can be analyzed in batch using automated image analysis software and compared with an existing profile database to identify the target. Compounds with completely unique cellular targets will form distinct categories that will be high priority for further analysis. The power of the analysis increases over time as more molecules with known mechanisms of action are characterized.

Identifying the Mode of Action of Spirohexenolide A. We next used BCP to provide information on the MOA of spirohexenolide A (Fig. S7A) (25), a spirotetronate natural product with a previously unknown MOA that kills mammalian cells, Gram positive bacteria, including MRSA, as well as the *E. coli lptD4213* mutant (26). Although spirohexenolide A was recently reported to inhibit human macrophage migration inhibitor factor (hMIF), it likely has a different target in bacterial cells because bacteria do not contain hMIF (27). Spirohexenolide A-treated cells had an overall profile identical to nisin-treated cells (Fig. 4 A–C and Fig. S7), suggesting that spirohexenolide A has an MOA similar to nisin. Nisin binds lipid II and rapidly forms pores in the membrane (28) so we tested whether spirohexenolide A compromised membrane integrity using the membrane-impermeable DNA stain SYTOX Green, which cannot enter intact cells. Both nisin- and spirohexenolide A-treated cells showed increased SYTOX Green fluorescence intensity within 10 min of antibiotic exposure (Fig. 4 D and E), suggesting that spirohexenolide A rapidly permeabilized the cell membrane. Nisin also collapses the proton motive force (PMF) of bacteria (29) so we used the PMF sensitive dye DiBAC4(5) and Fluorescence-Activated Cell Sorting (FACS) to determine whether spirohexenolide A collapses the PMF (20, 30). Immediately upon addition of spirohexenolide A, cells were rapidly permeabilized and showed high fluorescence intensity of the DiBAC4(5) PMF dye, identical to nisin-treated cells (Fig. 4F), suggesting that spirohexenolide A rapidly depletes PMF. Thus, spirohexenolide A likely acts by disrupting the cytoplasmic membrane.

Discussion

Cytological profiling in eukaryotic cells relies upon measuring a large number of cytoskeletal markers (18). Because bacteria are 100 times smaller than the typical eukaryotic cell and lack all of the organelles and markers used in those studies, it has long been assumed that cytological profiling could not be applied to bacteria. Here, we show that BCP is a simple, one-step assay that provides an immensely powerful approach for identifying the cellular pathways targeted by molecules, a key step in determining the MOA. BCP has many advantages over other approaches: it is faster, provides higher resolution for identifying more pathways, and can be performed in very small (microliter scale) culture volumes. BCP also does not require a set of specialized strains like many other methods (13–17). Because a single BCP experiment is sufficient to identify the cellular pathway targeted, the BCP workflow is simple and can be performed in high throughput. BCP can therefore be used for primary screening of compounds to identify molecules that target specific cellular pathways without the need for slow and labor-intensive analysis. Because one can easily monitor changes in cell morphology after exposure to various concentrations of different molecules (Fig. 5), BCP high-throughput screening (BCP-HTS) does not require growth inhibition data, such as MIC or viable cell counts, before screening. This advantage makes the method suitable for primary whole-cell screening of newly made libraries. The power of interpreting cytological profiles increases over time as more molecules with known mechanisms of action are characterized. When compounds with completely unique cellular targets are profiled, they will form unique categories and might be given high priority for further analysis. Because bacteria have evolved resistance to nearly all known antibiotics, identifying molecules with different mechanisms of action is of high priority.

One limitation of BCP is that it does not identify the precise molecular target and is therefore complementary to approaches such as isolating resistant mutants or screening a large collection of sensitized strains. In addition, newly isolated compounds that represent the first known inhibitors of a pathway will require additional experimental methods to determine and validate their targets.

Why does BCP work? A bacterial cell is built by thousands of enzymes working in unison. We speculate that the various pathways are largely uncoupled by checkpoints so inactivating a single essential enzyme reduces one key product, while the rest of the cell continues to replicate, leading to unique cell-shape changes in response to each specific challenge. In nearly all cases, the cytological profiles produced in response to antibiotics can be explained in terms of their physiological effects. For example, compounds that block translation lead to chromosome compaction due to the interference with coordinated translation and insertion of proteins into the membrane (31, 32) whereas compounds that block transcription lead to chromosome decondensation due to the absence of active RNA polymerase (33). BCP takes advantage of the paucity of cell-cycle checkpoints in bacteria and the advent of high-resolution imaging to allow the rapid identification of the cell pathway affected by thousands of compounds, eliminating a longstanding bottleneck in academic programs and in antibiotic discovery programs. BCP can be applied to a wide range of studies that involve compounds that kill bacteria, including studies of the innate immune system, complex microbial communities, evolution of antibiotics and mechanisms of resistance, as well as efforts to find antibiotics that are active against multidrug resistant bacteria.

Materials and Methods

Strain and Antibiotics. *E. coli lptD4213* was used in this study (26). Forty-one antibiotics were used that include 26 structural classes of antibiotics used in the clinic (Table S1). Solutions of antibiotics in Table S1 were prepared using the recommended concentrations and solvents from the manufacturers.

Minimal Inhibitory Concentration Determination. Minimal inhibitory concentration (MIC) data shown in Table S1 were determined by the microdilution

method (34). Overnight cultures of *E. coli* were diluted 1:100 into LB medium and grown at 30 °C to an OD_{600} of 0.2 (early exponential phase). Exponential-phase cell cultures were diluted 1:100 into the LB medium containing different concentrations of each antibiotic in a 96-well plate. MIC was obtained after an overnight incubation at 30 °C.

Fluorescence Microscopy. Exponential-phase cell cultures were treated with 5x MIC and grown in a roller at 30 °C. Treated cultures were harvested after 2 h and stained with 1 µg·mL^{-1} FM4-64 (35), 2 µg·mL^{-1} DAPI, and 0.5 µM SYTOX-Green (Molecular Probes/Invitrogen). Cultures were then centrifuged at $3,300 \times g$ for 30 s in a microcentrifuge and resuspended in 1/10 volume of the original cultures. Three microliters of concentrated cells were transferred onto an agarose pad containing 1.2% agarose and 20% LB medium for microscopy. Microscopy was performed as previously described (20). Exposure time of each wavelength was the same throughout every experiment included in the statistical analysis of all training sets of antibiotics.

Cytological Profiling. Cell morphology was measured by the ImageJ v1.46 according to the analyze tool parameters. Briefly, polygons were drawn on an experimental field using membrane or nucleoid as a guide to measure area (µm^2), perimeter (µm), length (µm), width (µm), and circularity of both membrane and nucleoid. Performing on nondeconvolved images, average DAPI and SYTOX Green intensity per pixel was determined using the membrane outline, and then subtracted by its own background intensity. Finally, DAPI and SYTOX Green intensity of treated cells was normalized by untreated cells intensity of the same set of experiments, making intensity data from different experimental sets comparable. Decondensation of the nucleoid was defined by the ratio of corrected nucleoid area and membrane area.

Statistical Analysis. Cell-morphology parameters in Tables S2 and S3 from each antibiotic were obtained from three or more independent experiments. The deviation shown in Tables S2 and S3 represents the SEM. Profiling data were obtained from, if possible, every cell in the imaging fields ($n > 30$ for the elongated cell phenotype, $n > 50$ for the others). Variables reduction was performed using a Principal Component Analysis (PCA) from the XLSTAT (version 2012.5.01) program on Microsoft Excel for Mac 2011 (version 14.1.0). Spearman's rank correlation and unweighted variables were used in PCA. Clustering of each subclass was performed using the Euclidean distance (average linkage) method on MultiExperiment Viewer (v4.7.3). The boundaries of the subgroups (boxes) drawn on the PCA graphs were determined empirically from the training set using compounds with known MOA and a Euclidean distance cluster map.

Double-Blind Tests. Eighteen antibiotics targeting different pathways and two controls (water and DMSO) were included in a double-blinded BCP experiment. Samples were divided into three sets containing 10 compounds in each set and relabeled as A1–A10, B1–B10, and C1–C10. Both the tester and the administrator were not aware of what compound belonged to which subclass of antibiotic, and each set was tested independently.

Flow Cytometry. Analysis of the *E. coli* proton motive force (PMF) by flow cytometry was carried out as described in ref. 20. Cell cultures were treated with spirohexenolide A or nisin at 30 °C for 10 min.

1. Hooper LV, Littman DR, Macpherson AJ (2012) Interactions between the microbiota and the immune system. *Science* 336(6086):1268–1273.
2. Hill DA, Artis D (2010) Intestinal bacteria and the regulation of immune cell homeostasis. *Annu Rev Immunol* 28:623–667.
3. Ley RE, Peterson DA, Gordon JI (2006) Ecological and evolutionary forces shaping microbial diversity in the human intestine. *Cell* 124(4):837–848.
4. Tremaroli V, Bäckhed F (2012) Functional interactions between the gut microbiota and host metabolism. *Nature* 489(7415):242–249.
5. Romero D, Traxler MF, López D, Kolter R (2011) Antibiotics as signal molecules. *Chem Rev* 111(9):5492–5505.
6. Zasloff M (2002) Antimicrobial peptides of multicellular organisms. *Nature* 415(6870):389–395.
7. Nikaido H (2009) Multidrug resistance in bacteria. *Annu Rev Biochem* 78:119–146.
8. Silver LL (2011) Challenges of antibacterial discovery. *Clin Microbiol Rev* 24(1):71–109.
9. Payne DJ, Gwynn MN, Holmes DJ, Pompliano DL (2007) Drugs for bad bugs: Confronting the challenges of antibacterial discovery. *Nat Rev Drug Discov* 6(1):29–40.
10. Cotsonas King A, Wu L (2009) Macromolecular synthesis and membrane perturbation assays for mechanisms of action studies of antimicrobial agents. *Current Protocols in Pharmacology*, eds Enna SJ, et al. (Wiley, Hoboken, NJ).
11. Bandow JE, Hecker M (2007) Proteomic profiling of cellular stresses in *Bacillus subtilis* reveals cellular networks and assists in elucidating antibiotic mechanisms of action. *Systems Biological Approaches in Infectious Diseases*, eds Boshoff HI, Barry CE (Birkhäueser, Basel, Switzerland), pp 79–101.
12. Donald RGK, et al. (2009) A *Staphylococcus aureus* fitness test platform for mechanism-based profiling of antibacterial compounds. *Chem Biol* 16(8):826–836.
13. Freiberg C, Fischer HP, Brunner NA (2005) Discovering the mechanism of action of novel antibacterial agents through transcriptional profiling of conditional mutants. *Antimicrob Agents Chemother* 49(2):749–759.
14. Xu HH, Real L, Bailey MW (2006) An array of *Escherichia coli* clones over-expressing essential proteins: A new strategy of identifying cellular targets of potent antibacterial compounds. *Biochem Biophys Res Commun* 349(4):1250–1257.
15. Nichols RJ, et al. (2011) Phenotypic landscape of a bacterial cell. *Cell* 144(1):143–156.
16. Singh SB, Phillips JW, Wang J (2007) Highly sensitive target-based whole-cell antibacterial discovery strategy by antisense RNA silencing. *Curr Opin Drug Discov Devel* 10(2):160–166.
17. Li X, et al. (2004) Multicopy suppressors for novel antibacterial compounds reveal targets and drug efflux susceptibility. *Chem Biol* 11(10):1423–1430.
18. Mitchison TJ (2005) Small-molecule screening and profiling by using automated microscopy. *ChemBioChem* 6(1):33–39.
19. Mayer TU, et al. (1999) Small molecule inhibitor of mitotic spindle bipolarity identified in a phenotype-based screen. *Science* 286(5441):971–974.
20. Lamsa A, Liu WT, Dorrestein PC, Pogliano K (2012) The *Bacillus subtilis* cannibalism toxin SDP collapses the proton motive force and induces autolysis. *Mol Microbiol* 84(3):486–500.
21. Jana S, Deb JK (2006) Molecular understanding of aminoglycoside action and resistance. *Appl Microbiol Biotechnol* 70(2):140–150.
22. Peske F, Savelsbergh A, Katunin VI, Rodnina MV, Wintermeyer W (2004) Conformational changes of the small ribosomal subunit during elongation factor G-dependent tRNA-mRNA translocation. *J Mol Biol* 343(5):1183–1194.
23. Guan L, Blumenthal RM, Burnham JC (1992) Analysis of macromolecular biosynthesis to define the quinolone-induced postantibiotic effect in *Escherichia coli*. *Antimicrob Agents Chemother* 36(10):2118–2124.
24. Menzel TM, et al. (2011) Mode-of-action studies of the novel bisquaternary bis-naphthalimide MT02 against *Staphylococcus aureus*. *Antimicrob Agents Chemother* 55(1):311–320.
25. Kang MJ, et al. (2009) Isolation, structure elucidation, and antitumor activity of spirohexenolides A and B. *J Org Chem* 74(23):9054–9061.
26. Ruiz N, Falcone B, Kahne D, Silhavy TJ (2005) Chemical conditionality: A genetic strategy to probe organelle assembly. *Cell* 121(2):307–317.
27. Yu W-L, et al. (2013) Spirohexenolide A targets human macrophage migration inhibitory factor (hMIF). *J Nat Prod* 76(5):817–823.
28. Wiedemann I, et al. (2001) Specific binding of nisin to the peptidoglycan precursor lipid II combines pore formation and inhibition of cell wall biosynthesis for potent antibiotic activity. *J Biol Chem* 276(3):1772–1779.
29. Bruno ME, Kaiser A, Montville TJ (1992) Depletion of proton motive force by nisin in *Listeria monocytogenes* cells. *Appl Environ Microbiol* 58(7):2255–2259.
30. Sims PJ, Waggoner AS, Wang CH, Hoffman JF (1974) Studies on the mechanism by which cyanine dyes measure membrane potential in red blood cells and phosphatidylcholine vesicles. *Biochemistry* 13(16):3315–3330.
31. Cabrera JE, Cagliero C, Quan S, Squires CL, Jin DJ (2009) Active transcription of rRNA operons condenses the nucleoid in *Escherichia coli*: Examining the effect of transcription on nucleoid structure in the absence of transertion. *J Bacteriol* 191(13):4180–4185.
32. Hud NV, Downing KH (2001) Cryoelectron microscopy of λ phage DNA condensates in vitreous ice: The fine structure of DNA toroids. *Proc Natl Acad Sci USA* 98(26):14925–14930.
33. Jin DJ, Cabrera JE (2006) Coupling the distribution of RNA polymerase to global gene regulation and the dynamic structure of the bacterial nucleoid in *Escherichia coli*. *J Struct Biol* 156(2):284–291.
34. Matthew AW (2006) Methods for Dilution Antimicrobial Susceptibility Tests for Bacteria That Grow Aerobically; Approved Standard. Seventh Edition (CLSI, Wayne, PA), pp 14–18.
35. Pogliano J, et al. (1999) A vital stain for studying membrane dynamics in bacteria: a novel mechanism controlling septation during *Bacillus subtilis* sporulation. *Mol Microbiol* 31(4):1149–1159.

Supporting Information
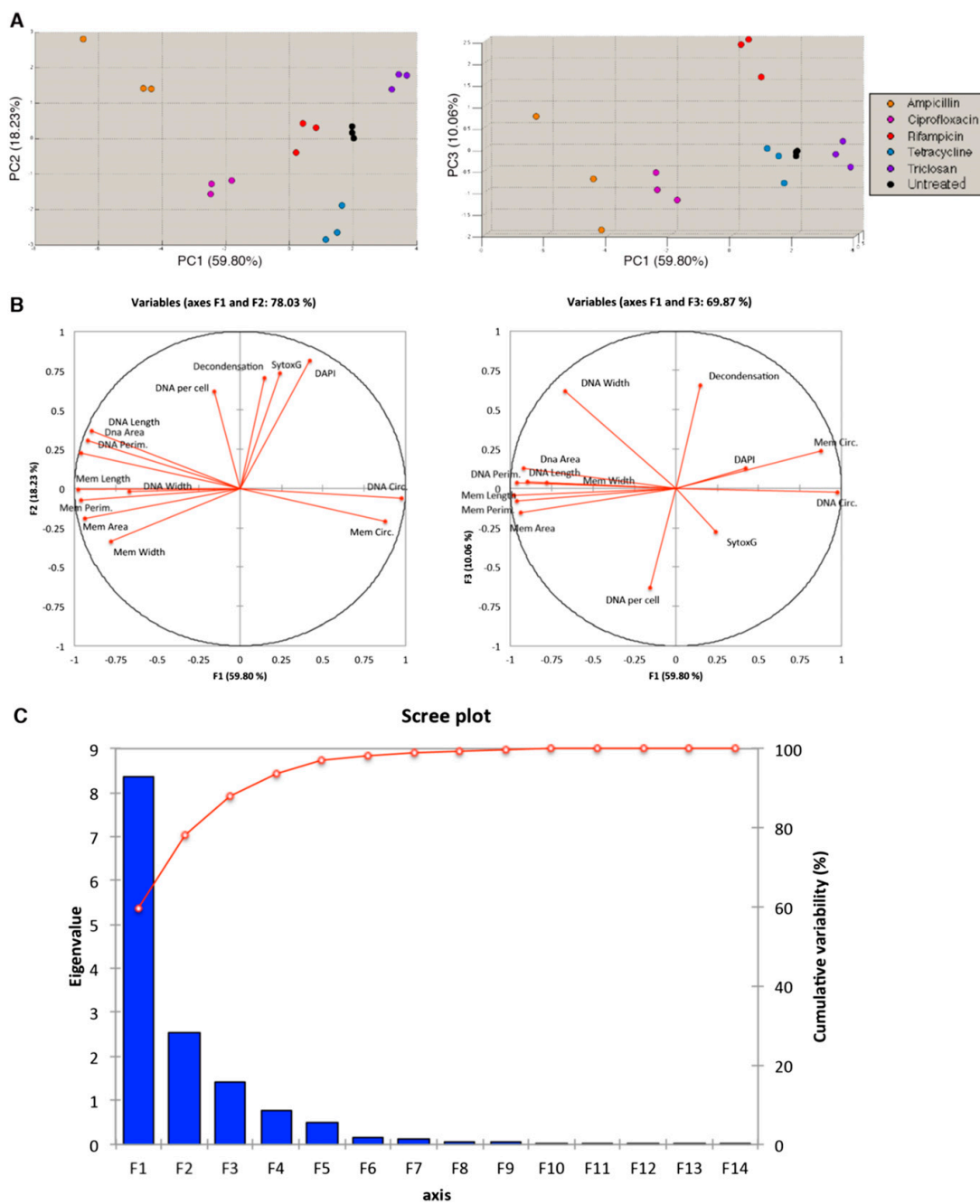
Nonejuie et al. 10.1073/pnas.1311066110

Fig. S1. (*A*) Principal component analysis (PCA) graphs using unweighted variables: PC1 (59.80%), PC2 (18.23%), and PC3 (10.06%). (*B*) Diagrams of correlations between variables and factors (PC). (*C*) A scree plot of eigenvalue and cumulative variability (%) of all factors.

Fig. S2. PCA and clustering of protein-translation inhibitors. (*A*) *Escherichia coli* cells were treated with each protein-translation inhibitor and stained with FM4-64 (red) and DAPI (blue). (Scale bar, 1 μm.) (*B*) A 3D (*Upper*) and a 2D (*Lower*) PCA graph using unweighted variables: PC1 (41.17%), PC2 (26.39%), and PC3 (12.83%). (*C*) Diagrams of correlations between variables and factors (PC). (*D*) A scree plot of eigenvalue and cumulative variability (%) of all factors in the protein-translation inhibitors PCA. (*E*) Cluster map of the protein-translation inhibitor training set, using PC1, PC2, and PC3 value from the PCA.
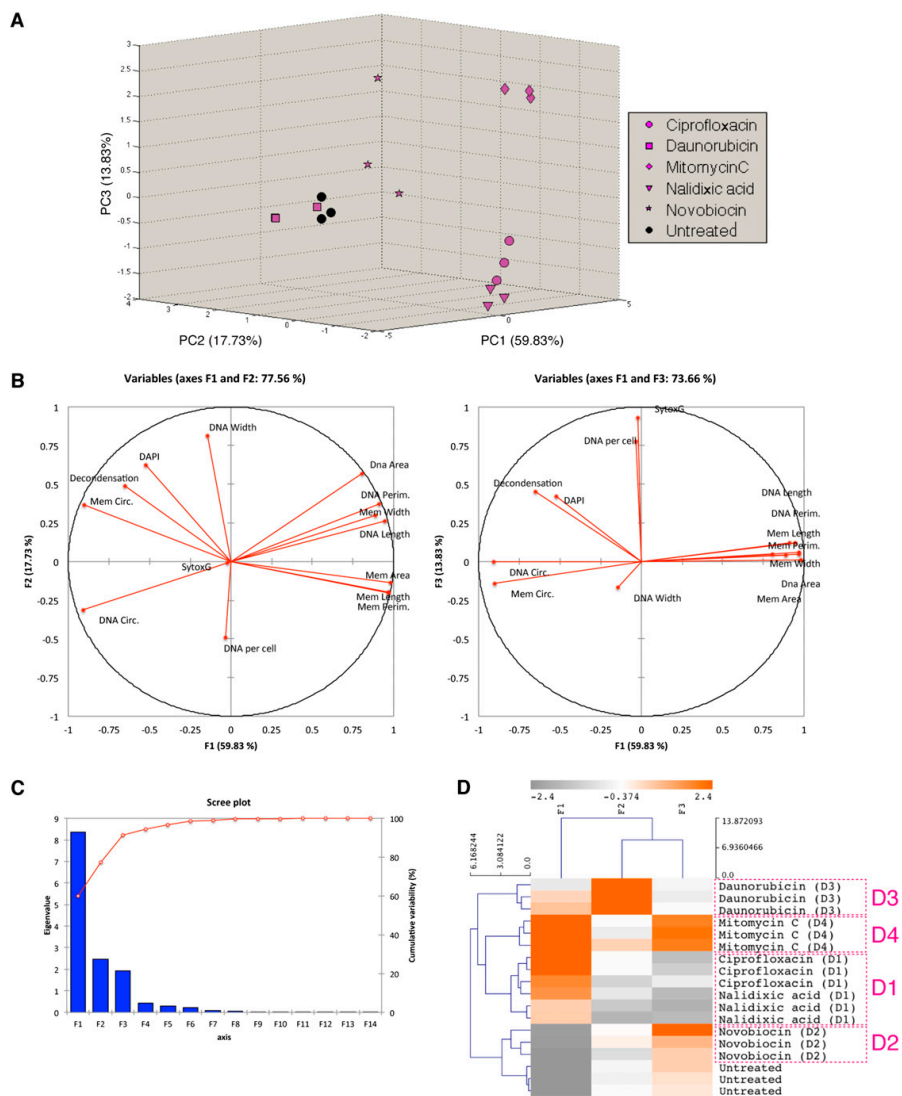
Fig. S3. PCA and clustering of DNA replication inhibitors. (*A*) A 3D PCA graph using unweighted variables: PC1 (59.83%), PC2 (17.73%), and PC3 (13.83%). (*B*) Diagrams of correlations between variables and factors (PC). (*C*) A scree plot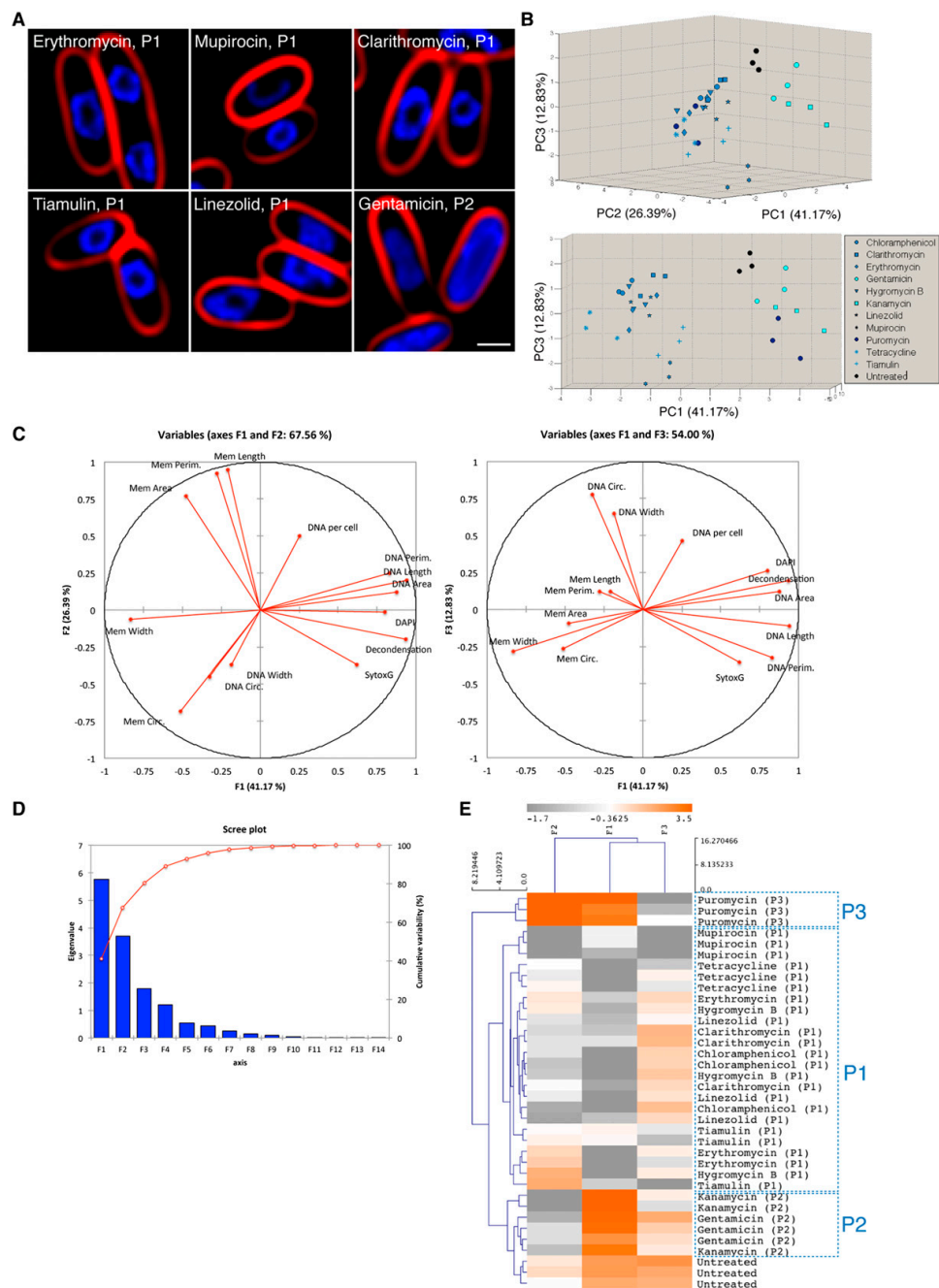 of eigenvalue and cumulative variability (%) of all factors in the DNA replication inhibitors PCA. (*D*) Cluster map of the DNA replication inhibitor training set, using PC1, PC2, and PC3 value from the PC.
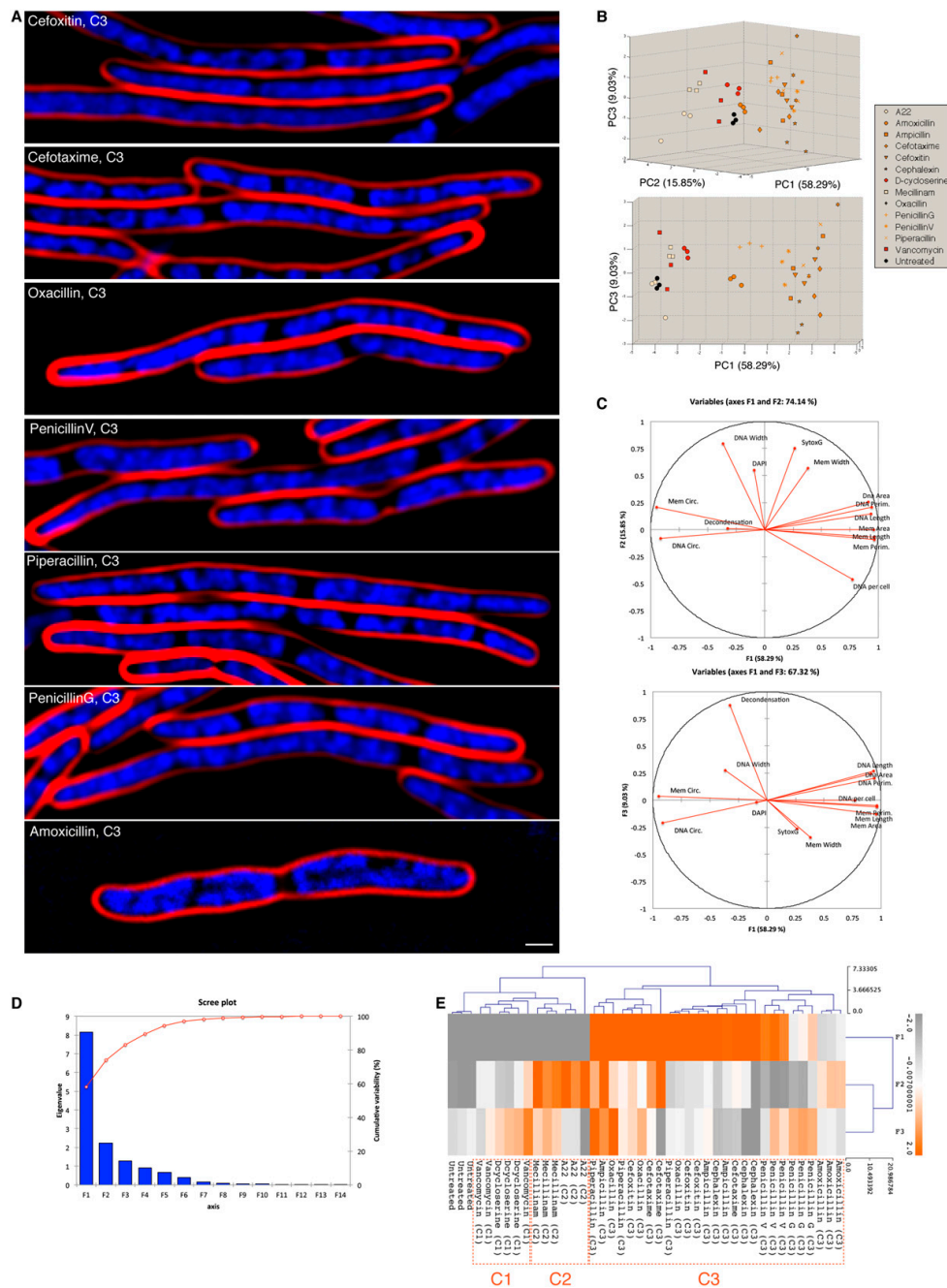
Fig. S4. PCA and clustering of cell-wall synthesis inhibitors. (*A*) *E. coli* cells were treated with each cell-wall synthesis inhibitor and stained with FM4-64 (red) and DAPI (blue). (Scale bar, 1 μm.) (*B*) A 3D (*Upper*) and a 2D (*Lower*) PCA graph using unweighted variables: PC1 (58.29%), PC2 (15.85%), and PC3 (9.03%). (*C*) Diagrams of correlations between variables and factors (PC). (*D*) A scree plot of eigenvalue and cumulative variability (%) of all factors in the cell-wall synthesis inhibitors PCA. (*E*) Cluster map of the cell-wall synthesis inhibitor training set, using PC1, PC2, and PC3 value from the PCA.
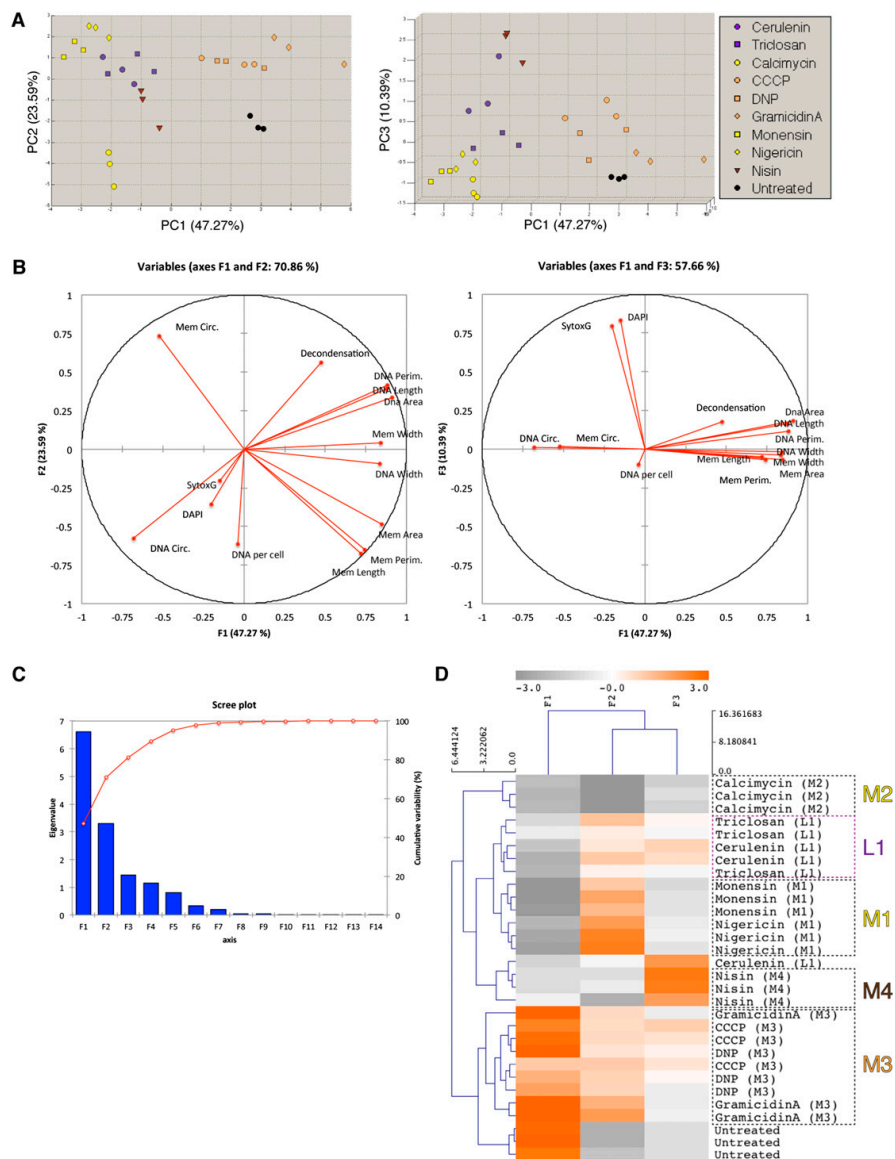
Fig. S5. PCA and clustering of membrane active compounds and lipid biosynthesis inhibitors. (*A*) PCA graphs using unweighted variables: PC1 (47.27%), PC2 (23.59%), and PC3 (10.39%). (*B*) Diagrams of correlations between variables and factors (PC). (*C*) A scree plot of eigenvalue and cumulative variability (%) of all factors in the membrane active compounds and lipid biosynthesis inhibitors PCA. (*D*) Cluster map of the membrane active compound and lipid biosynthesis inhibitor training set, using PC1, PC2, and PC3 value from the PCA.
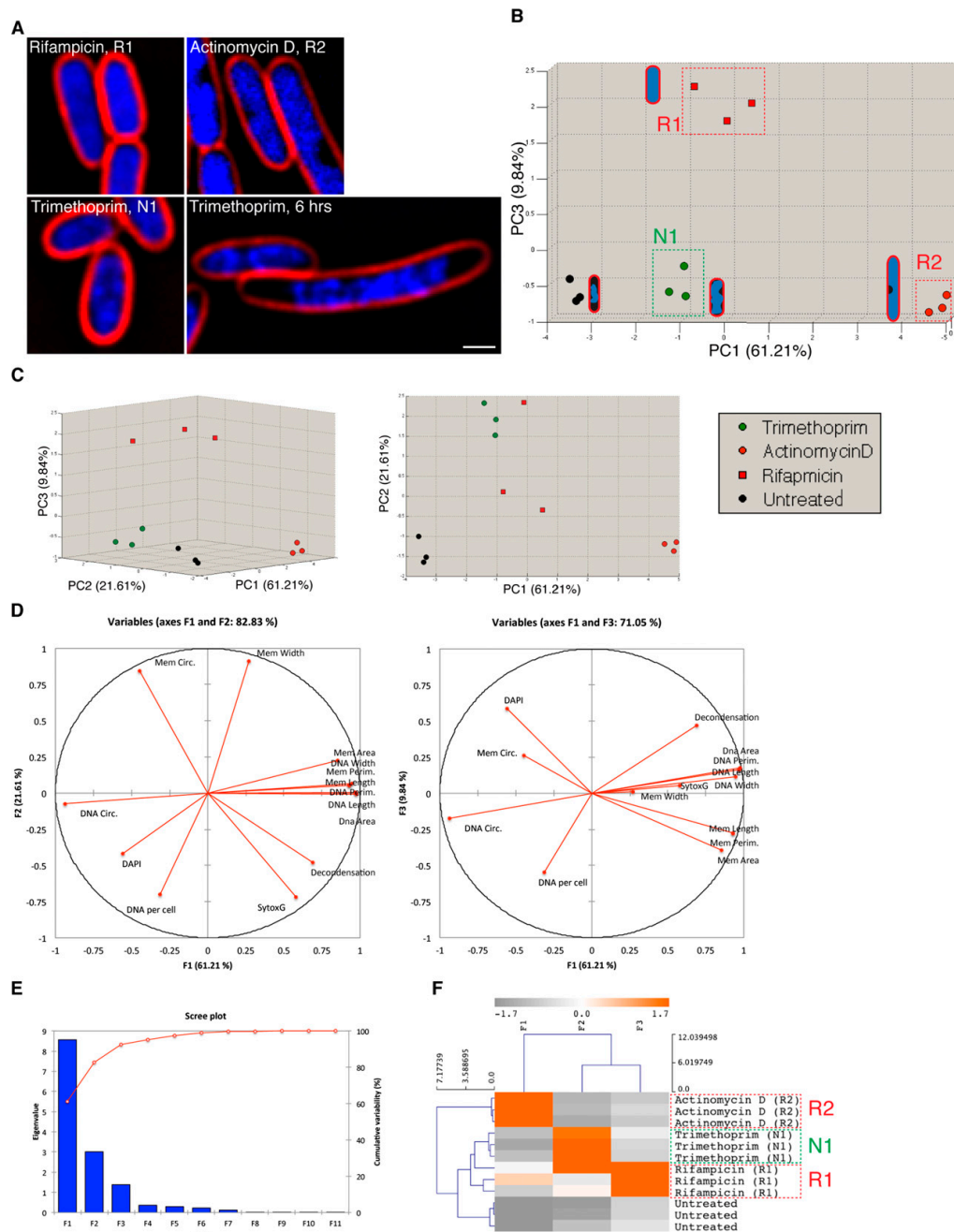
Fig. S6. Cytological profiles of cell treated with RNA-transcription and nucleotide-synthesis inhibitors. RNA-transcription inhibitor profiles were divided into two subgroups (R1 and R2). (*A*) *E. coli* cells were treated with each antibiotic and stained with FM4-64 (red) and DAPI (blue). (Scale bar, 1 μm.) (*B* and *C*) PCA graphs using unweighted variables: PC1 (61.21%), PC2 (21.61%), and PC3 (9.84%). The boundaries of the subgroups (boxes) were determined empirically from the training set using compounds with known mechanisms of action and the Euclidean distance cluster map shown in *F*. (*D*) Diagrams of correlations between variables and factors (PC). (*E*) A scree plot of eigenvalue and cumulative variability (%) of all factors in the RNA-transcription and nucleotide-synthesis inhibitors PCA. (*F*) Cluster map of the RNA-transcription and nucleotide-synthesis inhibitor training set, using PC1, PC2, and PC3 value from the PCA.

Fig. S7. PCA of spirohexenolide A, membrane-active compounds, and lipid-synthesis inhibitors. (*A*) Spirohexenolide A structure. (*B*) PCA graphs, PC1 (46.56%), PC2 (22.45%), and PC3 (11.76%), using unweighted variables. (*C*) Diagrams of correlations between variables and factors (PC). (*D*) A scree plot of eigenvalue and cumulative variability (%) of all factors in PCA.
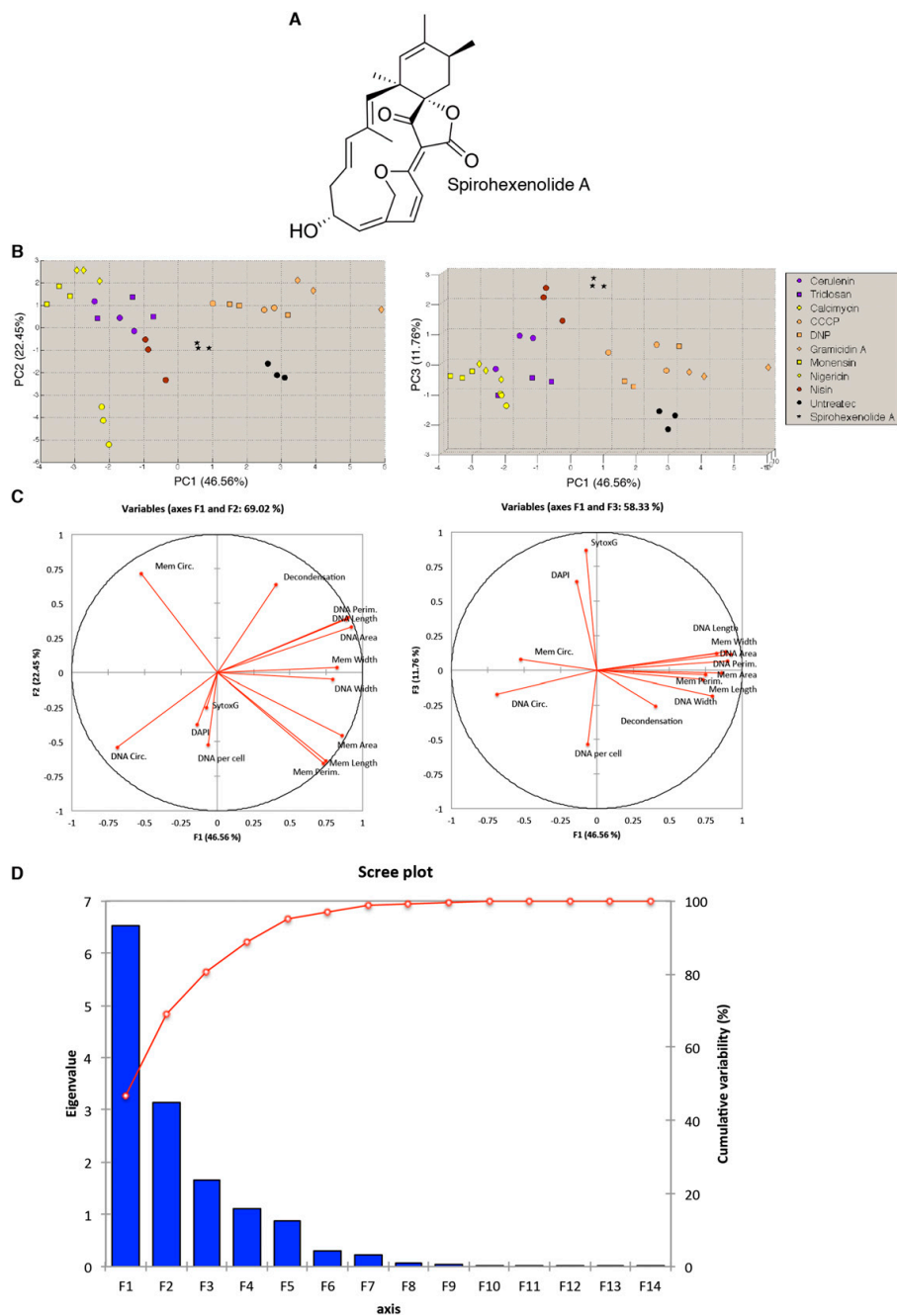
Table S1. List of antibiotics for bacterial cytological profiling

Antibiotic class	Antibiotic name	MIC, mg/L	Phenotype	Target (1, 2, 3–6)
		Protein synthesis		
Aminoglycoside	Gentamicin	0.625	P2	30S ribosome (promote mistranslation)
	Hygromycin B	10	P1	30S ribosome (inhibit translocation)
	Kanamycin	2	P2	30S ribosome (promote mistranslation)
Aminonucleoside	Puromycin	10	P3	50S ribosome (cause premature chain termination)
Amphenicols	Chloramphenicol	2	P1	50S ribosome (inhibit peptidyl transferase)
Macrolide	Clarithromycin	0.1	P1	50S ribosome (interfere aminoacyl translocation)
	Erythromycin	0.1	P1	50S ribosome (interfere aminoacyl translocation)
Monoxycarbolic acid	Mupirocin	0.25	P1	Isoleucyl t-RNA synthetase
Oxazolidinones	Linezolid	5	P1	50S ribosome (inhibit initiation complex formation)
Pleuromutilin	Tiamulin	0.25	P1	50S ribosome (inhibit peptidyl transferase)
Tetracycline	Tetracycline	0.5	P1	30S ribosome (inhibit aminoacyl tRNA binding)
		DNA synthesis and segregation		
Aminocoumarin	Novobiocin	0.5	D2	DNA gyrase B
Anthracycline	Daunorubicin	3.5	D3	Intercalates DNA, topoisomeraseII
Fluoroquinolone	Ciprofloxacin	0.005	D1	DNA gyrase A
	Nalidixic acid	1	D1	DNA gyrase A
Others	Mitomycin C	0.03	D4	Crosslink DNA strand
		RNA transcription		
Actinomycines	Actinomycin D	0.05	R2	Binds DNA at the transcription initiation
Rifamycin	Rifampicin	0.005	R1	DNA-dependent RNA polymerase
		Nucleotide synthesis		
Diaminopyridine	Trimethoprim	2	N1	Dihydrofolate reductase
		Cell wall synthesis		
Cephalosporins	Cefotaxime	0.0015	C3	Penicillin-binding proteins (PBPs)
	Cefoxitin	0.625	C3	Penicillin-binding proteins (PBPs)
	Cephalexin	2	C3	Penicillin-binding proteins (PBPs)
Glycopeptide	Vancomycin	1	C1	Binds D-Ala-D-Ala terminal, PBPs
Penicillin	Ampicillin	0.2	C3	Penicillin-binding proteins (PBPs)
	Amoxicillin	0.25	C3	Penicillin-binding proteins (PBPs)
	Oxacillin	1	C3	Penicillin-binding proteins (PBPs)
	Penicillin G	2	C3	Penicillin-binding proteins (PBPs)
	Penicillin V	3	C3	Penicillin-binding proteins (PBPs)
	Piperacillin	0.006	C3	Penicillin-binding proteins (PBPs)
	Mecillinam	0.01	C2	Penicillin-binding proteins (PBPs)
Others	D-Cycloserine	7	C1	Prevents D-Ala-D-Ala synthesis, PBPs
	A22	1	C2	Rod shape-determining protein MreB
		Lipid synthesis		
Polychloro phenoxy phenols	Triclosan	0.004	L1	Binds bacterial enoyl-acyl carrier protein reductase
Others	Cerulenin	3	L1	Binds fatty acid synthase
		Membrane active compounds		
Ionophore (divalent)	Calcimycin	1.25	M2	Mn^{2+}, Ca^{2+} and Mg^{2+} selective ionophore
Ionophores (carboxilic)	Nigericin	1.8	M1	K^+ ionophore
	Monensin	20	M1	Na^+ ionophore
Ionophores (polypeptide)	Gramicidin A	1.25	M3	Increase the permeability of bacterial membrane
Lantibiotics	Nisin	0.5	M4	Binds lipid II cause pore structure on membrane
Oxidative phosphorylation uncoupling agents	Carbonyl cyanide m-chlorophenyl hydrazone (CCCP)	2.05	M3	Energy poisoning agents
	2,4-Dinitrophenol (DNP)	184	M3	Energy poisoning agents
		Unknown		
Spirotetronate	Spirohexenolide A	20.375		

1. Peske F, Savelsbergh A, Katunin VI, Rodnina MV, Wintermeyer W (2004) Conformational changes of the small ribosomal subunit during elongation factor G-dependent tRNA-mRNA translocation. *J Mol Biol* 343(5):1183–1194.
2. Wiedemann I, et al. (2001) Specific binding of nisin to the peptidoglycan precursor lipid II combines pore formation and inhibition of cell wall biosynthesis for potent antibiotic activity. *J Biol Chem* 276(3):1772–1779.
3. Kohanski MA, Dwyer DJ, Collins JJ (2010) How antibiotics kill bacteria: From targets to networks. *Nat Rev Microbiol* 8(6):423–435.
4. Wilson DN (2009) The A-Z of bacterial translation inhibitors. *Crit Rev Biochem Mol Biol* 44(6):393–433.
5. Pressman BC (1976) Biological applications of ionophores. *Annu Rev Biochem* 45:501–530.
6. Typas A, Banzhaf M, Gross CA, Vollmer W (2012) From the regulation of peptidoglycan synthesis to bacterial growth and morphology. *Nat Rev Microbiol* 10(2):123–136.

Table S2. Bacterial cell morphology measurements

Antibiotics	Membrane area, μm²	DNA area, μm²	Membrane perimeter, μm	DNA perimeter, μm	Membrane length, μm	DNA length, μm	No. of nucleoids per cell
A22	2.522 ± 0.161	2.327 ± 0.151	6.282 ± 0.211	6.995 ± 0.243	2.264 ± 0.105	2.090 ± 0.110	1.000 ± 0.000
Actinomycin D	4.250 ± 0.146	4.202 ± 0.254	12.895 ± 0.444	12.510 ± 0.637	5.951 ± 0.172	5.281 ± 0.102	1.287 ± 0.057
Amoxicillin	6.801 ± 0.068	3.810 ± 0.095	18.062 ± 0.454	12.494 ± 1.113	7.781 ± 0.194	4.424 ± 0.180	1.608 ± 0.051
Ampicillin	12.248 ± 0.770	6.042 ± 1.824	35.957 ± 1.966	20.225 ± 5.276	13.489 ± 0.176	7.265 ± 1.250	1.767 ± 0.172
Calcimycin	1.641 ± 0.086	0.537 ± 0.039	6.584 ± 0.452	2.710 ± 0.131	2.978 ± 0.237	0.926 ± 0.046	1.276 ± 0.066
CCCP	1.587 ± 0.137	1.482 ± 0.144	5.937 ± 0.285	5.642 ± 0.301	2.621 ± 0.122	2.426 ± 0.144	1.117 ± 0.069
Cefotaxime	14.328 ± 0.777	5.488 ± 0.721	47.562 ± 1.190	18.736 ± 2.325	14.908 ± 0.424	7.137 ± 0.657	2.133 ± 0.227
Cefoxitin	12.909 ± 1.536	5.505 ± 0.723	42.187 ± 2.327	18.581 ± 1.307	14.304 ± 0.384	6.930 ± 0.647	2.076 ± 0.281
Cephalexin	14.283 ± 0.520	3.585 ± 0.483	48.402 ± 5.308	13.195 ± 1.256	14.172 ± 0.483	4.947 ± 0.489	2.916 ± 0.164
Cerulenin	1.097 ± 0.127	0.925 ± 0.061	4.941 ± 0.359	4.303 ± 0.138	2.158 ± 0.162	1.734 ± 0.080	1.147 ± 0.086
Chloramphenicol	2.510 ± 0.181	1.097 ± 0.006	7.239 ± 0.186	4.586 ± 0.096	3.143 ± 0.082	1.469 ± 0.011	1.119 ± 0.013
Ciprofloxacin	7.611 ± 0.480	3.080 ± 0.252	27.350 ± 1.614	11.562 ± 0.668	10.158 ± 0.183	4.655 ± 0.390	1.083 ± 0.047
Clarithromycin	2.474 ± 0.098	1.274 ± 0.161	7.457 ± 0.097	4.865 ± 0.239	3.297 ± 0.057	1.704 ± 0.120	1.089 ± 0.033
Daunorubicin	5.011 ± 0.626	3.964 ± 0.346	14.230 ± 1.493	12.591 ± 1.030	6.450 ± 0.634	4.482 ± 0.319	1.000 ± 0.000
Dcycloserine	3.497 ± 0.275	2.460 ± 0.188	10.490 ± 0.491	8.320 ± 0.110	4.481 ± 0.394	2.949 ± 0.288	1.623 ± 0.073
DNP	1.630 ± 0.197	1.473 ± 0.080	6.002 ± 0.389	5.530 ± 0.325	2.643 ± 0.169	2.342 ± 0.215	1.114 ± 0.071
Erythromycin	2.791 ± 0.059	1.107 ± 0.144	7.857 ± 0.090	4.999 ± 0.241	3.452 ± 0.042	1.602 ± 0.109	1.170 ± 0.032
Gentamycin	2.189 ± 0.055	1.851 ± 0.143	7.014 ± 0.167	6.111 ± 0.168	3.102 ± 0.090	2.540 ± 0.076	1.117 ± 0.017
GramicidinA	1.852 ± 0.261	1.860 ± 0.130	6.357 ± 0.639	6.515 ± 0.384	2.805 ± 0.275	2.568 ± 0.136	1.000 ± 0.000
Hygromycin B	2.806 ± 0.303	1.159 ± 0.027	7.807 ± 0.633	4.889 ± 0.265	3.436 ± 0.317	1.602 ± 0.078	1.150 ± 0.028
Kanamycin	2.040 ± 0.074	1.815 ± 0.038	6.727 ± 0.108	6.195 ± 0.107	2.984 ± 0.038	2.577 ± 0.027	1.049 ± 0.050
Linezolid	2.291 ± 0.152	0.992 ± 0.035	7.028 ± 0.283	4.472 ± 0.190	3.083 ± 0.140	1.498 ± 0.026	1.135 ± 0.005
Mecillinam	3.343 ± 0.196	3.014 ± 0.220	8.280 ± 0.191	8.232 ± 0.320	3.482 ± 0.079	2.895 ± 0.075	1.282 ± 0.028
Mitomycin C	10.057 ± 0.519	3.805 ± 0.401	38.097 ± 1.687	14.108 ± 1.001	11.939 ± 0.351	5.716 ± 0.297	1.625 ± 0.091
Monensin	0.963 ± 0.055	0.687 ± 0.068	4.239 ± 0.131	3.538 ± 0.182	1.787 ± 0.045	1.329 ± 0.077	1.077 ± 0.032
Mupirocin	2.131 ± 0.160	1.116 ± 0.068	6.217 ± 0.209	5.345 ± 0.166	2.572 ± 0.085	1.782 ± 0.050	1.036 ± 0.011
Nalidixic acid	6.555 ± 0.472	2.310 ± 0.325	23.713 ± 1.855	8.828 ± 0.876	8.960 ± 0.366	3.570 ± 0.397	1.136 ± 0.032
Nigericin	0.957 ± 0.054	0.817 ± 0.061	4.120 ± 0.163	4.035 ± 0.116	1.712 ± 0.089	1.503 ± 0.056	1.064 ± 0.061
Nisin	1.509 ± 0.127	0.928 ± 0.024	5.707 ± 0.396	3.990 ± 0.110	2.494 ± 0.231	1.522 ± 0.034	1.054 ± 0.056
Novobiocin	3.888 ± 0.224	1.958 ± 0.287	13.432 ± 0.634	6.927 ± 0.608	5.930 ± 0.283	2.821 ± 0.290	1.430 ± 0.011
Oxacillin	13.735 ± 0.350	6.517 ± 1.480	46.594 ± 1.738	21.493 ± 4.738	14.329 ± 0.666	7.782 ± 1.101	2.326 ± 0.073
PenicillinG	7.934 ± 0.954	3.703 ± 0.451	24.846 ± 2.977	12.494 ± 0.939	9.968 ± 0.801	5.274 ± 0.455	2.477 ± 0.034
PenicillinV	11.274 ± 0.778	4.123 ± 0.364	37.660 ± 0.784	14.363 ± 1.095	13.430 ± 0.318	5.770 ± 0.529	2.705 ± 0.161
Piperacillin	13.646 ± 0.371	5.752 ± 1.037	45.739 ± 1.278	18.438 ± 2.475	14.417 ± 1.009	6.948 ± 0.950	2.530 ± 0.134
Puromycin	3.285 ± 0.249	1.849 ± 0.116	10.600 ± 0.191	7.459 ± 0.458	4.861 ± 0.193	3.172 ± 0.208	1.301 ± 0.049
Rifampicin	2.495 ± 0.151	2.800 ± 0.267	7.731 ± 0.211	8.645 ± 0.584	3.428 ± 0.120	3.549 ± 0.230	1.009 ± 0.009
SpirohexenolideA	1.630 ± 0.051	1.131 ± 0.036	6.094 ± 0.130	4.725 ± 0.149	2.626 ± 0.056	1.911 ± 0.068	1.054 ± 0.047
Tetracycline	2.791 ± 0.185	0.946 ± 0.052	7.628 ± 0.128	4.485 ± 0.202	3.308 ± 0.025	1.395 ± 0.050	1.031 ± 0.015
Tiamulin	2.602 ± 0.327	1.299 ± 0.112	7.636 ± 0.597	5.745 ± 0.297	3.350 ± 0.221	1.936 ± 0.077	1.052 ± 0.047
Triclosan	1.205 ± 0.105	0.932 ± 0.107	4.776 ± 0.322	4.031 ± 0.349	2.006 ± 0.145	1.510 ± 0.154	1.248 ± 0.059
Trimethoprim	2.768 ± 0.109	1.946 ± 0.141	8.043 ± 0.303	6.874 ± 0.159	3.541 ± 0.120	2.521 ± 0.118	1.148 ± 0.068
Vancomycin	2.827 ± 0.231	2.057 ± 0.296	7.838 ± 0.383	6.660 ± 0.426	3.385 ± 0.174	2.360 ± 0.215	1.536 ± 0.080
Untreated	1.972 ± 0.025	1.294 ± 0.023	7.167 ± 0.319	5.103 ± 0.075	3.173 ± 0.121	1.989 ± 0.070	1.434 ± 0.070

Table S3. Bacterial cell morphology measurements (continued)

Antibiotics	Membrane width, μm	DNA width, μm	Membrane circularity	DNA circularity	SytoxG intensity	DAPI intensity	Decondensation
A22	1.413 ± 0.089	1.396 ± 0.030	0.813 ± 0.011	0.646 ± 0.025	6.281 ± 6.203	1.090 ± 0.333	0.924 ± 0.063
Actinomycin D	0.904 ± 0.009	1.034 ± 0.032	0.338 ± 0.010	0.375 ± 0.037	2.046 ± 0.070	0.649 ± 0.064	1.271 ± 0.038
Amoxicillin	1.075 ± 0.027	1.058 ± 0.032	0.286 ± 0.017	0.357 ± 0.050	7.870 ± 1.141	0.889 ± 0.191	0.901 ± 0.041
Ampicillin	1.159 ± 0.068	0.988 ± 0.124	0.129 ± 0.008	0.232 ± 0.029	3.665 ± 1.550	1.060 ± 0.180	0.854 ± 0.151
Calcimycin	0.701 ± 0.020	0.716 ± 0.016	0.494 ± 0.036	0.902 ± 0.019	23.734 ± 8.366	1.617 ± 0.144	0.419 ± 0.046
CCCP	0.771 ± 0.035	0.770 ± 0.027	0.585 ± 0.007	0.598 ± 0.002	43.956 ± 11.027	1.897 ± 0.289	1.044 ± 0.091
Cefotaxime	1.249 ± 0.048	0.903 ± 0.030	0.090 ± 0.006	0.254 ± 0.027	8.600 ± 8.060	1.523 ± 0.205	0.812 ± 0.058
Cefoxitin	1.183 ± 0.133	0.906 ± 0.041	0.098 ± 0.004	0.261 ± 0.025	2.605 ± 0.534	1.076 ± 0.219	0.882 ± 0.093
Cephalexin	1.312 ± 0.045	0.809 ± 0.048	0.084 ± 0.021	0.359 ± 0.047	4.202 ± 3.669	0.921 ± 0.152	0.732 ± 0.102
Cerulenin	0.644 ± 0.032	0.676 ± 0.014	0.587 ± 0.025	0.649 ± 0.012	2.373 ± 0.658	3.346 ± 1.009	0.976 ± 0.151
Chloramphenicol	1.008 ± 0.049	0.948 ± 0.008	0.611 ± 0.016	0.690 ± 0.010	0.469 ± 0.293	0.430 ± 0.151	0.490 ± 0.033
Ciprofloxacin	0.952 ± 0.049	0.837 ± 0.047	0.139 ± 0.010	0.314 ± 0.015	1.015 ± 0.262	0.259 ± 0.120	0.438 ± 0.010
Clarithromycin	0.952 ± 0.039	0.938 ± 0.054	0.574 ± 0.021	0.697 ± 0.017	0.171 ± 0.069	0.544 ± 0.115	0.561 ± 0.081
Daunorubicin	0.975 ± 0.039	1.094 ± 0.054	0.333 ± 0.035	0.329 ± 0.041	1.007 ± 0.084	1.083 ± 0.062	0.795 ± 0.069
Dcycloserine	0.983 ± 0.053	1.020 ± 0.056	0.434 ± 0.022	0.475 ± 0.034	1.742 ± 0.283	0.915 ± 0.169	1.142 ± 0.056
DNP	0.782 ± 0.052	0.785 ± 0.029	0.589 ± 0.018	0.616 ± 0.034	11.951 ± 5.068	1.243 ± 0.448	1.016 ± 0.134
Erythromycin	1.026 ± 0.014	0.871 ± 0.050	0.581 ± 0.003	0.606 ± 0.033	0.106 ± 0.032	0.719 ± 0.133	0.465 ± 0.068
Gentamycin	0.896 ± 0.024	0.925 ± 0.049	0.579 ± 0.017	0.643 ± 0.015	3.188 ± 1.205	1.638 ± 0.196	0.947 ± 0.107
GramicidinA	0.834 ± 0.051	0.899 ± 0.041	0.587 ± 0.036	0.563 ± 0.053	1.193 ± 0.497	0.454 ± 0.051	1.011 ± 0.072
Hygromycin B	1.033 ± 0.036	0.907 ± 0.030	0.591 ± 0.037	0.643 ± 0.046	0.341 ± 0.087	0.743 ± 0.205	0.478 ± 0.039
Kanamycin	0.869 ± 0.018	0.891 ± 0.019	0.586 ± 0.002	0.621 ± 0.012	10.016 ± 6.965	1.659 ± 0.204	0.933 ± 0.043
Linezolid	0.942 ± 0.021	0.840 ± 0.013	0.594 ± 0.006	0.660 ± 0.045	0.406 ± 0.082	0.617 ± 0.024	0.493 ± 0.049
Mecillinam	1.206 ± 0.059	1.310 ± 0.056	0.623 ± 0.023	0.587 ± 0.011	2.889 ± 0.609	1.487 ± 0.218	1.155 ± 0.033
Mitomycin C	1.048 ± 0.045	0.805 ± 0.053	0.099 ± 0.005	0.311 ± 0.015	1.571 ± 0.295	0.807 ± 0.176	0.614 ± 0.060
Monensin	0.686 ± 0.021	0.652 ± 0.031	0.691 ± 0.002	0.708 ± 0.011	1.255 ± 0.042	0.860 ± 0.084	0.769 ± 0.083
Mupirocin	1.048 ± 0.044	0.792 ± 0.029	0.700 ± 0.012	0.524 ± 0.016	2.399 ± 0.994	0.512 ± 0.215	0.545 ± 0.059
Nalidixic acid	0.937 ± 0.043	0.814 ± 0.039	0.160 ± 0.015	0.406 ± 0.031	0.602 ± 0.091	0.420 ± 0.044	0.399 ± 0.031
Nigericin	0.713 ± 0.001	0.691 ± 0.033	0.723 ± 0.014	0.655 ± 0.048	15.267 ± 23.800	0.861 ± 0.094	0.909 ± 0.079
Nisin	0.763 ± 0.004	0.773 ± 0.029	0.600 ± 0.028	0.741 ± 0.042	434.161 ± 155.326	2.503 ± 0.729	0.650 ± 0.043
Novobiocin	0.820 ± 0.025	0.868 ± 0.047	0.284 ± 0.021	0.537 ± 0.017	1.840 ± 0.705	1.047 ± 0.170	0.720 ± 0.102
Oxacillin	1.267 ± 0.122	0.959 ± 0.082	0.087 ± 0.004	0.234 ± 0.037	2.718 ± 1.384	0.798 ± 0.149	1.100 ± 0.225
PenicillinG	0.966 ± 0.031	0.863 ± 0.026	0.202 ± 0.028	0.345 ± 0.013	2.059 ± 1.459	1.142 ± 0.133	1.156 ± 0.010
PenicillinV	1.080 ± 0.069	0.862 ± 0.009	0.110 ± 0.010	0.295 ± 0.023	1.552 ± 0.668	0.667 ± 0.187	0.990 ± 0.088
Piperacillin	1.227 ± 0.058	0.952 ± 0.062	0.090 ± 0.002	0.281 ± 0.033	3.782 ± 2.553	1.131 ± 0.203	1.064 ± 0.181
Puromycin	0.850 ± 0.037	0.730 ± 0.011	0.383 ± 0.016	0.445 ± 0.036	1.598 ± 1.776	0.822 ± 0.086	0.733 ± 0.036
Rifampicin	0.934 ± 0.082	0.987 ± 0.037	0.549 ± 0.049	0.492 ± 0.015	1.055 ± 0.892	1.084 ± 0.288	1.136 ± 0.136
SpirohexenolideA	0.795 ± 0.043	0.722 ± 0.020	0.577 ± 0.044	0.632 ± 0.018	488.924 ± 41.312	2.595 ± 0.415	0.731 ± 0.037
Tetracycline	1.068 ± 0.064	0.865 ± 0.037	0.612 ± 0.019	0.650 ± 0.041	1.288 ± 1.707	0.304 ± 0.035	0.350 ± 0.012
Tiamulin	0.980 ± 0.060	0.844 ± 0.035	0.575 ± 0.022	0.537 ± 0.038	0.271 ± 0.026	0.569 ± 0.131	0.529 ± 0.061
Triclosan	0.762 ± 0.020	0.784 ± 0.010	0.685 ± 0.021	0.742 ± 0.037	5.883 ± 0.466	1.850 ± 0.100	0.964 ± 0.057
Trimethoprim	0.992 ± 0.012	0.961 ± 0.035	0.553 ± 0.011	0.534 ± 0.023	0.672 ± 0.090	0.664 ± 0.191	0.809 ± 0.090
Vancomycin	1.053 ± 0.041	1.073 ± 0.077	0.593 ± 0.019	0.596 ± 0.042	2.127 ± 0.838	1.201 ± 0.219	1.128 ± 0.246
Untreated	0.790 ± 0.016	0.825 ± 0.013	0.495 ± 0.023	0.649 ± 0.005	1.000 ± 0.000	1.000 ± 0.000	0.941 ± 0.044

Table S4. Double-blind test of known antibiotics
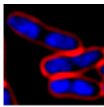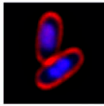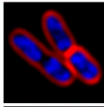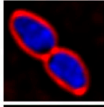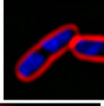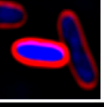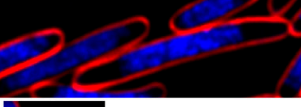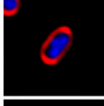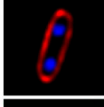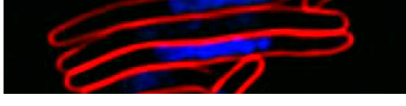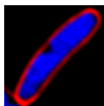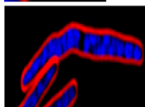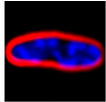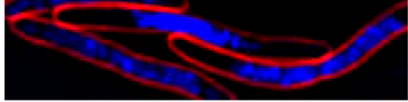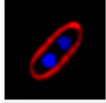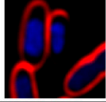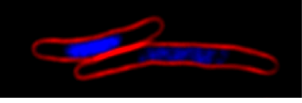
Test ID	Input molecules	Observed morphologies	BCP readout
		Set A	
A1	Water		Untreated
A2	Nisin (M4)		Membrane active (M4)
A3	DMSO		Untreated
A4	Mecillinam (C2)		Cell wall synthesis (C2)
A5	Water		Untreated
A6	DNP (M3)		Membrane active (M3)
A7	Daunorubicin (D3)		DNA replication (D3)
A8	Monensin (M1)		Membrane active (M1)
A9	Calcimycin (M2)		Membrane active (M2)
A10	Nalidixic acid (D1)		DNA replication (D1)
		Set B	
B1	Actinomycin D (R2)		RNA transcription(R2)
B2	Ampicillin (C3)		Cell wall synthesis (C3)

Table S4. Cont.

Test ID	Input molecules	Observed morphologies	BCP readout
B3	Ampicillin (C3)		Cell wall synthesis (C3)
B4	Mitomycin C (D4)		DNA replication (D4)
B5	Puromycin (P3)		Protein synthesis (P3)
B6	Kanamycin (P2)		Protein synthesis (P2)
B7	Chloramphenicol (P1)		Protein synthesis (P1)
B8	Chloramphenicol (P1)		Protein synthesis (P1)
B9	Novobiocin (D2)		DNA replication (D2)
B10	D-cycloserine (C1)		Cell wall synthesis (C1)

Set C

Test ID	Input molecules	Observed morphologies	BCP readout
C1	Trimethoprim (N1)		Nucleotide synthesis (N1)
C2	Triclosan (L1)		Lipid biosynthesis (L1)
C3	Rifampicin (R1)		RNA transcription (R1)
C4	Water		Untreated
C5	Daunorubicin (D3)		DNA replication (D3)

Table S4. Cont.

Test ID	Input molecules	Observed morphologies	BCP readout
C6	D-cycloserine (C1)		Cell wall synthesis (C1)
C7	Mitomycin C (D4)		DNA replication (D4)
C8	Calcimycin (M2)		Membrane active (M2)
C9	Kanamycin (P2)		Protein synthesis (P2)
C10	Nalidixic acid (D1)		DNA replication (D1)

Acknowledgements

Chapter 3

Treatment of High-Level Gentamicin-Resistant *Enterococcus faecalis* Endocarditis with Daptomycin plus Ceftaroline

Treatment of High-Level Gentamicin-Resistant *Enterococcus faecalis* Endocarditis with Daptomycin plus Ceftaroline

George Sakoulas,[a] Poochit Nonejuie,[b] Victor Nizet,[a] Joseph Pogliano,[b] Nancy Crum-Cianflone,[c] Fadi Haddad[d]

Department of Pediatric Pharmacology and Drug Discovery[a] and Department of Biology,[b] University of California San Diego School of Medicine, La Jolla, California, USA; Division of Infectious Diseases, Naval Medical Center San Diego, San Diego, California, USA[c]; Sharp Grossmont Hospital, La Mesa, California, USA[d]

A recurrent case of left-sided endocarditis caused by high-level aminoglycoside-resistant *Enterococcus faecalis* was successfully treated with ceftaroline and daptomycin. This combination demonstrated excellent synergy *in vitro*. Mechanistically, ceftaroline enhanced binding of daptomycin to the cell membrane and sensitized *E. faecalis* to killing by human cathelicidin LL-37, a cationic innate host defense peptide. Daptomycin plus ceftaroline may be considered in salvage therapy in *E. faecalis* endovascular infections and requires further study.

A 63-year-old man with a past medical history significant for hypertension presented with fevers for 1 month. The patient received levofloxacin and doxycycline for presumed prostatitis. Physical examination revealed a grade 2 systolic murmur and grade 1 diastolic murmur. Blood cultures were positive for *Enterococcus faecalis*. The patient was admitted to the hospital and started on ampicillin-sulbactam and gentamicin. The white blood cell count (WBC) was 10,100 cells/mm^3, hemoglobin was 14 g/dl, and the chest X-ray was normal. Repeat blood cultures showed ampicillin-susceptible *E. faecalis* with high-level gentamicin resistance (HLGR). A transesophageal echocardiogram revealed a 5-mm vegetation on the noncoronary cusp of the aortic valve. On the third hospital day, gentamicin was discontinued and ceftriaxone at 1 g intravenously (i.v.) every 12 h (q12h) was started, along with ampicillin at 2 g i.v. q4h. Blood cultures became negative after 96 h of treatment. The patient remained asymptomatic thereafter, and blood cultures remained negative during and after 6 weeks of therapy.

Two weeks after completion of therapy, the patient presented to the emergency department with a temperature of 39.2°C. Examination revealed a grade 3 systolic heart murmur and grade 1 diastolic murmur. A transesophageal echocardiogram showed severe aortic regurgitation and an increase in the size of the vegetation to 10 mm. *E. faecalis* was recovered from blood cultures without any change from the previous susceptibility profile. Ampicillin at 12 g, continuous infusion over 24 h, and ceftriaxone at 1 g i.v. q12h were started initially. On hospital day 2, ceftriaxone was switched to daptomycin at 8 mg/kg i.v. daily, based on prior data showing synergy between these antibiotics against enterococci and successful clinical use (1, 2). The patient became afebrile after 24 h of therapy. Blood cultures that were repeated after 48 and 96 h of daptomycin plus ampicillin therapy turned positive for the same isolate after 4 and 3 days, respectively.

Based on unpublished *in vitro* observations in our laboratory, which have demonstrated synergy between daptomycin and ceftaroline against several clinical bloodstream isolates of *E. faecalis* and *Enterococcus faecium*, and a published report of synergy between daptomycin and ceftaroline against MRSA (3), ampicillin was discontinued and ceftaroline at 600 mg i.v. every 8 h was added to the daptomycin treatment, and there was successful clearance of the bacteremia. The patient was discharged on a regimen of daptomycin at 8 mg/kg i.v. daily and ceftaroline at 600 mg

TABLE 1 Reduction of daptomycin MIC in Mueller-Hinton broth supplemented to 50 mg/liter Ca^{2+} and containing incrementally higher concentrations of ceftaroline or ampicillin[a]

AMP or CPT (mg/liter)	DAP MIC (mg/liter) in presence of:	
	CPT	AMP
0	2	2
0.5	0.5	2
1.0	0.5	2
2.0	0.5	2
4.0	0.5	2
8.0	0.5	0.5
16.0	0.5	
32.0	0.25	

[a] DAP, daptomycin; CPT, ceftaroline; AMP, ampicillin.

i.v. every 8 h, and he was readmitted after 2 weeks for elective aortic valve replacement. Preoperative blood cultures were negative. Aortic valve tissue culture grew *E. faecalis* with high aminoglycoside resistance only from broth. Daptomycin plus ceftaroline therapy was continued for 4 weeks after surgery, and blood cultures obtained 1 week after completion of therapy were negative. The patient was deemed cured 6 weeks after completion of therapy.

Based on this excellent clinical and microbiological response, we performed checkerboard assays and determined kill curves at clinically relevant antibiotic concentrations (4–7) in Mueller-Hinton broth supplemented to 50 mg/liter Ca^{2+} to assess the synergy of daptomycin and ceftaroline against the relapse *E. faecalis* isolate from this patient. Daptomycin, ampicillin, ceftaroline, and ceftriaxone MICs were 2, 16, >32, and >32 mg/liter, respectively. The organism was qualitatively negative for beta-lactamase production by nitrocefin disk test. The checkerboard assay showed a
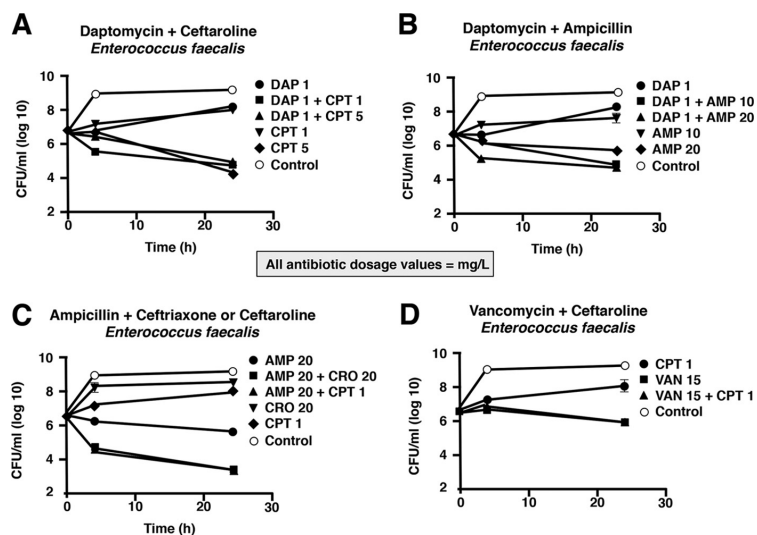
FIG 1 (A and B) Time-kill assays (24 h) in Mueller-Hinton broth supplemented to 50 mg/liter Ca^{2+}, evaluating the activity of daptomycin (DAP) alone or with ceftaroline (CPT) (A) or ampicillin (AMP) (B) against *E. faecalis*. (C and D) Results of similar experiments, showing an effect of AMP with either ceftriaxone (CRO) or CPT (C) and vancomycin (VAN) with CPT (D) against *E. faecalis*. Data are means of three experiments, with duplicate plating in each experiment. The limit of detection was 3.0 $\log_{10}$ CFU/ml.

4-fold reduction in the daptomycin MIC with ceftaroline at 0.5 to 16 mg/liter and ampicillin at 8 mg/liter (Table 1). No differences in the MIC were observed in checkerboard studies between ampicillin and ceftaroline or ampicillin and ceftriaxone.

Kill curve assays with daptomycin at 1 mg/liter plus ceftaroline at 1 or 5 mg/liter confirmed synergy, as had been observed in prior data with other clinical isolates, which prompted selection of this combination for this patient (Fig. 1A). In order to provide a context for this degree of killing with this combination compared to other regimens clinicians consider, we performed similar assays to determine relative synergy of daptomycin and ampicillin (Fig. 1B), ceftriaxone or ceftaroline with ampicillin (Fig. 1C), and vancomycin and
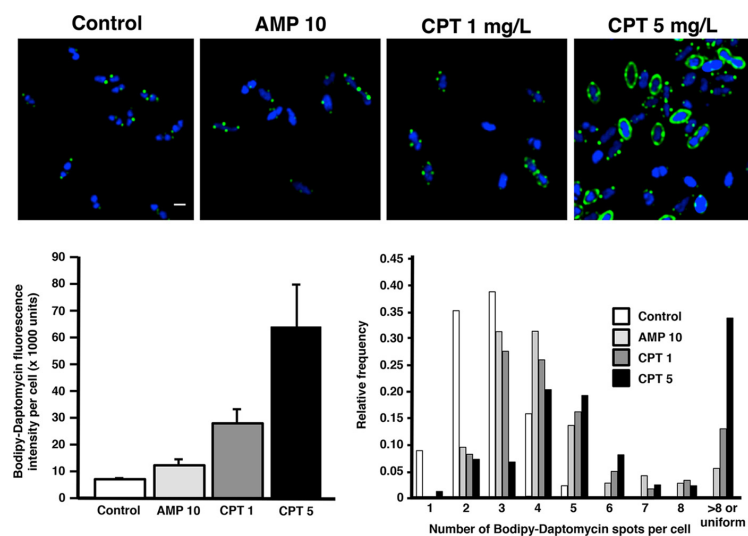
FIG 2 *E. faecalis* labeled with bodipy-daptomycin (16 mg/liter; 4× MIC; baseline MIC, 4 mg/liter) in LB broth for 15 min after a 45-min treatment with either ampicillin (AMP) at 10 mg/liter or ceftaroline (CPT) at 1 mg/liter or 5 mg/liter, compared to control untreated cells. The normalized total intensity of signal per cell (bottom left) and number of binding spots per cell (bottom right) are shown. Microscopy method details have been described elsewhere (2, 8).
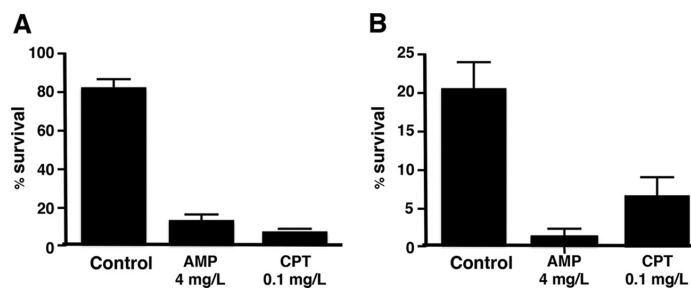
FIG 3 Percent survival of *E. faecalis* after 2 h of exposure to 64 μM (A) or 128 μM (B) cathelicidin LL37 in untreated controls compared to cells grown overnight in either ampicillin (AMP) at 4 mg/liter or ceftaroline (CPT) at 0.1 mg/liter. Method details have been described previously (2).

ceftaroline (Fig. 1D). These experiments showed the following: (i) bacteriostatic activity of vancomycin at 15 mg/liter and ampicillin at 20 mg/liter alone against this isolate, as anticipated; (ii) comparable synergy with ampicillin at 20 mg/liter and either ceftriaxone at 20 mg/liter or ceftaroline at 1 mg/liter; (iii) a lack of synergy for ceftaroline with vancomycin.

In agreement with our previous studies, which showed that ampicillin enhanced the binding of daptomycin to ampicillin-resistant *E. faecium* (2), using previously published methods (2, 8), growth of the present *E. faecalis* isolate in broth media containing either ampicillin at 10 mg/liter or ceftaroline at 1 or 5 mg/liter resulted in significantly increased daptomycin binding to the bacterial membrane compared to control bacteria grown in antibiotic-free LB broth (Fig. 2).

Also similar to what we had observed with *E. faecium* (2), growth of this *E. faecalis* strain in ampicillin or ceftaroline resulted in increased susceptibility to human cathelicidin LL-37 killing at 64 and 128 μM (Fig. 3). Note that this strain was much more susceptible to ampicillin and ceftaroline than the previously described *E. faecium*, and therefore much lower concentrations of drugs were used to allow growth under experimental conditions. Interestingly, this *E. faecalis* strain was much more resistant to cathelicidin LL-37 (MIC, 64 μM) than we observed for *E. faecium* (MIC, 8 μM), with both isolates from patients with endocarditis. This pattern may represent another interesting reflection of the β-lactam–antimicrobial peptide susceptibility seesaw effect across the enterococcal species, and it is a potential area for further study regarding the differences in endovascular pathogenicity between *E. faecium* and *E. faecalis*.

Assessment of surface charge with or without ceftaroline or ampicillin in cytochrome *c* binding assays showed no significant differences in this property (data not shown), which is perhaps an indication of the lack of significant surface charge effects when low concentrations of β-lactams are used.

This is the first case demonstrating a successful clinical outcome with use of daptomycin plus ceftaroline in a case of *E. faecalis* endocarditis, with supporting *in vitro* data demonstrating synergy between these drugs against *E. faecalis* and enhancement of cathelicidin peptide activity and daptomycin binding by ceftaroline. We point out that the ceftriaxone dose utilized initially was lower than that recommended in the literature and may have led to treatment failure (9). While limited to a single case, these results point to several alternative avenues of therapy that need to be studied clinically for the

treatment of serious enterococcal endovascular infections. Treatment of these infections can be hampered by the lack of a validated bactericidal monotherapy, as shown in this case, and intrinsic and acquired antimicrobial resistance in *E. faecium* superimposed on many host comorbidities. In treating *E. faecalis* endocarditis, use of ampicillin and gentamicin appears straightforward in treatment guidelines (10). However, in the practical clinical world, when not limited by HLGR as in this case, the otovestibular toxicity, nephrotoxicity, and therapeutic drug monitoring that accompanies prolonged aminoglycoside administration is something that patients and clinicians should not have to contend with in the 21st century. Alternative therapies need to be defined for these infections, as there appear to be safer and more convenient alternatives available that await validation in larger clinical studies. This patient demonstrated bacteremia clearance and had a successful clinical outcome with daptomycin plus ceftaroline along with appropriately timed valve replacement surgery. The fact that the valvular tissue was still culture positive despite 2 weeks of therapy underscores the importance of surgical intervention in these cases, and it is unknown if medical therapy alone would have sufficed in this case, particularly with potential relapse after a regimen of ampicillin plus ceftriaxone that provided comparable killing *in vitro*.

REFERENCES

1. **Rand KH, Houck HJ.** 2004. Daptomycin synergy with rifampin and ampicillin against vancomycin-resistant enterococci. J. Antimicrob. Chemother. **53:**530–532.
2. **Sakoulas G, Bayer AS, Pogliano J, Tsuji BT, Yang SJ, Mishra NN, Nizet V, Yeaman MR, Moise PA.** 2012. Ampicillin enhances daptomycin- and cationic host defense peptide-mediate killing of ampicillin and vancomycin-resistant *Enterococcus faecium.* Antimicrob. Agents Chemother. **56:** 838–844.

3. **Rose WE, Schultz LT, Andes D, Striker R, Berti AD, Hutson PR, Shukla SK.** 2012. Addition of ceftaroline to daptomycin after emergence of daptomycin-nonsusceptible Staphylococcus aureus during therapy improves antibacterial activity. Antimicrob. Agents Chemother. **56:**5296–5302.

4. **Forest Laboratories, Inc.** 2012. Ceftaroline fosamil package insert. http://www.accessdata.fda.gov/drugsatfda_docs/label/2010/200327s000lbl.pdf. Accessed 10 October 2012.

5. **Dvorchik BH, Brazier D, DeBruin MF, Arbeit RD.** 2003. Daptomycin pharmacokinetics and safety following administration of escalating doses once daily to healthy subjects. Antimicrob. Agents Chemother. **47:**1318–1323.

6. **Foulds G.** Pharmacokinetics of sulbactam/ampicillin in humans: a review. Rev. Infect. Dis. **8**(Suppl 5):S503–S511.

7. **Patel IH, Chen S, Parsonnet Hackman MR, Brooks MA, Konikoff J, Kaplan SA.** 1981. Pharmacokinetics of ceftriaxone in humans. Antimicrob. Agents Chemother. **20:**634–641.

8. **Pogliano J, Pogliano N, Silverman J.** 2012. Daptomycin mediated reorganization of membrane architecture causes mislocalization of essential cell division proteins. J. Bacteriol. **194:**4494–4504.

9. **Gavalda J, Len O, Miro JM, Munoz P, Montejo M, Alarcon A, de la Torre-Cisneros J, Pena C, Martinez-Lacasa X, Sarria C, Bou G, Aguado JM, Navas E, Romeu J, Marco F, Torres C, Tornos P, Planes A, Falco V, Almirante B, Pahissa A.** 2007. Brief communication: treatment of Enterococcus faecalis endocarditis with ampicillin plus ceftriaxone. Ann. Intern. Med. **146:**574–579.

10. **Baddour LM, Wilson WR, Bayer AS, Fowler Jr, Bolger VGAF, Levison ME, Ferrieri P, Gerber MA, Tani LY, Gewitz MH, Tong DC, Steckelberg JM, Baltimore RS, Shulman ST, Burns JC, Falace DA, Newbuger JW, Pallasch TJ, Takahashi M, Taubert KA.** 2005. Infective endocarditis: diagnosis, antimicrobial therapy, and management of complications: a statement for healthcare professionals from the Committee on Rheumatic Fever, Endocarditis, and Kawasaki Disease, Councils on Cardiovascular Disease in the Young, and the Councils on Clinical Cardiology, Stroke, and Cardiovascular Surgery and Anesthesia, American Heart Association. Endorsed by the Infectious Diseases Society of America. Circulation **111:** e394–e434.

Acknowledgements

Chapter 4

Roles of polymyxin B in bacterial membrane fluidity

Abstract

The spread of multidrug resistant (MDR) bacteria in hospitals is one of the major threats of a patients' life. While much research effort was put into finding cures for antibiotic resistant MDR Gram-positive bacteria, Gram-negative bacteria infections are more problematic to treat because the bacterial outer membrane provides an extra barrier against antibiotic treatments. Polymyxin B, a lipopeptide antibiotic, is very potent against Gram-negative pathogens and serves as the last line of defense against pathogens when other antibiotics fail. However, its mechanism of action is still debatable. Here I used bacterial cytological profiling (BCP) to show that polymyxin B-treated cells have a similar cell morphology to CHIR-090-treated cells suggesting that mechanism of action of polymyxin B against *E. coli* is similar to the *lpxC* inhibitor CHIR-090. Fluorescence recovery after photobleaching (FRAP) data of FM4-64 dye showed that the outer membrane polymyxin B- and CHIR-090-treated cells are dynamic. I hypothesize that polymyxin B might play role in lipopolysaccharide production leading to membrane synthesis alteration.

Introduction

The growing numbers of resistant Gram-negative bacteria together with the lack of new antibiotics are a major concern in the health science community. The widely spread multidrug-resistant (MDR) bacteria *Enterococcus* spp., *Staphylococcus aureus*, *Klebsiella* spp., *Acinetobacter baumannii*, *Pseudomonas aeruginosa* and *Enterobacter* spp., known as the "ESKAPE" pathogens, are among the most troublesome (1). Also, some MDR Gram-negative pathogens are now resistant to all antibiotics available in the clinic (2). Even though the antibiotic discovery situation in the last decade has shown a positive look due to the introduction of five new classes of antibiotics; oxazolidinone, lipopeptide, pleuromutilin, tiacumicin, and diarylquinoline, they are all narrowly active against only Gram-positive bacteria (2). Thus, new Gram-negative antibiotics are urgently in needed.

Discovery of Gram-negative antibiotics is far more difficult than those for Gram-positives due to the Gram-negative outer membrane (OM) which provides an extra barrier to antibiotic penetration (3, 4). Unlike the cytoplasmic membrane, the OM of Gram-negative bacteria is an asymmetric bilayer of phospholipid and lipopolysaccharides (LPS) (Figure 1A). A LPS molecule consists of three main components: 1) lipid A, a non-phospholipid core, 2) oligosaccharide core, and 3) an extremely variable O-antigen. The six saturated fatty acids chains of the lipid A core make LPS highly hydrophobic, which is the key of the OM strength against antibiotic (3).

When physicians encounter MDR Gram-negative pathogens and all other drugs fail for treatment, they turn to polymyxin B as the last line of defense (5). Developed in

the 1960s, polymyxin B was widely used against Gram-negative pathogens until the 1970s due to its neurotoxicity and nephrotoxicity, and doctor preference toward less toxic aminoglycosides (5–7). Albeit its toxicity, polymyxin B and colistin (polymyxin E) are very effective against MDR Gram-negative pathogens and the occurrence of resistance is relatively rare. Although polymyxin B has re-emerged as the last resort of antibiotic and is widely used today, its mechanism of action is still unclear (5). The most widely accepted model is the "self-promoted mechanism" achieved by inserting itself to the LPS layer and displacing divalent cations that maintain the LPS organization leading to instability of the OM and eventually OM disruption. Once the OM has collapsed, the polymyxin B gains access to the cytoplasmic membrane and disrupts the membrane leading to cell death (8, 9). However, other MOA for polymyxin B have been proposed (10). Various antimicrobial peptides not only effect membrane integrity, but also has intracellular targets (11). Thus, it is possible that polymyxin B also targets a specific cellular pathway.

In accordance to a possibility that polymyxin B possesses an alternative MOA in some bacteria, resistances that confer polymyxin B resistance show multiple hits of its possible targets summarized in previous review (5), including mutations in *lpxC*. The complete loss of LPS by *lpxABC* gene deletion, genes involved in early steps of lipid A biosynthesis, results in colistin resistance in *Acinetobacter baumannii* (12, 13). LpxC is a critical enzyme in the biosynthesis of lipid A (14, 15); thus, many efforts have been invested to find LpxC inhibitors (16–18). Among many LpxC inhibitors, CHIR-090 showed the most promising future in drug development (15). It was first introduced in 2004 and characterized in 2005 (19). Besides the well studied mutations in two

component signaling system pmrA/pmrB or its regulator phoP/phoQ (5, 7), the fact that *lpxC* mutants showed up in colistin resistance is very interesting and urges us to search for an alternative target of polymyxin B using the new method of Bacterial Cytological Profiling (BCP).

BCP is a fluorescence microscopy based method for studying the MOA of antibiotics (12). This method shows high resolution in dissecting the MOA of antibiotics. BCP can efficiently separate antibiotics that are known to inhibit the same cellular pathways into two or more subgroups based on their specific targets. In particular, BCP can separate membrane active compounds, previously grouped as nuisance compounds by other methods, into many different subgroups that correlate with their specific functions or ion selectivity. We hypothesize that, at certain concentrations, polymyxin B, which shows strong killing activity against Gram-negative bacteria and is grouped with other membrane disrupting molecules, will show a specific target. Here we use the BCP technique to show that polymyxin B and CHIR-090 have a similar effect on bacterial cell morphology, suggesting a possible role of polymyxin B in LPS production.

Results

FM4-64 stains the outer membrane of *E. coli*

A lipophilic styryl fluorescent dye FM4-64, described as a cytoplasmic membrane stain by the manufacturer, has been used extensively in bacterial membrane studies (20–22). While FM4-64 usage in Gram-positive bacteria is straightforward since they have only one cytoplasmic membrane (CM), applications of FM4-64 in Gram-negative bacteria are more complicated. The LPS layer of the outer membrane (OM) of Gram-negative bacteria is more hydrophobic than the CM and it serves as the first barrier against extracellular molecules in environment; thus, the OM is potentially a better target for FM4-64 than the CM (Figure 1A). A previous study in *Agrobacterium tumefaciens* (23) showed that FM4-64 binds to the OM of the bacteria. Here, we observed similar results in *Escherichia coli*. We used MalF-GFP, a cytoplasmic membrane component of the maltose transport system, as a CM indicator and showed that MalF-GFP binds the CM while FM4-64 stains the OM (Figure 1B).   To further evaluate staining patterns in the OM and CM, we performed fluorescence recovery after photobleaching (FRAP) experiments (Figure 1C). The FRAP data indicated that FM4-64 showed no recovery after photobleaching. This observation is in agreement with the nature of the OM which is far less dynamic than the CM due to its high content of LPS (3, 24). In contrast, the MalF-GFP signal was recovered after photobleaching due to the highly dynamic CM. Altogether, these data suggest that FM4-64 binds to the OM, not the CM of *E. coli*.
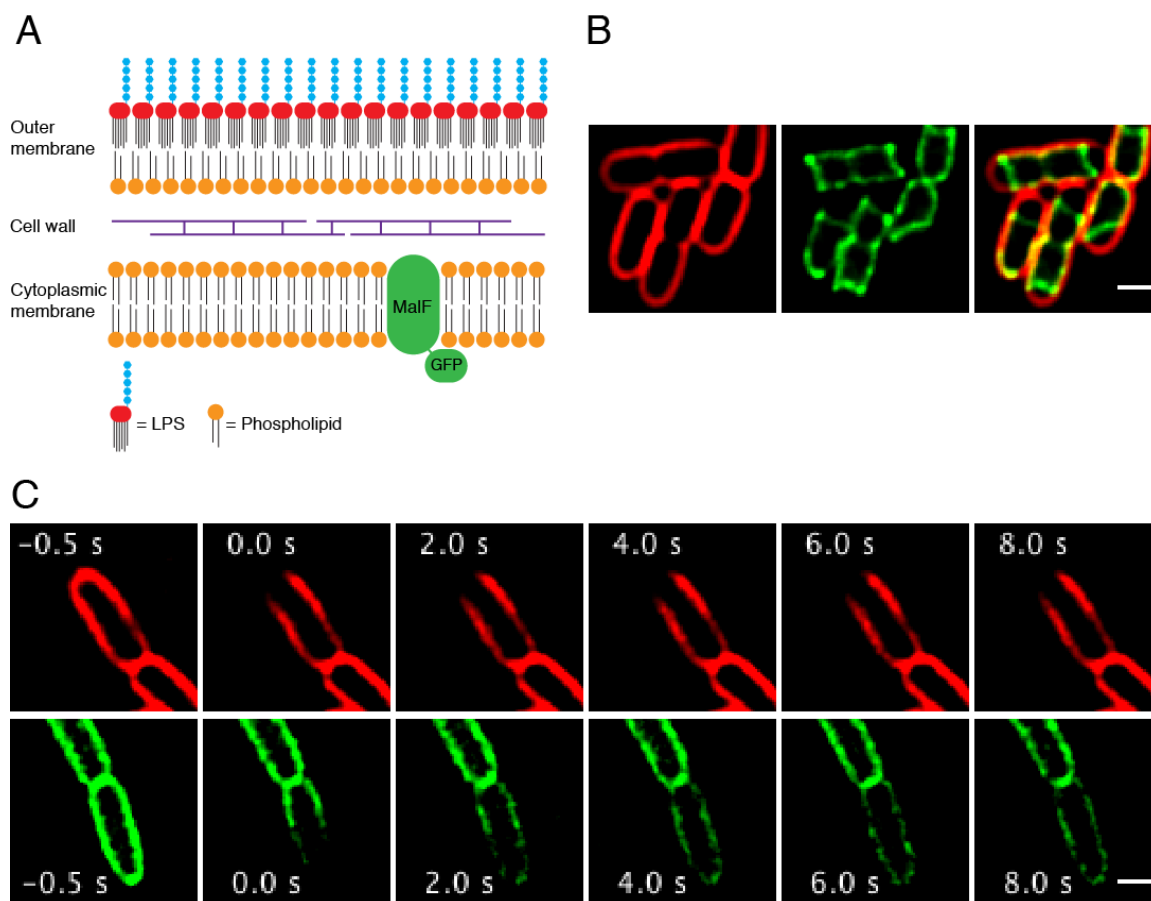
Figure 4.1 FM4-64 binds to outer membrane of *E. coli*. (A) A cartoon demonstrates double membrane of Gram-negative bacteria. An outer membrane consists of asymmetric bilayer of LPS and phospholipids providing rigid membrane structure. (B) 0.4M sucrose plasmolysed *E. coli* cells showing separated OM (indicated by FM4-64, red) and CM (indicated by MalF-GFP, green). (C) FRAP data of FM4-64 (upper panel, red) showed no recovery after photobleaching. MalF-GFP (lower panel, green) showed recovery after 2 s of bleaching event. Scale bars represent 1 micron.

The lptD mutant outer membrane is dynamic

To test if the LPS content of the OM plays a role in membrane fluidity, we used the *E. coli lptD* mutant (25–27), which has a defect in LPS transportation to an outer leaflet of OM thus containing significantly less LPS in the OM (Figure 2A). Even though the OM of the *lptD* mutant showed higher permeability to many hydrophobic molecules

(25), here we confirmed that FM4-64 still binds to the OM and no FM4-64 signal was detected in the CM (Figure 2B). FRAP analysis data indicated that the OM of the *lptD* mutant is highly dynamic since the FM4-64 signal recovered after photobleaching (Figure 2C) similar to MalF-GFP signal (Figure 1C). This FM4-64 recovery was also observed in the *Bacillus subtilis* membrane where LPS is absent (Figure 2E). These data indicate that the absence of LPS molecules on the OM increases the OM fluidity and therefore results in FM4-64 recovery after photobleaching.
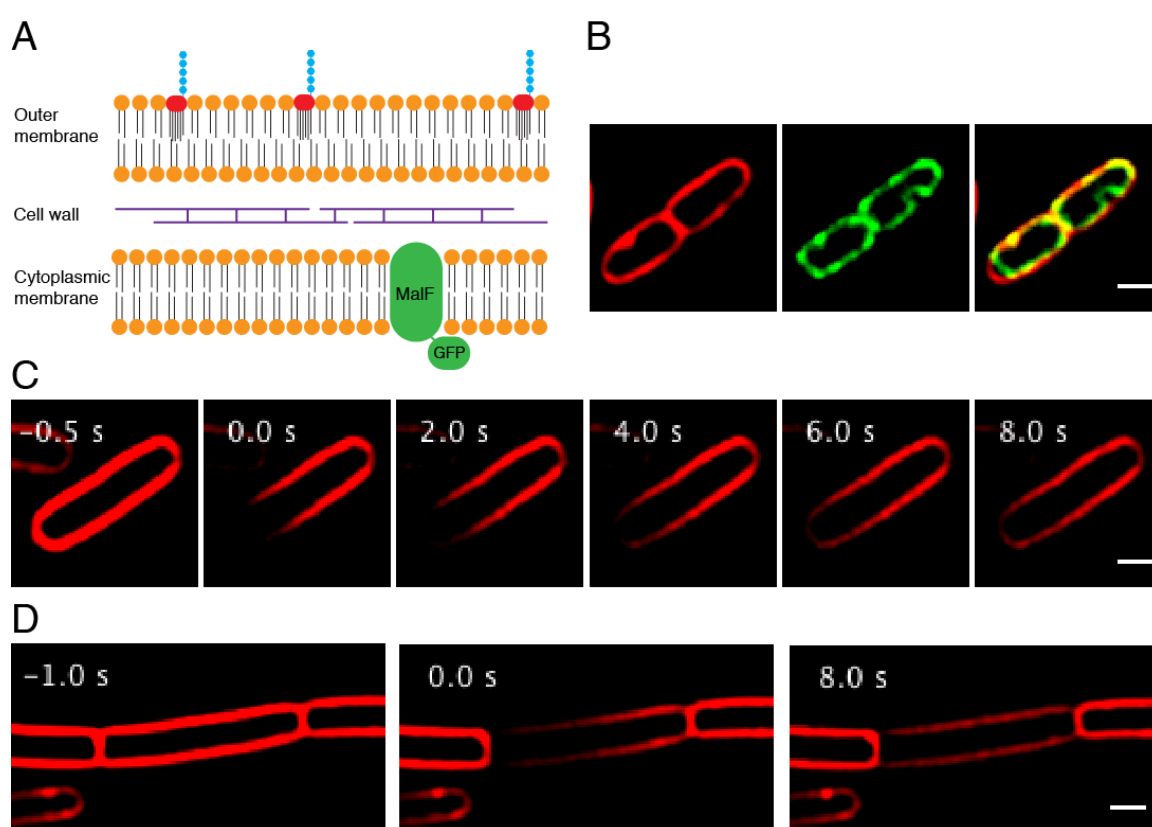
Figure 4.2 Outer membrane of *lptD E. coli* is dynamic similar to that of *B. subtilis* cytoplasmic membrane. (A) A cartoon demonstrates *lptD E. coli* membrane consisting of less LPS on the OM. (B) 0.4M sucrose plasmolysed *lptD E. coli* cells showing separated OM (indicated by FM4-64, red) and CM (indicated by MalF-GFP, green). (C) and (D) FRAP data of FM4-64 (red) showed recovery after photobleaching in *lptD E. coli* and *B. subtilis*, respectively. Scale bar represent 1 micron.

Cytological profiles of polymyxin B-treated bacteria are similar to those treated with CHIR-090

We used BCP to determine if polymyxin B shows a similar morphological profile to CHIR-090. Since polymyxin B at 5X MIC concentrations led to cell lysis, we performed polymyxin B and CHIR-090 treatment at 1-2X MIC in order to analyze cell morphological changes. BCP revealed that polymyxin B and CHIR-090 treated cells showed similar morphological changes unlike any other antibiotics described in previous studies (21, 22). Both antibiotics cause bacterial cells to grow in long chains where multiple cells were attached to each other forming a chain-liked cell structure (Figure 3). However, polymyxin B at higher concentration caused cell lysis as indicated by the exploded cells and SYTOX-Green dye stain (Figure 3, bottom left panel). This BCP data suggested that polymyxin B, at lower concentration, has a MOA similar to CHIR-090, while at higher concentrations, polymyxin B showed its conventional and well studied MOA (5, 8, 9).
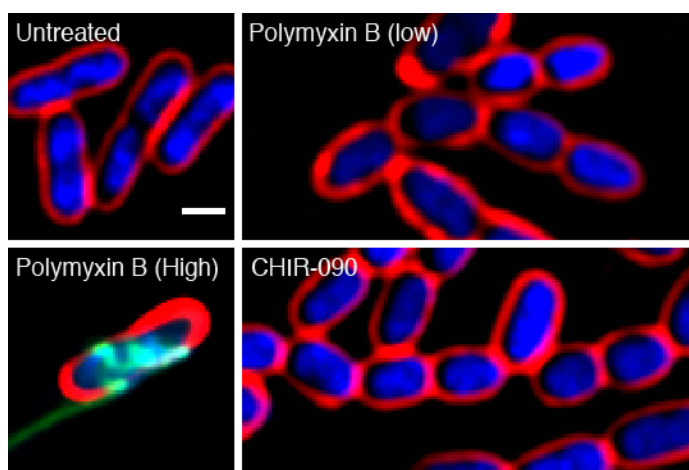
Figure 4.3 Bacterial cytological profiles of *E. coli* treated with polymyxin B are similar to those treated with CHIR-090. Cells were stained with FM4-64 (red), DAPI (blue), and SYTOX green (green). SYTOX green stains only cells with permeabilized membranes. A scale bar represents 1 micron.

Polymyxin B treatment leads to higher OM fluidity

CHIR-090 is a small molecule that inhibits an early step of lipid A production, a critical component of LPS and the OM (24, 28, 29). We assumed that the cell morphology change we observed in CHIR-090 treated cells is a result of a complete loss of LPS prior to cell death. Since polymyxin B at lower concentrations showed similar morphological changes to CHIR-090, we tested if LPS production in polymyxin B-treated cells is inhibited. We first performed FRAP analysis of the OM and the CM of CHIR-090-treated cells. The result showed that CHIR-090-treated cells, when photobleaching occurred in the middle cell of the chain, showed FM4-64 recovery while MalF-GFP signal did not (Figure 4A). This paradoxical data indicated that the CM was completely separated from neighboring cells; thus, no GFP signal recovery was observed in the CM. Under CHIR-090 treatment, the OM, previously showed no recovery (Figure 1D), revealed FM4-64 recovery due to the LPS synthesis inhibition and the increase in membrane fluidity (Figure 4B). Polymyxin B showed similar FRAP analysis to CHIR-090 (Figure 4C). Polymyxin B-treated cells showed no recovery in MalF-GFP signal indicating that the CM was complete and separated from other cells. However, some of the polymyxin B-treated cells did not show FM4-64 recovery (Figure 4C, bottom panel). We hypothesized that, unlike CHIR-090, polymyxin B partially inhibits LPS production thus LPS composition on the OM of some treated cells is enough to maintain its rigidity and static property (Figure 4D). An optimal concentration of polymyxin B is needed in order to see the phenotype associated with LPS inhibition; at higher concentrations cell lyse due to its membrane disruption activity. The importance of having the proper ratio of cells to antibiotics has been seen for other cell envelope targeted molecules such as

vancomycin and daptomycin in order to see different phenotypes microscopically. At appropriate concentrations, vancomycin shows peptidoglycan synthesis inhibition phenotype rather than just cell lysis (22). Similarly, daptomycin at lower concentrations revealed its interaction with the cell division protein DivIVA (30).

Future experiments

Analysis of LPS production upon polymyxin B treatment

To confirm that LPS production was inhibited during polymyxin B treatment, we will examine the presence of LPS in polymyxin B- and CHIR-090-treated cells. LPS from bacteria treated with under conditions will be extracted using Tri-Reagent method (31). Bacterial cells from each treatment will be collected and resuspended in 200 μl of Tri-Reagent at room temperature for 10 min. After incubation, 20 μl of chloroform will be added into the cell suspensions, vortexed vigorously, and incubated for 10 minute at room temperature. Phase separation will be done by 12,000 x g centrifugation for 10 minute. The aqueous phase will be transferred to a new tube. Repeat the phase separation steps by adding 100 μl of water into organic phase, vortex, and incubate 10 minute for the total of four times. The pooled aqueous phase will be dried using speed vac and resuspended in 100 μl of water to get crude LPS extract. LPS will be separated using SDS-PAGE and visualized by Pro-Q® Emerald 300 Lipopolysaccharide Gel Stain Kit or a modified silver staining protocol (32).
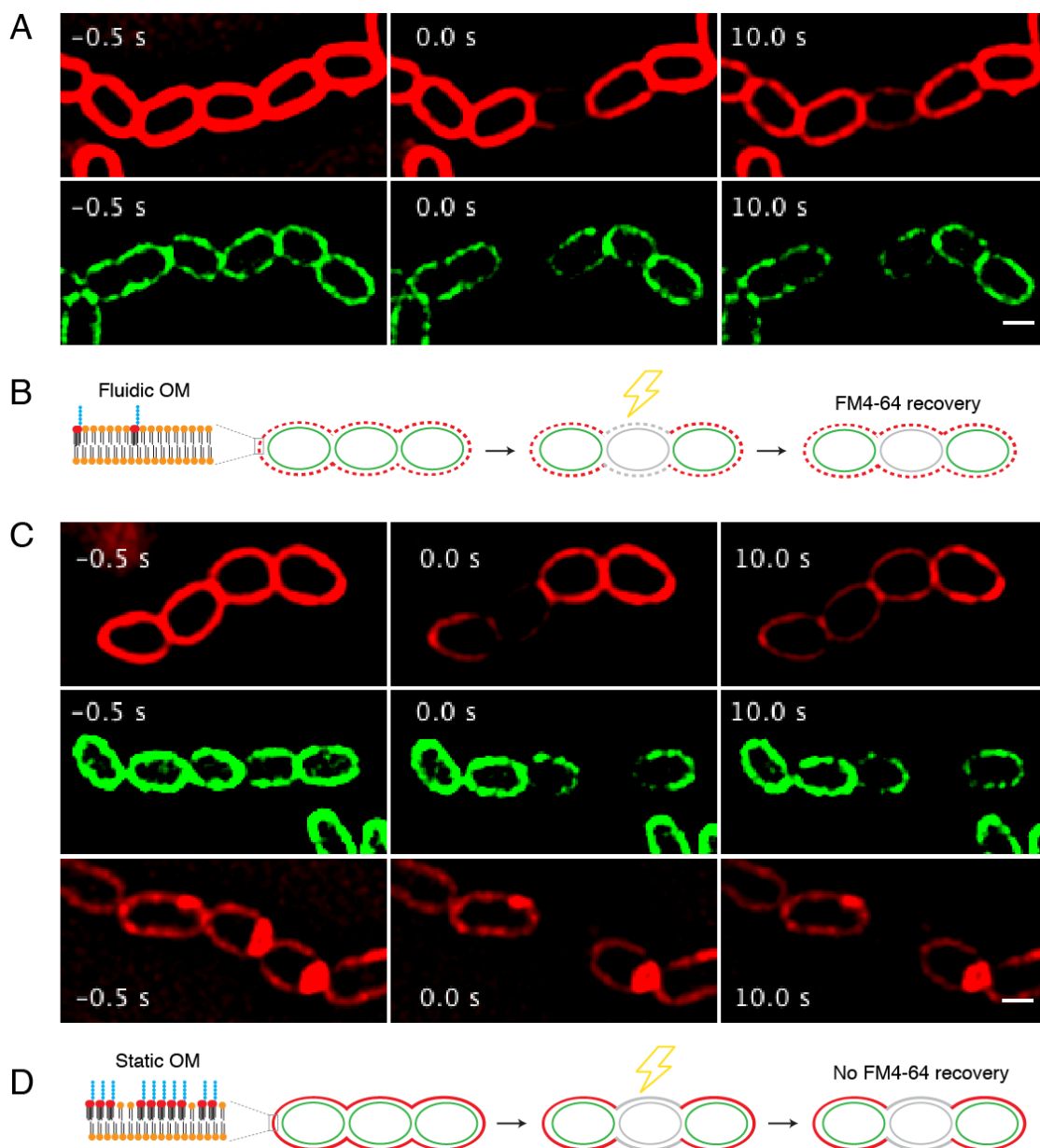
Figure 4.4 Polymyxin B and CHIR-090 effect outer membrane fluidity. (A) FRAP data of CHIR-090-treated cells. FM4-64 (upper panel, red) showed recovery after photobleaching while MalF-GFP (lower panel, green) did not. (B) A model of fluidic OM (containing no or little LPS content) with a complete CM separation during FRAP. (C) FRAP data of polymyxin B-treated cells. FM4-64 (upper panel, red) showed recovery after photobleaching while MalF-GFP (middle panel, green) did not. Some of polymyxin B-treated cells showed no recovery of FM4-64 signal as well (bottom panel). (D) A model of static OM (containing high LPS content) with a completed CM separation during FRAP.

Discussions

The outer membrane of Gram-negative bacteria is a crucial component that provides them higher antibiotic resistance (3, 24). Understanding the OM is an important step to gain insight into Gram-negative pathogenesis. Here we show that FM4-64 can be used as a tool for bacterial membrane study, not only used as a vital membrane stain. In *E. coli*, FM4-64 binds to the OM and cannot penetrate to the cytoplasmic membrane regardless of the OM hydrophobicity. This phenomenon was also observed in *A. tumefaciens* (23). Without the OM, FM4-64 binds to the cytoplasmic membrane of Gram-positive bacteria, the first hydrophobic barrier that it encounters. However, we found that FM4-64 can stain both the OM and the CM at the same time in some conditions. When FM4-64 was added prior to plasmolysis or cells were grown with FM4-64, low signal of FM4-64 can be found in the CM as well. Using FM4-64 for OM study, we demonstrated that LPS is a critical component that strongly affects OM membrane dynamics. In *lptD E. coli* with reduced LPS content, there was higher membrane fluidity similar to the CM. Thus, we hypothesized that inhibiting LPS production will result in a more dynamic OM. CHIR-090 is a small molecule that inhibits LPS production at the early step. We demonstrated that the OM of *E. coli* treated with CHIR-090 showed higher fluidity from FRAP analysis.

Bacterial cytological profiles of polymyxin B-treated cells showed that polymyxin B triggered similar morphological responses to CHIR-090-treated cells, which led us to hypothesize that polymyxin B possibly targets LPS production pathway. Our results are consistent with the fact that the complete loss of LPS due to mutations in *lpx* operon in *A. baumannii* conferred colistin resistance (13). Also, the OM of *E. coli* treated with

polymyxin B showed FM4-64 recovery from FRAP analysis similar to those treated with CHIR-090. Thus, polymyxin B might inhibit LPS production. In the case of polymyxin B-treated cells that showed FM4-64 recovery, we ruled out the possibility that polymyxin B permeabilized the OM resulting in FM4-64 signal in both OM and CM since we saw no recovery in MalF-GFP in CM. We will perform biochemical assays to examine the level of LPS production in treated cells to confirm what we observed *in vivo*. When complete, this data might support the previous observations which showed that low concentrations of polymyxin B are synergistic with many other antibiotics against Gram negative bacteria (5, 33–35). We hypothesize that, at the lower concentration, polymyxin B inhibits LPS production resulting in the membrane that is more vulnerable to other hydrophobic antibiotics leading to the synergistic effect. However, LPS profiles of treated samples must be completed in order to prove our hypothesis.

Fluorescence microscopy is becoming a major technique in antibiotic studies. Here we used BCP, a method based on bacterial cell morphology, to unveil another possible function of polymyxin B in LPS production. Even though BCP did not identify the specific protein targets of polymyxin B, it uncovered a polymyxin B function that has never been observed by other methods. Polymyxin B was omitted from the previous study (22) because at high concentration polymyxin B causes cell lysis and thus we were not able to score cell morphology to include into the analysis. This study highlights the importance of the concentration of the antibiotic used in the studies, especially antibiotics that are sensitive to the ratio of cells and antibiotic molecules. The cell density differences not only effect the readouts of MIC, here we showed that it also effect the MOA analysis as well.

Materials and Methods

Strains and antibiotics

Strains used in this study are *E. coli* MC4100 (27, 36) and *lptD* mutant (27) with and without plasmid containing MalF-GFP. Polymyxin B sulfate salt was purchased from Sigma-Aldrich and stocks were made according to the manufacturer recommendations.

Minimal inhibitory concentration (MIC) determination

MIC of antibiotics were examined by a microdilution method as described previously (22). Bacteria were first grown in LB broth overnight. Then, overnight cultures were diluted 1:100 into fresh media and grown at 30°C to early exponential phase (an OD_{600} of 0.2). The exponential phase cells were diluted 1:100 again in the media containing different concentrations of antibiotics and grown at 30°C. The MIC data were collected after 24 hours incubation.

Plasmolysis

Plasmolysis experiments were performed as previously described (37). Briefly, bacteria cells were first grown to an OD_{600} of 0.4. Prior to cells harvest, 1 µg/ml FM4-64 dye was added into bacteria cultures and incubated for 1 minute. Then, 1 ml of stained bacteria cultures were collected by centrifugation at 3,300 x g for 30 second and resuspended in 0.4 M sucrose for 2 minute. Plasmolysed cells were put onto a slide for fluorescence microscopy.

Fluorescence Microscopy

Bacterial cells sample preparation and microscopy for bacterial cytological profiling (BCP) were performed as previously described (22). Plasmolysed cells were put onto a 1.2% agarose pad containing 0.4 M sucrose to maintain osmolality difference throughout the course of experiments. For FRAP analysis, three images were collected prior to photobleaching by 0.5 second exposure of 488 nm laser beam. Post-bleach images were taken every 0.5 seconds for 30 seconds.

Acknowledgements

Chapter 4, in part, is being prepared for submission for publication of the material. Poochit Nonejuie, Chiara Ricci-Tam, Joe Pogliano "Roles of polymyxin B in bacterial membrane fluidity". I was a primary author and performed all of the fluorescence microscopy and images analysis.

References

1. H. W. Boucher, G. H. Talbot, J. S. Bradley, J. E. Edwards, D. Gilbert, L. B. Rice, M. Scheld, B. Spellberg, J. Bartlett, Bad Bugs, No Drugs: No ESKAPE! An Update from the Infectious Diseases Society of America, *Clin. Infect. Dis.* **48**, 1–12 (2009).

2. K. Lewis, Platforms for antibiotic discovery, *Nat. Rev. Drug Discov.* **12**, 371–387 (2013).

3. A. H. Delcour, Outer membrane permeability and antibiotic resistance, *Biochim. Biophys. Acta BBA-Proteins Proteomics* **1794**, 808–816 (2009).

4. A. R. Coates, *Antibiotic resistance, Handbook of Experimental Pharmacology.* **211,** (Springer, 2012)

5. S. Biswas, J.-M. Brunel, J.-C. Dubus, M. Reynaud-Gaubert, J.-M. Rolain, Colistin: an update on the antibiotic of the 21st century, *Expert Rev. Anti Infect. Ther.* **10**, 917–934 (2012).

6. D. Landman, C. Georgescu, D. A. Martin, J. Quale, Polymyxins Revisited, *Clin. Microbiol. Rev.* **21**, 449–465 (2008).

7. M. E. Falagas, S. K. Kasiakou, L. D. Saravolatz, Colistin: the revival of polymyxins for the management of multidrug-resistant gram-negative bacterial infections, *Clin. Infect. Dis.* **40**, 1333–1341 (2005).

8. P. J. Bergen, C. B. Landersdorfer, J. Zhang, M. Zhao, H. J. Lee, R. L. Nation, J. Li, Pharmacokinetics and pharmacodynamics of "old" polymyxins: what is new?, *Diagn. Microbiol. Infect. Dis.* **74**, 213–223 (2012).

9. J. Li, R. L. Nation, J. D. Turnidge, R. W. Milne, K. Coulthard, C. R. Rayner, D. L. Paterson, Colistin: the re-emerging antibiotic for multidrug-resistant Gram-negative bacterial infections, *Lancet Infect. Dis.* **6**, 589–601 (2006).

10. T. Mogi, K. Kita, Gramicidin S and polymyxins: the revival of cationic cyclic peptide antibiotics, *Cell. Mol. Life Sci.* **66**, 3821–3826 (2009).

11. K. A. Brogden, Antimicrobial peptides: pore formers or metabolic inhibitors in bacteria?, *Nat. Rev. Microbiol.* **3**, 238–250 (2005).

12. T. Wu, A. C. McCandlish, L. S. Gronenberg, S. S. Chng, T. J. Silhavy, D. Kahne, Identification of a protein complex that assembles lipopolysaccharide in the outer membrane of Escherichia coli, *Proc. Natl. Acad. Sci.* **103**, 11754–11759 (2006).

13. J. H. Moffatt, M. Harper, P. Harrison, J. D. F. Hale, E. Vinogradov, T. Seemann, R. Henry, B. Crane, F. St. Michael, A. D. Cox, B. Adler, R. L. Nation, J. Li, J. D. Boyce, Colistin Resistance in Acinetobacter baumannii Is Mediated by Complete Loss of Lipopolysaccharide Production, *Antimicrob. Agents Chemother.* **54**, 4971–4977 (2010).

14. M. S. Anderson, H. G. Bull, S. M. Galloway, T. M. Kelly, S. Mohan, K. Radika, C. R. Raetz, UDP-N-acetylglucosamine acyltransferase of Escherichia coli. The first step of endotoxin biosynthesis is thermodynamically unfavorable., *J. Biol. Chem.* **268**, 19858–19865 (1993).

15. A. W. Barb, P. Zhou, Mechanism and inhibition of LpxC: an essential zinc-dependent deacetylase of bacterial lipid A synthesis, *Curr. Pharm. Biotechnol.* **9**, 9 (2008).

16. J. Bérdy, Thoughts and facts about antibiotics: Where we are now and where we are heading, *J. Antibiot. (Tokyo)* **65**, 385–395 (2012).

17. L. L. Silver, Challenges of Antibacterial Discovery, *Clin. Microbiol. Rev.* **24**, 71–109 (2011).

18. M. S. Butler, M. A. Blaskovich, M. A. Cooper, Antibiotics in the clinical pipeline in 2013, *J. Antibiot. (Tokyo)* **66**, 571–591 (2013).

19. A. L. McClerren, S. Endsley, J. L. Bowman, N. H. Andersen, Z. Guan, J. Rudolph, C. R. H. Raetz, A Slow, Tight-Binding Inhibitor of the Zinc-Dependent Deacetylase LpxC of Lipid A Biosynthesis with Antibiotic Activity Comparable to Ciprofloxacin [†], *Biochemistry (Mosc.)* **44**, 16574–16583 (2005).

20. J. Pogliano, N. Osborne, M. D. Sharp, A. D. Mello, A. Perez, Y. L. Sun, K. Pogliano, A vital stain for studying membrane dynamics in bacteria: a novel mechanism controlling septation during Bacillus subtilis sporulation, *Mol. Microbiol.* **31**, 1149–1159 (2002).

21. A. Lamsa, W. T. Liu, P. C. Dorrestein, K. Pogliano, The Bacillus subtilis cannibalism toxin SDP collapses the proton motive force and induces autolysis, *Mol. Microbiol.* (2012).

22. P. Nonejuie, M. Burkart, K. Pogliano, J. Pogliano, Bacterial cytological profiling rapidly identifies the cellular pathways targeted by antibacterial molecules, *Proc. Natl. Acad. Sci.* **110**, 16169–16174 (2013).

23. J. R. Zupan, T. A. Cameron, J. Anderson-Furgeson, P. C. Zambryski, Dynamic FtsA and FtsZ localization and outer membrane alterations during polar growth and cell

division in Agrobacterium tumefaciens, *Proc. Natl. Acad. Sci.* **110**, 9060–9065 (2013).

24. H. Nikaido, Molecular Basis of Bacterial Outer Membrane Permeability Revisited, *Microbiol. Mol. Biol. Rev.* **67**, 593–656 (2003).

25. H. Nikaido, Restoring Permeability Barrier Function to Outer Membrane, *Chem. Biol.* **12**, 507–509 (2005).

26. N. Ruiz, B. Falcone, D. Kahne, T. J. Silhavy, Chemical Conditionality, *Cell* **121**, 307–317 (2005).

27. B. Sampson, R. Misra, S. Benson, Identification and characterization of a new gene of Escherichia coli K-12 involved in outer membrane permeability., *Genetics* **122**, 491–501 (1989).

28. K. Bodewits, C. R. H. Raetz, J. R. Govan, D. J. Campopiano, Antimicrobial Activity of CHIR-090, an Inhibitor of Lipopolysaccharide Biosynthesis, against the Burkholderia cepacia Complex, *Antimicrob. Agents Chemother.* **54**, 3531–3533 (2010).

29. R. E. Caughlan, A. K. Jones, A. M. DeLucia, A. L. Woods, L. Xie, B. Ma, S. W. Barnes, J. R. Walker, E. R. Sprague, X. Yang, C. R. Dean, Mechanisms Decreasing In Vitro Susceptibility to the LpxC Inhibitor CHIR-090 in the Gram-Negative Pathogen Pseudomonas aeruginosa, *Antimicrob. Agents Chemother.* **56**, 17–27 (2011).

30. J. Pogliano, N. Pogliano, J. A. Silverman, Daptomycin-Mediated Reorganization of Membrane Architecture Causes Mislocalization of Essential Cell Division Proteins, *J. Bacteriol.* **194**, 4494–4504 (2012).

31. E. C. Yi, M. Hackett, Rapid isolation method for lipopolysaccharide and lipid A from Gram-negative bacteria, *The Analyst* **125**, 651–656 (2000).

32. C.-M. Tsai, C. E. Frasch, A sensitive silver stain for detecting lipopolysaccharides in polyacrylamide gels, *Anal. Biochem.* **119**, 115–119 (1982).

33. A. Elemam, J. Rahimian, M. Doymaz, In Vitro Evaluation of Antibiotic Synergy for Polymyxin B-Resistant Carbapenemase-Producing Klebsiella pneumoniae, *J. Clin. Microbiol.* **48**, 3558–3562 (2010).

34. D. Landman, Citywide emergence of Pseudomonas aeruginosa strains with reduced susceptibility to polymyxin B, *J. Antimicrob. Chemother.* **55**, 954–957 (2005).

35. G. A. Pankey, D. S. Ashcraft, The detection of synergy between meropenem and polymyxin B against meropenem-resistant Acinetobacter baumannii using Etest® and time-kill assay, *Diagn. Microbiol. Infect. Dis.* **63**, 228–232 (2009).

36. M. J. Casadaban, Transposition and fusion of the lac genes to selected promoters in Escherichia coli using bacteriophage lambda and Mu, *J. Mol. Biol.* **104**, 541–555 (1976).

37. P. O. Scheie, Plasmolysis of Escherichia coli B/r with Sucrose, *J. Bacteriol.* **98**, 335–340 (1969).

Chapter 5

Alp7R Regulates Expression of the Actin-Like Protein Alp7A in *Bacillus subtilis*

Alp7R Regulates Expression of the Actin-Like Protein Alp7A in *Bacillus subtilis*

Alan I. Derman, Poochit Nonejuie, Brittany C. Michel, Bao D. Truong, Akina Fujioka, Marcella L. Erb, and Joe Pogliano

Division of Biological Sciences, University of California San Diego, La Jolla, California, USA

Alp7A is a bacterial actin from *Bacillus subtilis* plasmid pLS20 that functions in plasmid segregation. Alp7A's function requires that it assemble into filaments that treadmill and exhibit dynamic instability. These dynamic properties require the two other components of the *alp7A* operon, the downstream *alp7R* gene and the upstream *alp7C* sequence, as does the ability of Alp7A to form filaments at its physiological concentration in the cell. Here, we show that these two other components of the operon also determine the amount of Alp7A that is produced in the cell. The deletion of *alp7R* leads to overproduction of Alp7A, which assembles into large, amorphous, static filaments that disrupt chromosome segregation and cell division. The product of the *alp7R* gene is a DNA-binding protein that represses transcription of the *alp7A* operon. Purified Alp7R protein binds specifically to *alp7C*, which contains two σ^A promoters embedded within a series of near-repeats of a 10-mer. Alp7R also shows the typical nonspecific binding activity of a DNA-binding protein: Alp7R-GFP (green fluorescent protein) associates with the chromosomes of cells that lack *alp7C*. When Alp7A-GFP is produced in *B. subtilis* along with untagged Alp7R, Alp7A-GFP also colocalizes with the chromosome, indicating that Alp7R associates with Alp7A. Hence Alp7R, determines both the activity and the cellular concentration of Alp7A, and it can associate with Alp7A even if it is not bound to *alp7C*.

Bacteria have very many actin-like proteins (Alps) whose amino acid sequences indicate that they are only distantly related to the very highly conserved eukaryotic actin (4). The Alps are themselves evolutionarily diverse and so, in order to lay the groundwork for understanding this diversity, we have organized them into families whose members show at least 30% amino acid identity (4, 47). Although only a small number of Alp families have been studied to date, it has become apparent that the Alps share the basic properties of eukaryotic actin. Their crystal structures approximate that of actin and they polymerize into filaments (35). The Alps participate in a variety of central processes relating to cell architecture and growth or to the movement and positioning of large structures within the cell.

There are fundamental differences between the few families of Alps that are encoded on bacterial chromosomes and the many families that are encoded on mobile genetic elements. The chromosomal Alps are highly conserved. Members of the MreB family, for example, are required for the proper cell morphology of nonspherical bacteria and are present in most rod-shaped bacteria (8, 9, 22, 24, 43, 49). FtsA, the other prominent chromosomal Alp, is a critical component of the cell division machinery and is well represented in eubacteria (7, 14, 21, 48). There are, in contrast, at least 30 distinct families of Alps that are encoded on a variety of mobile genetic elements, and many of these Alps perform the same function. For example, Alp7A, AlfA, and ParM represent three distantly related families of Alps; they are encoded on three different plasmids, yet they all segregate plasmids (1, 4, 27, 32, 47). Their identical function notwithstanding, these Alps have been shown to differ in their cell biological and in their biophysical properties (1, 4, 10, 11, 26, 32). Studying these proteins provides an opportunity for us to comprehend the scope of actin-based solutions to the challenge of plasmid segregation and at the same time to gain insights into the plasticity of actin that the study of eukaryotic actin or the few chromosomal Alps of bacteria cannot provide.

We have focused on Alp7A, a plasmid segregation protein from the 55-kb *Bacillus subtilis* plasmid pLS20 (4, 25). Alp7A shares only 13% primary sequence identity with eukaryotic actin but contains its five signature nucleotide binding motifs. Alp7A-GFP (green fluorescent protein), which retains the full function of Alp7A in plasmid segregation, polymerizes into filaments in *B. subtilis* that display the characteristic dynamic properties of both eukaryotic actin and tubulin; Alp7A filaments treadmill and exhibit dynamic stability. Mutations of amino acids that would be expected, in the manner of eukaryotic actin, to be involved in the binding or hydrolysis of nucleotide either eliminate these dynamic properties or prevent Alp7A from assembling into filaments (4).

The *alp7A* gene is the first of two genes that comprise a small operon adjacent to the pLS20 origin of replication (4, 25). A mini-pLS20 plasmid built from the operon and adjacent origin is, like pLS20 itself, completely stable over more than 30 generations of exponential growth. Deletion of the operon or of the *alp7A* gene from the operon leads to the rapid loss of mini-pLS20. Alp7A must be able to assemble into dynamic actin-like filaments in order to function in plasmid segregation; the mutations that prevent Alp7A filament formation or deprive Alp7A filaments of their dynamic properties also destabilize the plasmid. The dynamic properties of Alp7A also require that the other components of the operon be present in the cell either in *cis* or in *trans*. In the absence of the promoter region and the smaller downstream gene *alp7R*, only static filaments are formed, and these lack the uniform appearance of their dynamic counterparts. The other components of the operon also determine the critical concentration for Alp7A

filament formation in the cell. When these components are present, dynamic filaments are observed if Alp7A is present at the level ordinarily found in a cell containing pLS20. When they are absent, filaments are observed only if Alp7A is present at more than 5-fold higher levels, and these filaments are static (4).

In the case of *alp7A* then, the activity and therefore the function of a bacterial actin is regulated by the other components of the operon. There is regulation of actin function and activity in other actin-based plasmid segregation systems, but it can be of a very different sort. In the *parMR* operon of the *Escherichia coli* plasmid R1, for example, the *parM* gene codes for another bacterial actin that is distantly related to eukaryotic actin, to the *alp7* family, and to the other bacterial actin families (4, 12, 13, 45, 47). ParM, like Alp7A, is a plasmid segregation determinant, and filaments of both this prototypical ParM and the ParM of plasmid pB171 exhibit dynamic instability (10, 11, 34, 37, 41). Biophysical experiments with the ParM proteins have demonstrated, though, that this dynamic instability requires no extrinsic factors and that the critical concentration for filament formation is low enough that filaments would be expected to form spontaneously within the cell (10, 41). Experiments with an *in vitro* reconstitution of the entire system indicate that the product of the downstream *parR* gene, bound to the *parC* site that is situated upstream of *parM*, squelches the dynamic instability of ParM filaments and prevents their catastrophic disassembly (11).

The *parMR* promoter is embedded in the *parC* site such that by binding at *parC*, the ParR protein also represses transcription of the operon. Transcriptional repression has been demonstrated in the *parM* operon from plasmid R1 and also in the *parM* operon of plasmid pB171 (20, 26, 40). Complete repression of the R1 operon requires all 10 of the short repeat elements that comprise *parC* (2).

Comparatively little is known about *alp7R* and *alp7C*, the corresponding components of the *alp7A* operon, although they are a key to understanding the fundamental differences in behavior between the ParM and Alp7A systems. As more of these systems are studied closely, it has become apparent that even though all are actin-based plasmid segregation machineries, they do not function identically. Among the systems that have been studied— ParM, AlfA, the ParM of plasmid pSK41 (actually distantly related to the prototypical ParM and a member of another Alp family), and Alp7A—differences have been observed in nucleotide binding and hydrolysis parameters, in the kinetics of filament formation, and in filament structure and filament behavior (4, 10, 11, 26, 32–37, 41). These differences no doubt reflect the great evolutionary distances between these Alp families. As a necessary step toward cataloging and explaining the differences between the Alp7A system and these other actin-based plasmid segregations systems, we turned our attention to the regulatory components of the *alp7A* operon.

MATERIALS AND METHODS

Molecular biology. The standard techniques of molecular biology were used. Genomic DNA was purified from *Bacillus* with a modification of a protocol developed for Gram-negative bacteria (29). Plasmids and DNA fragments, including products of PCR amplifications, were purified with kits from Qiagen, Invitrogen, or Fermentas. DNA modification enzymes, polymerases, and other molecular biology reagents were obtained from New England BioLabs unless noted otherwise. Shrimp alkaline phosphatase was obtained from Roche Diagnostics, and RNase was obtained from Qiagen. Deoxynucleoside triphosphates (dNTPs) were obtained from a variety of sources, including Roche Diagnostics and Fermentas. Other biochemicals and chemicals were obtained from Fisher, VWR, or Sigma. Agarose for routine electrophoresis was obtained from Denville Scientific. Oligonucleotide primers (see Table S1 in the supplemental material) were synthesized by Allele Biotechnology and Pharmaceuticals or by Integrated DNA Technologies. DNA sequencing was performed by Eton Bioscience or by Genewiz.

Plasmids were introduced into *E. coli* DH5α or BL21(DE3) by electroporation with a Gene Pulser Xcell (Bio-Rad) or by transformation of chemically competent cells (18).

Plasmids and plasmid constructions. The plasmids used in this study are listed in Table 1. The construction of plasmids pAID3129 (mini-pLS20), pAID3195 [mini-pLS20 (*alp7A-gfp*), where *gfp* encodes green fluorescent protein], pAID3169 [mini-pLS20 *alp7A(D212A)*], and pAID3171 (mini-pLS20 Δ*alp7AR*) was described in our previous study (4).

(i) Expression of *alp7R* and production of Alp7R. Plasmid pME7 (pP*ara*alp7R*) was constructed by PCR amplification with oligonucleotide primers P7 and P8 of the section of plasmid pAID3147 (mini-pLS20 Δ*alp7A* [4]) corresponding to 45 bp upstream of the *alp7A* initiation codon, the *alp7A* in-frame deletion, the 10-bp intergenic region, the *alp7R* gene, and the transcription terminator, followed by restriction of the amplicon with PstI and SphI and ligation of the product to plasmid pBAD33 (16) restricted with PstI and SphI. Plasmid pAID3204 (pP*xyl*alp7R*) was constructed by PCR amplification with oligonucleotide primers P1 and P2 of a section of plasmid pAID3147 corresponding to 45 bp upstream of the *alp7A* initiation codon, the *alp7A* in-frame deletion, the 10-bp intergenic region, the *alp7R* gene, and the transcription terminator, followed by restriction of the amplicon with BamHI and SphI and ligation of the product to plasmid pWH1520 (42) restricted with BamHI and SphI. Plasmid pAID3219 (pP*xyl*alp7R-gfp*) was constructed from plasmid pAID3211, which contains a fusion of *gfp* to *alp7R*. pAID3211 was constructed by PCR amplification with oligonucleotide primers P3 and P4 of a section of plasmid pAID3147 corresponding to 45 bp upstream of the *alp7A* initiation codon, the *alp7A* in-frame deletion, the 10-bp intergenic region, and the *alp7R* gene lacking its termination codon, followed by restriction of the amplicon with EagI and ligation of the product to pMUTIN-GFP+ (23) restricted with EagI. The *alp7R-gfp* gene codes for the 4-amino-acid linker ASID. pAID3211 DNA was amplified with oligonucleotide primers P5 and P6, and the amplicon was restricted with XmaI and SphI and ligated to pWH1520 restricted with XmaI and SphI. pAID3219 includes the *trpA* transcription terminator that follows *gfp* in pMUTIN-GFP+. Plasmid pAID3277 (pP*T7*His6*-alp7R*) was constructed from a preliminary pCR2.1-TOPO clone (Invitrogen). The *alp7R* gene lacking its initiation codon was amplified from pAID3147 by PCR with oligonucleotide primers P11 and P12, the amplicon was cloned into the pCR2.1-TOPO vector, and candidates were screened by DNA sequencing. The TOPO clone was restricted with NheI, and the 411-bp fragment containing the *alp7R* gene was ligated to pET28a (Novagen) restricted with NheI. The insert's orientation was determined by DNA sequencing.

(ii) Deletion of *alp7R*. Plasmid pAID3226 [mini-pLS20 *alp7A(D212A)* Δ*alp7R*] was constructed via a modification of the standard PCR-based site-directed mutagenesis protocol with mutagenic oligonucleotide primers P9 and P10 (52). The template for this mutagenesis was a derivative of plasmid pAID3169 that was generated by monomolecular ligation of its largest (6,847 bp) AatII restriction fragment (4). The 1,645-bp fragment resulting from restriction of pAID3169 with BsrGI and NheI was then replaced with the corresponding fragment from the mutagenized plasmid. Plasmid pAID3244 (mini-pLS20 Δ*alp7R*) was constructed by replacing the 1,035-bp BsrGI-BbvCI fragment of pAID3226 with the corresponding fragment from pAID3129. Plasmid pAID3232 [mini-pLS20 *alp7A(D212A)-gfp* Δ*alp7R*] was constructed by replacing the 2,840-bp AvrII-SphI fragment from pAID3195 (4) with a fragment that was generated by amplification of pAID3226 with oligonucleotide primers P11 and P12 and then restriction with AvrII and SphI. Plasmid pAID3261 [mini-pLS20 (*alp7A-gfp*) Δ*alp7R*] was constructed by re-

TABLE 1 Plasmids and strains used in this study

Plasmid or strain	Description or genotype	Reference and/or source
Plasmids		
pAID3129	Mini-pLS20	4
pAID3169	Mini-pLS20 *alp7A(D212A)*	4
pAID3171	Mini-pLS20 Δ*alp7AR*	4
pAID3195	Mini-pLS20 *alp7A-gfp*	4
pAID3204	pP$_{xyl}$*alp7R*	This study
pAID3219	pP$_{xyl}$*alp7R-gfp*	This study
pAID3226	Mini-pLS20 *alp7A(D212A)* Δ*alp7R*	This study
pAID3232	Mini-pLS20 *alp7A(D212A)-gfp* Δ*alp7R*	This study
pAID3244	Mini-pLS20 Δ*alp7R*	This study
pAID3261	Mini-pLS20 *alp7A-gfp* Δ*alp7R*	This study
pAID3277	pP$_{T7}$His$_6$-*alp7R*	This study
pME7	pP$_{ara}$*alp7R*	This study
Strains		
B. subtilis		
PY79	Prototroph, 168 lineage	53
JP3133	pAID3129 [mini-pLS20]/PY79	4
JP3161	PY79 *thrC*::(*xylR*⁺ P$_{xyl}$*alp7A-gfp erm*)	4
JP3169	pAID3169/PY79	4
JP3171	pAID3171/PY79	4
JP3196	pAID3195/PY79	4
JP3210	PY79 *thrC*::(*xylR*⁺ P$_{xyl}$*alp7R erm*)	This study
JP3223	pAID3219/PY79	This study
JP3233	pAID3232/JP3210	This study
JP3245	pAID3261/JP3210	This study
JP3247	pAID3226/JP3210	This study
JP3248	pAID3226/PY79	This study
JP3300	PY79 *amyE*::(*alp7C cat*)	This study
JP3302	pAID3244/JP3210	This study
JP3309	PY79 *amyE*::(*alp7C cat*) *thrC*::(*xylR*⁺ P$_{xyl}$*alp7A-gfp erm*)	This study
JP3311	pAID3204/JP3309	This study
JP3315	pAID3204/JP3161	This study
JP3322	pAID3219/JP3300	This study
E. coli		
JP313	F⁻ Δ*araBAD-714* [*araD139*]$_{B/r}$? Δ(*argF-lac*)*169* λ⁻ e14⁻ *flhD5301* Δ(*fruK-yeiR*)*725*(*fruA25*) *relA1* *rpsL150*(Str^r) *rbsR22* Δ(*fimB-fimE*)*632*(::IS*1*) *deoC1*	6
JP3227	pME7/JP313	This study
JP3277	pAID3277/BL21(DE3)	This study

placing the 695-bp AgeI fragment of pAID3244 with the corresponding fragment from pAID3195. All plasmids were recovered as transformants of strain JP3227. Transformants were isolated in the presence of 0.2% L-arabinose and were maintained and stored in the presence of 0.2% arabinose.

Bacterial strains, strain construction, and growth of bacteria. The strains used in this study are listed in Table 1. *E. coli* strain JP3227 was constructed by transformation of strain JP313 (6) with plasmid pME7. All physiology and microscopy experiments were carried out at 30°C in *B. subtilis* strain PY79 (53) or in derivatives of PY79. The construction of strain JP3161 (PY79 *thrC*::*xylR*⁺ P$_{xyl}$*alp7A-gfp erm*) was described in our previous study (4). Strain JP3210 [PY79 *thrC*::(*xylR*⁺ P$_{xyl}$*alp7R erm*)] was constructed by integration into the PY79 chromosome of a segment of plasmid pAID3204 containing the *xylR* gene and P$_{xyl}$*alp7R*. The derivative of chromosomal integration vector pDG1664 (15) containing P$_{xyl}$*alp7A* that had been constructed for making strain JP3206 [PY79 *thrC*::(*xylR*⁺ P$_{xyl}$*alp7A erm*)] (4) was restricted with SpeI and NruI, and the 7,703-bp fragment was ligated to the 823-bp fragment generated by restriction of pAID3204 with SpeI and NruI. The segment containing *xylR* and P$_{xyl}$*alp7R* was then integrated into the PY79 chromosome at *thrC* by a

double recombination event. Strain JP3300 (PY79 *amyE*::*alp7C*) was constructed by integration into the PY79 chromosome of a 531-bp segment corresponding to the 477 bp directly upstream of *alp7A*, the first 15 codons of *alp7A*, and the sequence ACCTAATGA. The segment was generated by PCR amplification of pAID3129 with oligonucleotide primers P15 and P16 and restriction of the amplicon with BamHI and HindIII. The product was ligated to *B. subtilis* chromosomal integration vector pDG1662 (15) restricted with BamHI and HindIII. The cloned segment was then integrated into the PY79 chromosome at *amyE* by a double recombination event. The chromosomal insert was verified by DNA sequencing. Strain JP3309 (PY79 *amyE*::*alp7C thrC*::*xylR*⁺ P$_{xyl}$*alp7A-gfp*) was constructed by transformation of JP3300 with genomic DNA from strain JP3161 (4). Strain JP3311 (pP$_{xyl}$*alp7R*/PY79 *amyE*::*alp7C thrC*:: *xylR*⁺ P$_{xyl}$*alp7A-gfp*) was constructed by transformation of strain JP3309 with plasmid pAID3204. All other *B. subtilis* strains were constructed by standard transformation of PY79 or of derivatives of PY79 with the plasmids described above (5).

Medium components were manufactured by Becton, Dickinson, and Co. Our LB formulation is 1% Bacto-tryptone, 0.5% yeast extract, 0.5% NaCl per liter, with no pH adjustment. Most antibiotics were obtained

from Sigma. Media for strains containing derivatives of pWH1520, including mini-pLS20 and its derivatives, were supplemented with 100 μg ml^{-1} ampicillin or carbenicillin for *E. coli* or with 10 μg ml^{-1} tetracycline for *Bacillus* strains. Chloramphenicol was used at 5 μg ml^{-1} and erythromycin at 2 μg ml^{-1} for *Bacillus* strains, kanamycin at 50 μg ml^{-1} for *E. coli*, and spectinomycin at 100 μg ml^{-1} for either *Bacillus* strains or *E. coli*.

Plasmid stability assays. Plasmid stability assays were carried out as described previously (4), except that the starter cultures contained 10 μg ml^{-1} tetracycline and 0.5% D-xylose, the shake flask cultures requiring xylose were supplemented hourly with xylose to 0.5%, and the nonselective medium for the plating of samples contained 0.5% xylose. For assays of plasmid retention, colonies were patched onto LB agar plates containing 0.5% xylose and onto LB agar plates containing 10 μg ml^{-1} tetracycline and 0.5% xylose.

Microscopy. Agarose pads contained 1.2% agarose (Invitrogen Ultra-Pure 15510-027), 25% LB medium, and 0.2 μg ml^{-1} FM4-64 [*N*-(3-triethylammoniumpropyl)-4-{6-[4-(diethylamino)phenyl]hexatrienyl}pyridinium dibromide; Molecular Probes/Invitrogen]. DAPI (4′,6-diamidino-2-phenylindole, dihydrochloride; Invitrogen), when included, was present at 0.01 μg ml^{-1}. Xylose was present at the concentrations indicated below. Pads were inoculated with colonies from an LB agar plate containing selective antibiotic and, when required for viability, 0.5% xylose, that had been streaked the previous day from frozen glycerol stocks and incubated overnight at 30°C. The pads were incubated at 30°C prior to and during imaging in the Weather Station temperature-controlled chamber outfitted to the microscope (Precision Control LLC.).

For slides prepared from liquid cultures, FM4-64 was added to 1 ml of culture to a concentration of 2 μg ml^{-1} and DAPI to a concentration of 2 μg ml^{-1}, the cells were pelleted for 0.5 min at 3,300 × *g* in a microcentrifuge and resuspended in approximately 5% of the supernatant, and 5.0 μl of the resuspension was applied to a polylysine-coated coverslip for imaging.

Microscopy was carried out as described previously (4). Unless otherwise noted, micrographs of GFP and DNA (DAPI) were prepared from undeconvolved images, and micrographs of membranes (FM4-64) were prepared from deconvolved images.

Immunoblotting. Cultures for immunoblotting were started with colonies from an LB agar plate containing 10 μg ml^{-1} tetracycline that had been streaked the previous day from frozen glycerol stocks and incubated overnight at 30°C. Several colonies were suspended in a small volume of LB medium, typically 0.5 ml, and equal volumes of the suspension were used to inoculate a set of 6-ml LB cultures containing 10 μg ml^{-1} tetracycline and the appropriate amount of xylose. The cultures were rolled at 30°C and supplemented hourly with xylose at the designated concentration.

Lysates were prepared from cells in exponential phase, at an optical density at 600 nm (OD$_{600}$) of approximately 0.5. Trichloroacetic acid was added to a final concentration of 5% to a volume of cells corresponding to 1 OD$_{600}$, and the cells were incubated on ice for 30 min, pelleted, and washed as described previously (31). Cells were lysed with 1 mg ml^{-1} chicken egg white lysozyme for 30 min at 37°C in 60 μl of a buffer consisting of 35% sucrose, 900 μM EDTA, 30 mM Tris-HCl, pH 8.0, that was supplemented with 160 μg ml^{-1} phenylmethylsulfonyl fluoride and 0.6 μl of a protease inhibitor cocktail (Sigma P2714). Two microliters of Triton X-100 was added at the end of the 30-min incubation. After the addition of 140 μl 2× SDS-PAGE sample preparation buffer, the samples were boiled for 5 min, vortexed, boiled once more for 3 min, and then pelleted at ambient temperature in a microcentrifuge at maximum speed. Fifteen microliters (0.075 OD$_{600}$) of the supernatant was loaded onto a polyacrylamide gel for SDS-PAGE. The preparation of the hexahistidine-tagged Alp7A, which was used as a molecular-weight standard, has been described previously (4).

Proteins were transferred to polyvinylidene fluoride (PDVF) mem-branes in Towbin buffer containing 20% (vol/vol) methanol (51). Incubation of the membrane with the primary antibody, a polyclonal antibody raised against Alp7A (4), used at 1:10,000, and with the secondary antibody, a horseradish peroxidase-linked anti-rabbit IgG (GE Healthcare), used at 1:3,000 or 1:5,000, was carried out in TBST, pH 8.0 (150 mM NaCl, 10 mM Tris-HCl, pH 8.0), to which was added 0.06% Tween 20 (vol/vol) and 5% (wt/vol) instant nonfat dry milk (Safeway). Washes were performed in TBST. The ECL Plus Western blotting detection system (GE Healthcare) was used for detection. Relative band intensities were computed from multiple exposures of a blot with the gel analysis feature of ImageJ 1.45m (38).

Purification of Alp7R. Shake flask cultures of strain JP3277 were grown at 30°C in LB medium supplemented with 50 μg ml^{-1} kanamycin, induced at an OD$_{600}$ of 0.4 with 750 μM isopropyl-β-D-thiogalactopyranoside (IPTG), and harvested 6 h later. The cells were lysed in CelLytic B cell lysis reagent (product no. B7435; Sigma) supplemented with 200 μg ml^{-1} chicken egg white lysozyme, 1 μg ml^{-1} RNase A (Qiagen), a protease inhibitor cocktail (product no. P2714; Sigma), and 150 μg ml^{-1} PMSF. The lysate was then treated with 40 units of DNase I (product code M0303; New England BioLabs) in the presence of 10 mM MgCl$_2$ and then centrifuged after supplementation with NaCl to 300 mM, imidazole to 12.5 mM, and HEPES to 50 mM, pH 8.0. His$_6$-Alp7R was purified from the lysate by nickel affinity chromatography. The lysate was loaded onto a column of His-Select nickel affinity gel (product no. P6611; Sigma), the column was washed with 300 mM NaCl, 12.5 mM imidazole, 0.1% Triton X-100, 50 mM HEPES, pH 8.0, and the protein was eluted in 300 mM NaCl, 250 mM imidazole, 50 mM HEPES, pH 8.0.

Approximately 2 mg of His$_6$-Alp7R from the most abundant fraction were treated with thrombin agarose (product no. T7151; Sigma) in 10 mM CaCl$_2$, 300 mM NaCl, 50 mM HEPES, pH 8.0, for 1 h or 2 h at ambient temperature. SDS-PAGE indicated that this treatment resulted in complete removal of the hexahistidine tag. The Alp7R protein was then dialyzed against 300 mM NaCl, 1 mM EDTA, 20 mM HEPES, pH 8.0. Protein concentration was determined on the basis of the calculated extinction coefficient of 7,450 M^{-1} cm^{-1} (30).

Electrophoretic mobility shift assay (EMSA). DNA substrates were generated by amplification of pAID3129 with oligonucleotide primers P17 and P18 (*alp7C*), P19 and P20 (*alp7R*), and P21 and P22 (*ori rep*). The *alp7C* amplicon was restricted with SspI. The sequences of the three amplicons are as follows: *alp7C* (182 bp), 5′-CGTAAAGCCCCGGGCCTGA AATCACTTTTCTCTACTGATTTCACTGATTTCATTTTTATTATAT AATCCTCAAATAGCCTGTATTCACTGATTTTAAATGTGATTTCAT TTTATTGACTTTAGTGATATAAGATGCTAGTATTGAGGAAAGTG AAATCAAAGGAGAGAATAAAAATATGAAT-3′; *alp7R* (189 bp), 5′-GAGCAGATTAGTACATTCAGTAAAGGTAAGAGTAAGGGTACCTTT AGAGAGTATGCCTTTCAGCTCATAGAAAGGGACATGCAACAACAG AAAGAGGAACAGCAGAATAGAGAAAAAGATCGTCATGTTCATGAT GAATTAATTGCCATGAGAGAAGAAATGAAGAAAGAATTTCGTGAT TTGAGGAAG-3′; and *ori rep* (191 bp), 5′-GACAGACATAGGCAATCG ATCAGATTTGAAACTAGCGTCATAGAGACGTCTGAGGTTTCCA GCTCTGCCTTGCTATCGCCAGGCTTTCGCCTGCCATGACCTTTT TACATACAATGCTTGTCCTGTATGCAACTTCTATGGGGTTTGTC TCGTGTTCTCTCACACGGTCACACTCAATTGTGTGCCGCTG-3′.

The DNA substrate was mixed with Alp7R protein in a 20-μl reaction mixture consisting of 300 mM NaCl, 5% polyethylene glycol (PEG) 8000, 1 mM EDTA, 25 μg ml^{-1} poly(dI-dC) (Sigma), 500 μg ml^{-1} bovine serum albumin (BSA; New England BioLabs), 20 mM HEPES, pH 7.5, and the mixture was incubated at ambient temperature for approximately 30 min. Typically, 100 ng of the *alp7C* DNA substrate and molar equivalents of the other two substrates were used. Two microliters of a dye mixture (2% xylene cyanol, 2% bromphenol blue, 300 mM NaCl, 1 mM EDTA, 20 mM HEPES, pH 7.5) was added to each reaction mixture, and the mixtures were fractionated on a 5% polyacrylamide gel (acrylamide/bis-acrylamide, 29:1 [Bio-Rad], 1× Tris-borate-EDTA [TBE], 1% PEG 8000, 10%
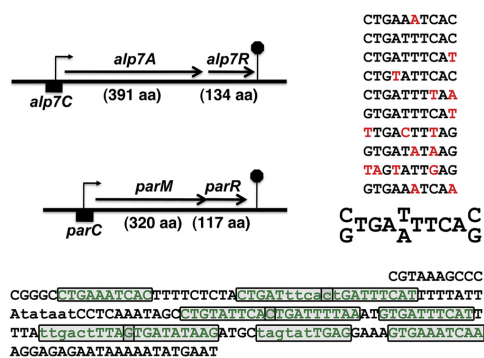
FIG 1 The *alp7AR* and *parMR* operons have similar structures. The *alp7AR* and *parMR* operons are diagrammed to scale, with the lengths of their gene products in amino acids (aa) shown. The *alp7C* sequence through the second codon of *alp7A* is presented below, with the *alp7A* initiation codon underlined. Two potential σ^A promoters are denoted in lowercase (17). The sequence contained in a set of near-repeat elements is indicated as green text; the individual repeats are boxed. As construed here, six of the repeats overlap an adjoining repeat by one base. An inferred consensus is presented in the upper right. The presence of a base or a pair of bases in the consensus requires at least six or more appearances at that position; deviations are indicated in red. Some deviations, as in repeats 7 and 9, appear to reflect promoter element constraints.

glycerol) in 1× TBE after a 30-min prerun. The gel was stained and destained briefly with ethidium bromide and then either photographed or visualized with a Typhoon 9400 variable mode imager (GE Healthcare). Band intensities were quantified with ImageJ 1.45m (38).

RESULTS

The *alp7A* operon of *B. subtilis* plasmid pLS20 is a plasmid stability determinant. A mini-pLS20 plasmid containing the *alp7A* operon and the adjacent pLS20 origin of replication is completely stable; deletion of *alp7A* or of the entire operon leads to loss of the plasmid (4). The *alp7A* gene is followed by a smaller gene, which we have designated *alp7R* (Fig. 1). We deleted *alp7R* from mini-pLS20 and assessed the stability of the resulting plasmid. The introduction of mini-pLS20 Δ*alp7R* into *B. subtilis* required that *alp7R* be present elsewhere in the genome (Fig. 2A), so the gene was placed under the control of the inducible P$_{xyl}$ promoter and installed on the chromosome. This requirement for *alp7R* suggested that mini-pLS20 Δ*alp7R* would be unstable, and moreover, that the plasmid most likely could not be tolerated by the cell. Plasmid stability assays confirmed this. A culture was grown for several generations in the presence of xylose and selective antibiotic and then assayed for antibiotic resistance at intervals following subculture into unsupplemented medium. Plasmid retention fell off precipitously starting at between 6 and 10 generations after the withdrawal of xylose, such that by about 10 generations, the plasmid was lost completely (Fig. 2B, red circles). During this period, the growth rate slowed greatly. Under the microscope, we observed aberrations in cell morphology, chromosome segregation, and cell division (Fig. 2C). Many cells appeared to be anucleate (Fig. 2C, arrows). If the culture was instead maintained in the presence of xylose (Fig. 2B, red squares), the plasmid was stable, the cells grew normally, and they were indistinguishable from cells of the strain containing intact mini-pLS20 (Fig. 2D and E).

We had seen similar disruptive effects on cell growth and via-
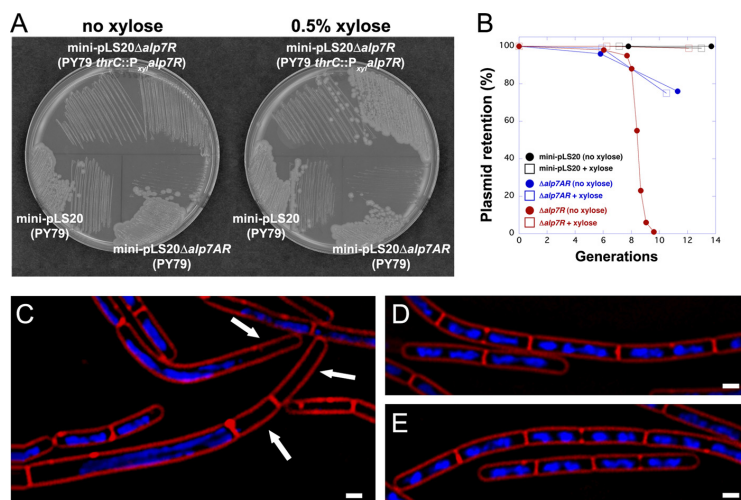
FIG 2 Deletion of *alp7R* destabilizes mini-pLS20 and is lethal to cells carrying the plasmid. (A) LB agar plates containing 10 μg ml^{-1} tetracycline with or without 0.5% D-xylose were incubated at 30°C for 24 h. Lower left, JP3133 (PY79 carrying mini-pLS20 [pLS20 origin of replication and *alp7AR* operon]); lower right, JP3171 (PY79 carrying mini-pLS20 Δ*alp7AR* [pLS20 origin of replication only]); top, JP3302 (PY79 with an integrated xylose-inducible copy of *alp7R*, carrying mini-pLS20 Δ*alp7R* [pLS20 origin of replication and *alp7AR* operon lacking *alp7R*]). (B) Exponential cultures grown in the absence of selection were sampled at regular intervals for plasmid retention as described in Materials and Methods. Black, JP3133; blue, JP3171; red, JP3302. Open squares, hourly supplementation with xylose to 0.5%; filled circles, no xylose supplementation. (C to E) Fluorescence microscopy images of strains supplemented or not supplemented with xylose. Exponential cultures grown in the absence of selection as in the plasmid stability assay were sampled for microscopy. Membranes were stained with FM4-64 (red), and DNA was stained with DAPI (blue). Scale bar equals 1 μm; all panels are at the same scale. (C) JP3302, with no xylose supplementation, at 4 h. Arrows indicate anucleate cells. (D) JP3302, supplemented hourly with 0.5% xylose, at 4 h. (E) JP3133, supplemented hourly with xylose to 0.5%, at 3 h.

bility in connection with the abnormal filament formation that follows from overproduction of Alp7A. Observations from a xylose titration were indeed consistent with a scenario in which limiting the amount of Alp7R results in Alp7A-GFP overproduction. When little or no xylose was provided to a culture, so that little or no Alp7R was produced, many cells contained thick ribbon-like filaments that seemed to fill them completely and in many cases distorted them to the point of inhibiting their normal growth and division (Fig. 3C and D). All of these filaments were static (see Fig. S1 in the supplemental material). At a high xylose concentration, many cells contained filaments that appeared normal and exhibited dynamic instability (Fig. 3E and F), a property of the fully functional protein (Fig. 3A and B; see also Fig. S2 and S3 in the supplemental material).

It appeared then that Alp7R was functioning as a negative regulator of the *alp7A* gene. It was nevertheless possible that Alp7R had no effect on the amount of Alp7A that was produced in the cell and that its function was simply to enable the Alp7A that was present to be assembled into normal dynamic filaments. In order to distinguish these two possibilities, we measured the steady-state levels of Alp7A in the presence and absence of Alp7R. When the chromosomal *alp7R* gene was left uninduced in strains containing Δ*alp7R* plasmids, the cells contained five to 10 times the Alp7A of a strain containing mini-pLS20 (Fig. 3G) and 50 times the Alp7A-GFP of a strain containing mini-pLS20 *alp7A-gfp* (Fig. 3H). Induction of the *alp7R* gene depressed Alp7A and Alp7A-GFP levels to that of mini-pLS20 or below (Fig. 3G and H).

We substituted *alp7A(D212A)* for the wild-type *alp7A* in mini-pLS20 Δ*alp7R* because this point mutation prevents filament formation when present in mini-pLS20 (4). We hoped by doing this to avoid the potential complications of studying regulation under lethal conditions. The resulting Δ*alp7R* strain did not require xylose for viability (Fig. 4A), but the steady-state level of Alp7A(D212A) was again elevated, to 20 times that found in the cell when the *alp7R* gene was intact (Fig. 4B). Although we had not seen Alp7A(D212A)-GFP polymerize into filaments before, this level of overproduction was sufficient to drive much of the protein into filaments, albeit filaments lacking dynamic properties (Fig. 4C and D; see also Fig. S4 in the supplemental material). As was the case for wild-type Alp7A, induction of the chromosomal *alp7R* gene led to a reduction in the steady-state level of Alp7A(D212A) or of Alp7A(D212)-GFP: the greater the induction, the lower the steady-state level (Fig. 4B to F). At the highest induction level, no filaments were observed, and soluble Alp7A(D212A)-GFP was distributed uniformly throughout the cell, as it was in a strain containing mini-pLS20 *alp7A(D212A)* with an intact *alp7R* gene (Fig. 4E and F).

Alp7R is therefore a negative regulator of *alp7A* gene expression and presumably of the *alp7A* operon. The structure of the *alp7A* operon closely resembles that of the *parM* operon (Fig. 1). The actin gene, *alp7A* or *parM*, is followed by a smaller gene, *alp7R* or *parR*, that codes for a protein with a high percentage of charged amino acid residues, many of which show up in short runs of two or more (4). ParR is a DNA-binding protein that binds at *parC*, a sequence directly upstream of the *parM* gene that contains 10 imperfect iterations of a 10-mer sequence which straddle the promoter (2, 3). The sequence directly upstream of *alp7A* contains a series of 10 imperfect iterations of a 10-mer sequence in which two putative σ^A promoters are embedded (Fig. 1). When expressed in *B. subtilis* PY79, an Alp7R-GFP fusion protein delineated the
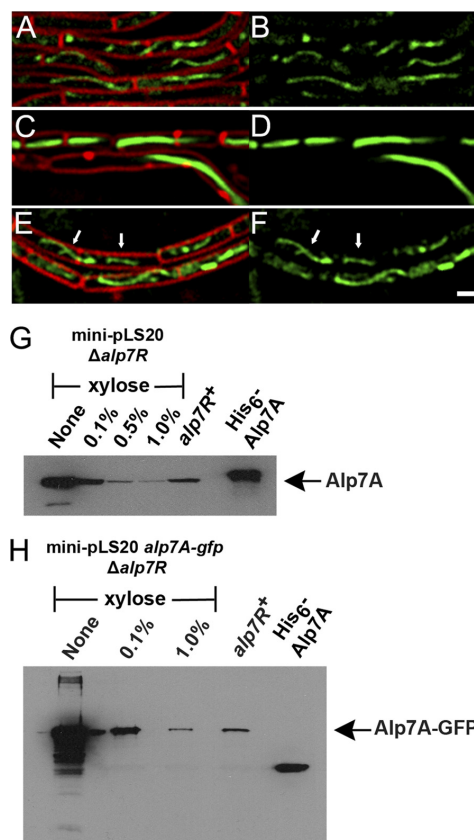

FIG 3 Depletion of Alp7R leads to overproduction of Alp7A. (A to F) Fluorescence microscopy images of strains grown in the presence or absence of D-xylose (agarose pads; scale bar equals 1 μm; all panels are at the same scale). (A and B) JP3196 (PY79 carrying mini-pLS20 *alp7A-gfp*) in the absence of xylose. (C to F) JP3245 (PY79 with an integrated xylose-inducible copy of *alp7R*, carrying mini-pLS20 *alp7A-gfp* Δ*alp7R*) in the absence of xylose (C and D) or in the presence of 0.5% xylose (E and F). Arrows denote filaments whose dynamic behavior can be tracked in the lower left section of the corresponding movie (see Fig. S2 in the supplemental material). (A, C, and E) Cell membranes (FM4-64) and GFP. (B, D, and F) GFP only. See also Fig. S1, S2, and S3 in the supplemental material. (G and H) Immunoblots prepared from lysates of JP3302 (PY79 with an integrated xylose-inducible copy of *alp7R*, carrying mini-pLS20 Δ*alp7R*) (G) or JP3245 (PY79 with an integrated xylose-inducible copy of *alp7R*, carrying mini-pLS20 *alp7A-gfp* Δ*alp7R*) (H) grown in the presence of various concentrations of xylose. The filter was probed with a polyclonal anti-Alp7A serum. Lanes are labeled with the xylose concentrations used. The lane labeled "*alp7R*⁺" shows the steady-state level of Alp7A that is present in JP3133 (PY79 carrying mini-pLS20) (G) or of Alp7A-GFP that is present in JP3196 (PY79 carrying mini-pLS20 *alp7A-gfp*) (H). The rightmost lane contains purified His₆-Alp7A (G and H).

chromosome in the manner of DAPI staining, indicating that it was bound to DNA nonspecifically (Fig. 5A, left). When the fusion protein was expressed in a variant of PY79 in which the *alp7C* sequence had been installed on the chromosome, discrete foci could be observed (Fig. 5A, right). In cells that contained these foci, the number ranged from one to four, as would be expected
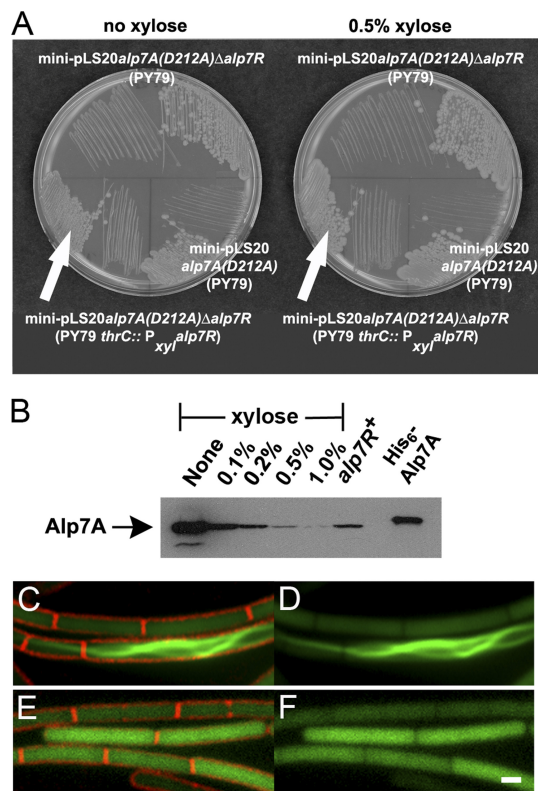
FIG 4 Deletion of *alp7R* causes Alp7A(D212A) to assemble into filaments. (A) LB agar plates containing 10 µg ml⁻¹ tetracycline with or without 0.5% D-xylose were incubated overnight at 30°C. Lower left, JP3247 [PY79 with an integrated xylose-inducible copy of *alp7R*, carrying mini-pLS20 *alp7A(D212A)* Δ*alp7R*]; lower right, JP3169 [PY79 carrying mini-pLS20 *alp7A(D212A)*]; top, JP3248 [PY79 carrying mini-pLS20 *alp7A(D212A)* Δ*alp7R*]. (B) Immunoblot prepared from lysates of JP3247 grown in the presence of various concentrations of xylose. The filter was probed with a polyclonal anti-Alp7A serum. Lanes are labeled with the xylose concentrations used. The lane labeled "*alp7R*⁺" shows the steady-state level of Alp7A(D212A) that is present in JP3169. The rightmost lane contains purified His₆-Alp7A. (C to F) Fluorescence microscopy images of strain overproducing Alp7A(D212A) (agarose pads; scale bar equals 1 µm, all panels are at the same scale). JP3233 [PY79 with an integrated xylose-inducible copy of *alp7R*, carrying mini-pLS20 *alp7A(D212A)-gfp* Δ*alp7R*] in the absence of xylose (C and D) or in the presence of 0.5% xylose (E and F). (C and E) Cell membranes (FM4-64) and GFP. (D and F) GFP only. See also Fig. S4 in the supplemental material.

under these growth conditions if a single focus were formed at each *alp7C* site. These findings suggested that Alp7R was a DNA-binding protein like ParR and that it bound specifically at *alp7C*.

EMSAs were therefore carried out to assess the nature and specificity of the binding. As the molar ratio of purified Alp7R protein to *alp7C* DNA was increased from 1 to 25, we observed a shift of the DNA from its normal migration position, owing to its incorporation into high-molecular-weight complexes (Fig. 5B and D). There was also shifting, but considerably diminished, of either of two alternative DNA fragments of similar size, one corresponding to part of the *alp7R* structural gene and the other to

part of the pLS20 origin of replication. This difference was particularly pronounced when competitor was included in the binding reaction mixtures (Fig. 5C). Even at a 25 molar excess of Alp7R, where more than 80% of the *alp7C* DNA shifted, nearly 80% of the other two DNA fragments failed to shift (Fig. 5C and D). These data confirmed our *in vivo* findings that Alp7R, although capable of binding to DNA nonspecifically, binds specifically to *alp7C*.

Having demonstrated binding of Alp7R at *alp7C*, we attempted to determine how Alp7A interacts with these other components. In order to do this, we took advantage of the observation that in the absence of *alp7C*, Alp7R binds nonspecifically to DNA (Fig. 5A, left). In place of *alp7R-gfp*, we expressed *alp7R* coordinately with *alp7A-gfp*. Interaction of Alp7A-GFP and Alp7R would be expected to give rise to a fluorescence pattern that resembled that of Alp7R-GFP. This turned out to be the case; the chromosome was again delineated in the manner of DAPI staining (Fig. 6A). Hence, Alp7A interacts with Alp7R and it can do so even if there is no *alp7C* present in the cell for Alp7R to bind to.

When we introduced *alp7C*, we reconstituted the complete system, albeit with its components dispersed: *alp7C* was on the chromosome, *alp7A-gfp* was in single copy elsewhere on the chromosome, and *alp7R* was on a multicopy plasmid. It was therefore not surprising that coordinate induction of *alp7A-gfp* and *alp7R* eventually gave rise to dynamic filaments in these cells (Fig. 6B; see also Fig. S5 in the supplemental material). Alp7R was required for this. In its absence, in a strain that contained only the chromosomal copies of *alp7C* and *alp7A-gfp* but no *alp7R* plasmid, only small static filaments were observed (Fig. 6C; see also Fig. S6 in the supplemental material), and this profile was indistinguishable from that of a strain containing only the chromosomal copy of *alp7A-gfp* (Fig. 6D; see also Fig. S7 in the supplemental material). So *alp7C* in the absence of *alp7R* has no effect on Alp7A activity, and Alp7R is therefore indispensable for the formation of dynamic filaments. There was also no fluorescent delineation of the chromosome in these cells (Fig. 6C and D), indicating that Alp7A-GFP is unable to interact directly with DNA and confirming that the fluorescence pattern in Fig. 6A could be generated only through an interaction between Alp7A-GFP and Alp7R.

DISCUSSION

In our previous study, we found that *alp7R* and *alp7C* regulate the activity of Alp7A, that *alp7R* and *alp7C* are required for Alp7A to assemble into dynamic filaments at its physiological concentration (4). In the present study, we have found that Alp7R and *alp7C* also regulate the production of Alp7A. When *alp7R* was deleted from mini-pLS20, the steady-state levels of Alp7A were increased up to 50-fold, and the cells were filled with large filaments of irregular shape that lacked dynamic properties. These rigid filaments that filled much of the cells' interior space were likely to interfere with chromosome segregation or with cell division and presumably account for the lethality that we observed.

Although Alp7R may contribute in more than one way to setting Alp7A levels in the cell, its principal contribution is at the level of transcription. Alp7R is a negative regulator of *alp7A* gene expression. The region immediately upstream of *alp7A*, which we call *alp7C* in analogy with *parC*, the corresponding region in the *parMR* operon, contains two potential σ^A promoters. The EMSA and cell biology data indicate that Alp7R binds preferentially at *alp7C*. Although we cannot rule out more sophisticated mechanisms, Alp7R seems to function as a simple transcriptional repres-
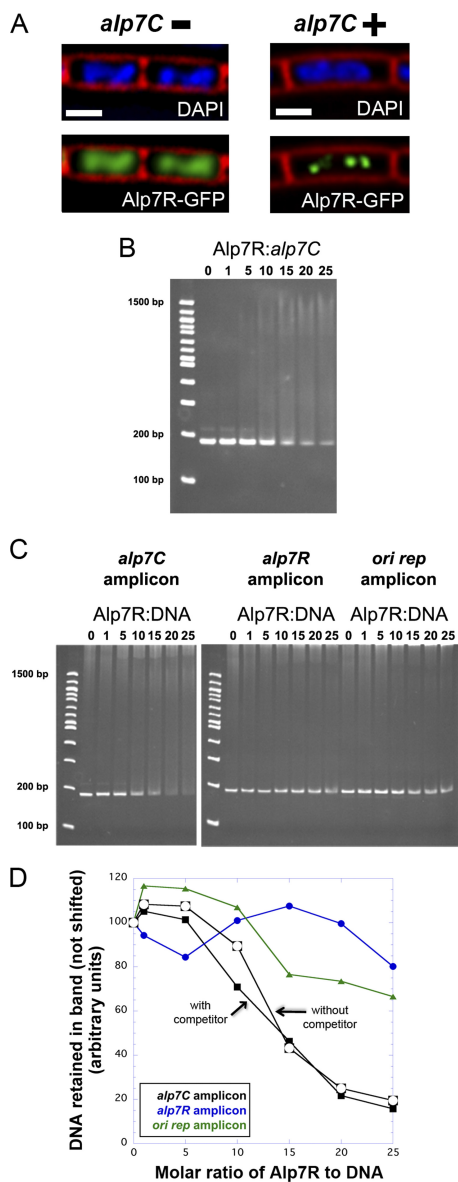
FIG 5 Alp7R is a DNA-binding protein that binds specifically at *alp7C*. (A) Fluorescence microscopy of strains expressing *alp7R-gfp* (agarose pads; scale bar equals 1 μm, all panels are at the same scale). Left, JP3223 (PY79 carrying pP$_{xyl}$*alp7R-gfp*) in the presence of 0.5% xylose. Right, JP3322 (PY79 with an integrated copy of *alp7C*, carrying pP$_{xyl}$*alp7R-gfp*) in the presence of 0.1% xylose. Top, cell membranes (FM4-64) and DNA (DAPI). Bottom, cell membranes and GFP. (B and C) Electrophoretic mobility shift assays (EMSA) of *alp7C* DNA by the Alp7R protein. See Materials and Methods. The number above each lane indicates the molar ratio of Alp7R protein to the DNA amplicon. (B) Competitor poly(dI-dC) was omitted from the binding reaction mixture. The high-molecular-weight material consists entirely of complex. (C) Competitor poly(dI-dC) was present in the binding reaction mixture at 25 μg ml^{-1}. At the higher Alp7R-to-*alp7C* ratios, the high-molecular-weight mate-
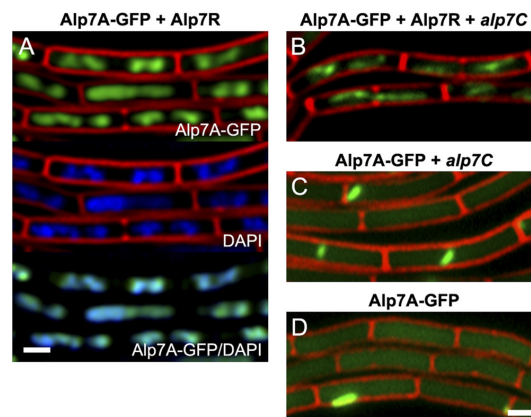

FIG 6 Alp7R and Alp7A interact; Alp7R is indispensable for the formation of dynamic Alp7A filaments. (A to D) Fluorescence microscopy images of strains expressing Alp7A-GFP by itself or in the presence of other components of the system (agarose pads containing 0.5% xylose; scale bar equals 1 μm, all panels are at the same scale). (A) JP3315 (PY79 with an integrated xylose-inducible copy of *alp7A-gfp*, carrying pP$_{xyl}$*alp7R*). Top, cell membranes (FM4-64) and GFP (Alp7A-GFP); middle, cell membranes (FM4-64) and DNA (DAPI); bottom, GFP (Alp7A-GFP) and DNA (DAPI). GFP panels were prepared from deconvolved images. (B) JP3311 (PY79 with an integrated xylose-inducible copy of *alp7A-gfp* and an integrated copy of *alp7C*, carrying pP$_{xyl}$*alp7R*). (C) JP3309 (PY79 with an integrated xylose-inducible copy of *alp7A-gfp* and an integrated copy of *alp7C*). (D) JP3161 (PY79 carrying an integrated xylose-inducible copy of *alp7A-gfp*). (B to D) Cell membranes and GFP. See also Fig. S5 to S7 in the supplemental material.

sor, impeding transcription by promoter occlusion. In this respect, *alp7AR* would resemble every actin-based bacterial plasmid segregation system whose regulation has been studied to date, including the *parMR* systems from plasmids R1 and pB171 (3, 20, 40) and two distantly related systems, the *parMR* system from plasmid pSK41 (46) and the *alfAB* system from plasmid pLS32 (1, 50). In each case, the product of the downstream gene is a DNA-binding protein that binds upstream of the actin gene and represses transcription. Alp7R presumably represses transcription of the entire operon, including the *alp7R* gene. The negative feedback loop that is established necessarily ensures that the appropriate amount of Alp7R is present in the cell to promote the formation of normal dynamic filaments. Disruption of this feedback loop leads to aberrant filament formation, perturbation of plasmid segregation, and cell death.

The sequence of Alp7R resembles that of ParR in its length and charge distribution (4). The crystal structures of ParR from pB171 and of the N-terminal portion of the DNA-binding protein from pSK41 in complex with a 20-mer derived from its binding site revealed that both proteins contain N-terminal ribbon-helix-helix

rial contains both competitor and complex. (D) The percentage of unshifted DNA in each lane of panels B and C is plotted against the molar ratio of Alp7R to DNA. Black filled symbols, *alp7C* amplicon with competitor, from the experiment represented in panel C; black open symbols, *alp7C* amplicon without competitor, from the experiment represented in panel B; blue, *alp7R* amplicon with competitor, from the experiment represented in panel C; green, origin of replication amplicon with competitor, from the experiment represented in panel C.

(RHH) domains, which places them in the MetJ/Arc family of gene regulators (28, 39, 46). The RHH domain, or more properly the surface that is formed from a pair of RHH domains upon protein dimerization, constitutes the DNA-binding moiety. The sequence diversity among MetJ/Arc family members and the small size of the DNA-binding domain make it difficult to determine, in the absence of structural information, whether Alp7R is a member of this family as well (44). That said, it is not hard to spot stretches of similarity between Alp7R and some RHH family members. For example, the sequence near the N terminus of Alp7R (PLFNVR) resembles that of the bacteriophage P22 repressor proteins Arc (PQFNLR) and Mnt (PHFNFR), two founding members of the family; in the RHH dimer, this short sequence gives rise to the β-sheet, or "ribbon," that contacts the DNA (44).

RHH protein dimers tend to interact cooperatively and give rise to higher-order structures (28, 44). This has turned out to be true in the case of the DNA-binding proteins associated with actin-driven plasmid segregation systems. The structure of the ParR-DNA complex was inferred from the pB171 ParR crystal structure and electron micrographs of the ParR protein of plasmid R1 with *parC* DNA. ParR dimers assembled into a ringlike helical formation, with 12 dimers comprising a full 360° turn of the ring (28). The cocrystal of the pSK41 RHH domain with its 20-mer binding site yielded a similar structure, a finding which was supported by electron microscopy. Each 20-mer was bound by two dimers, and as in the case of ParR, a total of 12 dimers were required for a full turn of the ring (46). In both structures, the bound DNA was wrapped around the outer circumference of the ring and the actin filament was proposed to interact with the interior of the ring (28, 46).

It is likely that *alp7C* is also bound by many copies of Alp7R. Alp7R-GFP forms bright foci on bacterial chromosomes that contain *alp7C*, and a single protein or dimer could not be expected to produce so bright a focus. The high-molecular-weight material generated in the EMSA experiments migrates as a diffuse band and may represent a collection of species, yet the apparent size of this collection does not change above a certain Alp7R-to-*alp7C* ratio (Fig. 5B). So the complexes are probably discrete species, with a fixed number of Alp7R monomers or dimers bound at *alp7C*. If one assumes that each complex contains a single copy of *alp7C*, the median molecular weight of the collection is consistent with a complex containing from 35 to 40 copies of Alp7R. It would follow that each of the 10 repeats is bound by about four copies of Alp7R, or two Alp7R dimers. This is a rough reckoning, but the numbers are of the same order as those in the ParR and pSK41 complexes, so it would not be surprising if the Alp7R/*alp7C* complex is of a similar configuration. And binding is likely to be cooperative as well, because Hill plots of the EMSA data yield Hill coefficients (n_H values) of 3.0 or greater (not shown).

Alp7R binds specifically at *alp7C*, but it also binds nonspecifically to unrelated DNA sequences, as is typical of DNA-binding proteins. When expressed in strains that lack *alp7C*, Alp7R-GFP delineated the chromosome. We found that replacement of Alp7R-GFP with Alp7R and Alp7A-GFP gave rise to a similar pattern of fluorescence, indicating that Alp7A interacts with Alp7R under these circumstances. We had inferred an interaction between Alp7A and Alp7R from our earlier observation that Alp7R/*alp7C* is required for Alp7A to assemble into dynamic filaments at its physiological concentration (4), but this is the first demonstration of the interaction. The interaction is likely to be direct, although we cannot rule out the possibility that it is mediated by other cellular proteins. It is noteworthy, though, that this interaction requires neither the Alp7R-*alp7C* centrosome complex nor that Alp7A be filamentous. We had expected the interaction between Alp7A and Alp7R to require binding of Alp7R at *alp7C*. Instead, Alp7R, bound nonspecifically to DNA in its search for *alp7C*, may already be associated with Alp7A.

We undertook the present study to extend our understanding of the Alp7A system and as part of an ongoing effort in the field to sort out which features are conserved and which vary among the great many actin-based plasmid segregation systems. Our findings add to the evidence that the DNA-binding protein in these systems, in addition to its function in the mechanics of plasmid segregation, invariably functions to regulate transcription of the operon. Evolution has allowed for differences in polymer structure, in the kinetics of polymerization, in the role that the DNA-binding protein has in regulating these parameters. But the DNA-binding protein as regulator of transcription would seem to be a constant.

REFERENCES

1. **Becker E, et al.** 2006. DNA segregation by the bacterial actin AlfA during *Bacillus subtilis* growth and development. EMBO J. **25**:5919–5931.
2. **Breuner A, Jensen RB, Dam M, Pedersen S, Gerdes K.** 1996. The centromere-like *parC* locus of plasmid R1. Mol. Microbiol. **20**:581–592.
3. **Dam M, Gerdes K.** 1994. Partitioning of plasmid R1. Ten direct repeats flanking the *parA* promoter constitute a centromere-like partition site *parC*, that expresses incompatibility. J. Mol. Biol. **236**:1289–1298.
4. **Derman AI, et al.** 2009. Phylogenetic analysis identifies many uncharacterized actin-like proteins (Alps) in bacteria: regulated polymerization, dynamic instability and treadmilling in Alp7A. Mol. Microbiol. **73**:534–552.
5. **Dubnau D, Davidoff-Abelson R.** 1971. Fate of transforming DNA after uptake by competent *Bacillus subtilis*. J. Mol. Biol. **56**:209–221.
6. **Economou A, Pogliano JA, Beckwith J, Oliver DB, Wickner W.** 1995. SecA membrane cycling at SecYEG is driven by distinct ATP binding and hydrolysis events and is regulated by SecD and SecF. Cell **83**:1171–1181.
7. **Feucht A, Lucet I, Yudkin MD, Errington J.** 2001. Cytological and biochemical characterization of the FtsA cell division protein of *Bacillus subtilis*. Mol. Microbiol. **40**:115–125.
8. **Figge RM, Divakaruni AV, Gober JW.** 2004. MreB, the cell shape-determining bacterial actin homologue, co-ordinates cell wall morphogenesis in *Caulobacter crescentus*. Mol. Microbiol. **51**:1321–1332.
9. **Formstone A, Errington J.** 2005. A magnesium-dependent *mreB* null mutant: implications for the role of *mreB* in *Bacillus subtilis*. Mol. Microbiol. **55**:1646–1657.
10. **Garner EC, Campbell CS, Mullins RD.** 2004. Dynamic instability in a DNA-segregating prokaryotic actin homolog. Science **306**:1021–1025.
11. **Garner EC, Campbell CS, Weibel DB, Mullins RD.** 2007. Reconstitution of DNA segregation driven by assembly of a prokaryotic actin homolog. Science **315**:1270–1274.
12. **Gerdes K, Moller-Jensen J, Ebersbach G, Kruse T, Nordstrom K.** 2004. Bacterial mitotic machineries. Cell **116**:359–366.
13. **Gerdes K, Moller-Jensen J, Jensen RB.** 2000. Plasmid and chromosome partitioning: surprises from phylogeny. Mol. Microbiol. **37**:455–466.
14. **Goley ED, et al.** 2011. Assembly of the *Caulobacter* cell division machine. Mol. Microbiol. **80**:1680–1698.

Derman et al.

15. **Guerout-Fleury AM, Frandsen N, Stragier P.** 1996. Plasmids for ectopic integration in *Bacillus subtilis*. Gene **180**:57–61.

16. **Guzman LM, Belin D, Carson MJ, Beckwith J.** 1995. Tight regulation, modulation, and high-level expression by vectors containing the arabinose pBAD promoter. J. Bacteriol. **177**:4121–4130.

17. **Haldenwang WG.** 1995. The sigma factors of *Bacillus subtilis*. Microbiol. Rev. **59**:1–30.

18. **Hanahan D.** 1985. Techniques for transformation of E. coli. *In* Glover DM (ed), DNA cloning: a practical approach. RL Press, Oxford, England.

19. Reference deleted.

20. **Jensen RB, Dam M, Gerdes K.** 1994. Partitioning of plasmid R1. The *parA* operon is autoregulated by ParR and its transcription is highly stimulated by a downstream activating element. J. Mol. Biol. **236**:1299–1309.

21. **Jensen SO, Thompson LS, Harry EJ.** 2005. Cell division in *Bacillus subtilis*: FtsZ and FtsA association is Z-ring independent, and FtsA is required for efficient midcell Z-ring assembly. J. Bacteriol. **187**:6536–6544.

22. **Jones L, Carballido-Lopez R, Errington J.** 2001. Control of cell shape in bacteria: helical, actin-like filaments in *Bacillus subtilis*. Cell **104**:913–922.

23. **Kaltwasser M, Wiegert T, Schumann W.** 2002. Construction and application of epitope- and green fluorescent protein-tagging integration vectors for Bacillus subtilis. Appl. Environ. Microbiol. **68**:2624–2628.

24. **Kruse T, Bork-Jensen J, Gerdes K.** 2005. The morphogenetic MreBCD proteins of *Escherichia coli* form an essential membrane-bound complex. Mol. Microbiol. **55**:78–89.

25. **Meijer WJ, de Boer AJ, van Tongeren S, Venema G, Bron S.** 1995. Characterization of the replication region of the *Bacillus subtilis* plasmid pLS20: a novel type of replicon. Nucleic Acids Res. **23**:3214–3223.

26. **Moller-Jensen J, et al.** 2003. Bacterial mitosis: ParM of plasmid R1 moves plasmid DNA by an actin-like insertional polymerization mechanism. Mol. Cell **12**:1477–1487.

27. **Moller-Jensen J, Jensen R, Lowe J, Gerdes K.** 2002. Prokaryotic DNA segregation by an actin-like filament. EMBO J. **21**:3119–3127.

28. **Moller-Jensen J, Ringgaard S, Mercogliano CP, Gerdes K, Lowe J.** 2007. Structural analysis of the ParR/*parC* plasmid partition complex. EMBO J. **26**:4413–4422.

29. **Neumann B, Pospiech A, Schairer HU.** 1992. Rapid isolation of genomic DNA from Gram-negative bacteria. Trends Genet. **8**:332–333.

30. **Pace CN, Vajdos F, Fee L, Grimsley G, Gray T.** 1995. How to measure and predict the molar absorption coefficient of a protein. Protein Sci. **4**:2411–2423.

31. **Pogliano K, Hofmeister AE, Losick R.** 1997. Disappearance of the sigma E transcription factor from the forespore and the SpoIIE phosphatase from the mother cell contributes to establishment of cell-specific gene expression during sporulation in *Bacillus subtilis*. J. Bacteriol. **179**:3331–3341.

32. **Polka JK, Kollman JM, Agard DA, Mullins RD.** 2009. The structure and assembly dynamics of plasmid actin AlfA imply a novel mechanism of DNA segregation. J. Bacteriol. **191**:6219–6230.

33. **Popp D, et al.** 2010. Polymeric structures and dynamic properties of the bacterial actin AlfA. J. Mol. Biol. **397**:1031–1041.

34. **Popp D, et al.** 2008. Molecular structure of the ParM polymer and the

mechanism leading to its nucleotide-driven dynamic instability. EMBO J. **27**:570–579.

35. **Popp D, Robinson RC.** 2011. Many ways to build an actin filament. Mol. Microbiol. **80**:300–308.

36. **Popp D, et al.** 2010. Structure and filament dynamics of the pSK41 actin-like ParM protein: implications for plasmid DNA segregation. J. Biol. Chem. **285**:10130–10140.

37. **Popp D, et al.** 2007. Concerning the dynamic instability of actin homolog ParM. Biochem. Biophys. Res. Commun. **353**:109–114.

38. **Rasband WS.** 2011. ImageJ. National Institutes of Health, Bethesda, MD. http://imagej.nih.gov/ij/.

39. **Raumann BE, Brown BM, Sauer RT.** 1994. Major groove DNA recognition by β-sheets: the ribbon-helix-helix family of gene regulatory proteins. Curr. Opin. Struct. Biol. **4**:36–43.

40. **Ringgaard S, Ebersbach G, Borch J, Gerdes K.** 2007. Regulatory crosstalk in the double par locus of plasmid pB171. J. Biol. Chem. **282**:3134–3145.

41. **Rivera CR, Kollman JM, Polka JK, Agard DA, Mullins RD.** 2011. Architecture and assembly of a divergent member of the ParM family of bacterial actin-like proteins. J. Biol. Chem. **286**:14282–14290.

42. **Rygus T, Hillen W.** 1991. Inducible high-level expression of heterologous genes in Bacillus megaterium using the regulatory elements of the xylose-utilization operon. Appl. Microbiol. Biotechnol. **35**:594–599.

43. **Schirner K, Errington J.** 2009. Influence of heterologous MreB proteins on cell morphology of *Bacillus subtilis*. Microbiology **155**:3611–3621.

44. **Schreiter ER, Drennan CL.** 2007. Ribbon-helix-helix transcription factors: variations on a theme. Nat. Rev. Microbiol. **5**:710–720.

45. **Schumacher M.** 2008. Structural biology of plasmid partition: uncovering the molecular mechanisms of DNA segregation. Biochem. J. **412**:1–18.

46. **Schumacher MA, et al.** 2007. Segrosome structure revealed by a complex of ParR with centromere DNA. Nature **450**:1268–1271.

47. **Shaevitz, JW, Gitai Z.** 2010. The structure and function of bacterial actin homologs. Cold Spring Harb. Perspect. Biol. **2**:a000364.

48. **Shiomi D, Margolin W.** 2007. Dimerization or oligomerization of the actin-like FtsA protein enhances the integrity of the cytokinetic Z ring. Mol. Microbiol. **66**:1396–1415.

49. **Soufo HJ, Graumann PL.** 2010. *Bacillus subtili*s MreB paralogues have different filament architectures and lead to shape remodelling of a heterologous cell system. Mol. Microbiol. **78**:1145–1158.

50. **Tanaka T.** 2010. Functional analysis of the stability determinant AlfB of pBET131, a miniplasmid derivative of *Bacillus subtilis* (*natto*) plasmid pLS32. J. Bacteriol. **192**:1221–1230.

51. **Towbin H, Staehelin T, Gordon J.** 1979. Electrophoretic transfer of proteins from polyacrylamide gels to nitrocellulose sheets: procedure and some applications. Proc. Natl. Acad. Sci. U. S. A. **76**:4350–4354.

52. **Wang W, Malcolm BA.** 1999. Two-stage PCR protocol allowing introduction of multiple mutations, deletions and insertions using QuikChange site-directed mutagenesis. Biotechniques **26**:680–682.

53. **Youngman P, Perkins JB, Sandman K (ed).** 1984. New genetic methods, molecular cloning strategies, and gene fusion techniques for *Bacillus subtilis* which take advantage of Tn*917* insertional mutagenesis. Academic Press, New York, NY.

Table S1 Oligonucleotide Primers

Oligonucleotide Primers

P1   5'-CTGTAGGATCCTAATGAGATGCTAGTATTGAGGAAAGTG-3'
P2   5'-GTACTGCATGCGTTGCTCAGGGCGTCTG-3'
P3   5'-CTGTACGGCCGGATGCTAGTATTGAGGAAAGTG-3'
P4   5'-GTACTCGGCCGATCGATGCTAGCAAAATCATAGTCGTATTCTTCTTC-3'
P5   5'-CTGTACCCGGGGATAATGAGATGCTAGTATTGAGGAAAGTG-3'
P6   5'-GTACTGCATGCGACCTCGTTTCCACCGGAATTAG-3'
P7   5'-GTACTGGCTGCAGGATGCTAGTATTGAGGAAAGTG-3
P8   5'-GTCTGCGGGACTCGTTGCGTACGGACATAG-3'
P9   5"-GAGGCACAATCAATTTAGGAGCCTGGATTAATCTAG-3'
P10   5'-CTAGATTAATCCAGGCTCCTAAATTGATTGTGCCTC-3'
P11   5'-GTACTCCTAGGGAGGCACAATCAATTTAGGAGCCTG-3'
P12   5'-GTAAGAGCCGCGAGCGATC-3'
P13   5'-CTGTAGCTAGCGGGAAAAACAAAAGAATTCCAC-3'
P14   5'-GTACTGCTAGCTCATTAAAAATCATAGTCGTATTCTTCTTC-3'
P15   5'-GTACTGGATCCGTGTTGACGTATACACTTGTTTTCG-3'
P16   5'-CTGTAAAGCTTTCATTAGGTGTACATACTGTTTCCAAAGTCCACGTTC-3'
P17   5'-CGTAAAGCCCCGGGCCTGAAATC-3'
P18   5'-GTTTCCAAAGTCCACGTTCATACGAGAAATATTC-3'
P19   5'-GAGCAGATTAGTACATTCAGTAAAG-3'
P20   5'-CTTCCTCAAATCACGAAATTCTTTC-3'
P21   5'-GACAGACATAGGCAATCGATCAG-3'
P22   5'-CAGCGGCACACAATTGAGTGTG-3'

Acknowledgements

Chapter 6
Discussion

My thesis research is focusing on developing the bacterial cytological profiling (BCP) technique that can be used to determine the mechanism of action (MOA) of antibacterial molecules based on bacterial cell morphological changes upon antibiotic treatment. The cytological profiles of known antibiotics were established and separated into subgroups based on their MOA. BCP was used to determine the MOA of a new antibacterial molecule, spirohexenolide A, as a membrane active compound similar to nisin (1). Similar to eukaryotic cytological profiling (2, 3), BCP relies on a large number of bacterial cell morphology parameters obtained from image analysis. Thus, it has long been assumed that BCP would not work since bacteria are much smaller than eukaryotic cells. Even if BCP works, it will require an ultra high-resolution microscope to accurately visualize the bacterial cell morphologies and significant image analysis to extract the data.

My thesis work shows that BCP is a simple one step technique that can be used in antibiotic discovery without the need for ultra high-resolution microscopy. BCP is faster than other conventional methods. The whole BCP process can take only a couple of hours to determine the MOA of new molecules yet provides higher resolution that other methods by unveiling dozens of different pathways in a single test. No special strain collections are needed in BCP unlike other methods (4); however, it is clear that certain specialized strains might be important in the future development of BCP in order to more precisely identify the molecular target. Also, BCP needs only small amount of molecules, so it is suitable for studying newly isolated molecules, which are usually available in small amount.

BCP is the new MIC

Antibiotic studies strictly rely upon an empirical test, growth or no growth test, before starting a MOA study. Minimal inhibitory concentration (MIC) is used as a reference concentration of antibiotic that kills all of the bacteria present in a culture. While it provides very useful information about killing activity, the MIC readout is highly fluctuating. Many MIC standard methods have been established in order to cope with its inaccuracy such as the disk diffusion method, an E-test method and a microdilution method but none of them alone provides perfectly consistent results. This inconsistency of MIC readout is mainly caused by the different ratio of antibiotic molecules and number of bacterial cells in each experiment. If a ratio of drug/cell is high in the experiment, the MIC from that experiment will be underestimated, and vice versa. Without the MIC data in hand, BCP can identify the MOA and demonstrate at which concentration of antibiotic the bacteria are killed by performing BCP under different concentrations. The lowest concentration of antibiotic that yields a noticeable phenotype can be called the minimal phenotypic change concentration (MPCC).

Also, some antibacterial molecules are highly unstable in bacteria growing in certain conditions or are detoxified by bacteria. Conventional empirical methods might overlook these unstable compounds. BCP can serve as an alternative single cell method to traditional MIC testing. We found that BCP worked very well with unstable compounds. For example, we use BCP to estimate the MIC of bacilleane, a protein translation inhibitor secreted from *Bacillus subtilis*. Bacilleane is very unstable in the

presence of oxygen, thus the conventional MIC method that relies on cell growth failed to determine its MIC.

BCP in species-specific antibiotics

BCP can be applied to species-specific whole cell screening which is considered to be the future trend of antibiotic discovery. Compounds that specifically inhibit particular pathogens are less likely to be a nuisance compound like detergent or DNA intercalating agents. Working closely with the Kit Pogliano lab, we are now expanding BCP to a Gram-positive model organism, *Bacillus subtilis*, and a pathogen, methicillin resistant *Staphylococcus aureus* (MRSA). *Pseudomonas* is also one of our top priorities; however, fluorescence techniques need to be optimized toward *Pseudomonas* screening due to its efflux pumps that can pump out many fluorescent dyes. Moreover, biofilm production can interfere with dye staining and antibiotic treatment. *Mycobacterium* is also particularly interesting. It is notoriously difficult to treat with conventional antibiotics due to its very slow growth and ability to stay dormant in the host body for many years. Unfortunately, most antibiotics work well against vegetative cells, not latent cells. This is why prodrug-like antibiotics are the key to treatment of these dormant bacteria. One possibility is that we could screen for a prodrug-like antibiotic using BCP. Since BCP uses a non-destructive fluorescence microscopy technique, it is possible to perform time-course imaging following single cells after prodrug exposure and eventually reveal the MOA.

Another benefit of species-specific antibiotics is that they exhibit fewer side effects on the human since the normal flora in human are not targeted (5). Unlike broad-spectrum antibiotics, species-specific antibiotics will reduce the risk of bacteria becoming resistant since they specifically kill the pathogens not the common bacteria. The more bacteria targeted by antibiotics, the higher chance of resistance to occur and eventually transfer to pathogenic strains.

BCP in natural product derived antibiotics research

Due to the relatively unsuccessful approach of target-based screening of chemically synthesized compound libraries (6), antibiotic discovery communities have turned back to long abandoned natural products in search of novel antibiotics. Natural products derived antibiotic screening is now one of the most promising approaches to find potential antibacterial candidates since compounds from natural production are much more complex and diverse than those from chemical synthesis. However, natural extracts contain a very high background of nuisance compounds impeding bioactive molecule identification. BCP can be used to screen through natural crude products for a specific activity and ignore the effects of unwanted background compounds; thus, resolving the bottleneck of natural product derived antibiotics research.

BCP can help with dereplication by reducing the rate of rediscovery of known antibiotics. Around 1% of actenomycetes in screening programs produce streptomycin and 0.4% make tetracycline (7, 8). Daptomycin was found after screening 10 million actinomycetes (8). Due to its sensitivity, BCP can be used to screen against crude extracts

and specify how many activities are present in the extracts. This advantage of BCP allows scientists to prioritize the extracts with favorable activities. Conventionally, the method to avoid rediscovery is 1) screen against resistant mutants (Cubist) (7) and 2) use antisense to knock down the expression of targeted genes (MERCK) all of which require specialized strain collections. BCP can bypass compound purification and identification steps in order to prioritize the extracts since the BCP data is enough to determine the MOA of molecules in crude extracts. However, it is undoubtedly easier when working with cleaner extracts. A simple fractionation step might be necessary for some crude extracts in order to reveal correct MOA.

BCP in bacterial interspecies interaction

In their natural habitat, microorganisms do not live alone. They are living among other species and form a complex community. To be able to co-exist, they have to adapt to microenvironments created by other species without disrupting each other yet maintaining their own environment. Interspecies interactions shape the environment and the host they live in. They are always exposed to molecules produced by others, either benefiting them or putting them at bay. This interspecies interaction is considered to be a new way of antibiotic production study in bacteria based on the fact that antibacterial molecules are secondary metabolites that are not normally produced in nutrient enriched and challenge-free environments. Competition between species will likely increase the rate of secondary metabolites production.

In the past, bacteria fermentation played an important role in antibiotic production by growing bacterial cultures until nutrients were depleted thus activating secondary metabolites production (5, 9). However, only a few metabolites or antibacterial molecules were obtained from fermentation compared to predicted molecules based on genome sequences. For example, some actinomycetes and myxobacteria contain more than 25 predicted gene clusters of polyketides synthases (PKS) and nonribosomal peptide synthetases (NRPS) that possibly produce secondary metabolites but only a few of these potential characterized molecules have been characterized to date (7, 8). Putting two or multiple bacteria together might increase the chance of bacteria to activate untapped gene clusters in normal environments and produce more secondary metabolites than we have never identified before. Similar to the study of natural products mentioned earlier, BCP can play role in rapidly detecting multiple antibacterial activities in crude extracts from bacterial interactions. It can be used as a quick screen through the combination of interactions before upscale interactions are needed for mass production of secondary metabolites.

Bacterial interaction studies with BCP can also apply to studies of human health. In humans, the gut microbe community or microbiome, are known to be closely linked to many human health conditions (10–12). It is very important to understand how bacteria interact with each other and what molecules are secreted during the interactions. BCP can be applied in microbiome interaction studies since it relies on a non-destructive microscopy technique meaning that BCP can monitor microbiome interactions in real time. Following the gradient of molecules secreted by bacteria is also possible by tracking morphological changes within the bacterial community over time and space.

BCP on chips

Due to its ability to perform rapidly and accurately, BCP can be used to screen for resistant bacteria in clinics. Conventionally, bacteria isolated from patients will go through strain purification, identification, and re-growing on proper bacterial culture media. Once enough cells were obtained, they are subjected to minimal inhibitory concentration (MIC) testing by standard methods, either E-test or the microdilution method. The whole process can take from two days to more than a week to know if pathogens are resistant to any antibiotics. BCP has the high potential to replace these time-consuming and laborious methods. Since BCP is a single-cell analysis method, all it needs is a few cells of the pathogen, which can be purified easily from patient. For example, bacteria can be filtered from a blood sample and used for BCP testing. Once bacteria are isolated from a patient's blood, we can apply BCP directly on isolated pathogens and test their sensitivity against different antibiotics. Clinicians will be able to determine a pathogen's antibiotic resistance phenotype within a couple hours instead of several days. This advantage of BCP can save many patients especially when quick decisions need to be made about treatment options. How are we going to bring everything needed for BCP to the hospital test kit? One possibility is microfluidic technology. We are currentlly working with Megan Dueck and Jeff Hasty at UCSD in merging microfluidic devices with BCP. When this project is complete, we will establish a prototype of BCP-on-chip device to be used in hospitals conveniently.

BCP current limitation and how to improve

The BCP technique is in its early stage of development and is far from being completely perfected. Like other new techniques, one limitation of BCP is its reliability in precisely identifying the target at the molecular level. Newly isolated molecules with novel MOAs need additional methods to fully understand their MOA similar to what I did to spirohexenolide A MOA study described in chapter 2. However, this limitation will be of less concern as more and more cytological profiles are generated for new molecules and are included into a BCP database or training set. Molecules with a new MOA will eventually form their own distinct profiles and separate themselves from other molecules with different or known MOA. BCP can turn its limitation to an advantage since any new profiles can theoretically lead to new targets, which are desired. As mentioned in chapter 1, there are many conserved proteins with no known chemical inhibitor. BCP can be a great tool to explore these untapped targets in bacteria.

BCP heavily relies on precise image analysis. In chapter 2, in order to get the most accurate data, I analyzed all the images in a semi-automated manner. Briefly, I chose the best image field of each antibiotic treatment, adjusted the image to get a correct threshold so that every cell in a field was included in the analysis, and finally I analyzed each image using ImageJ software and its measurement parameters. This process can take 15-60 min per image depending on the phenotype of the cells. Fully automated software is needed to speed up the whole analysis process and prevent human errors. Nowadays, our lab uses a more automated software, CellProfiler2.0, which can perform all the image analysis in batch, speeding up the whole process significantly, 1-2min per

image depending on the number of parameters analyzed (not including the preparation time of image files). However, we still rely on visual inspection in choosing the best field of the image. Ideally, limiting human involvement to zero will be important to move BCP into a high throughput screening method.

Concluding remarks

Long assumed impractical, here we demonstrated that BCP is very efficient in antibiotic MOA studies. Why does BCP work? Even though it is far less complex than eukaryotic cells, inside bacterial cells lie highly organized macromolecular molecules that maintain cell morphology. Thus, inhibiting one cellular pathway in bacteria, while the other pathways are left untouched and working properly, will lead to unique cell morphological changes in response to specific challenges. Also, bacterial profiles produced can be explained physiologically. For example, the toroidal-shape nucleoid found in translation inhibition is a low energy state form of the nucleoid when there is no external energy involved such as ribosomal translation and membrane insertion forces (13, 14). In summary, BCP takes advantages of both the lack of cell cycle checkpoints in bacteria and the non-destructive fluorescence microscopy techniques in rapidly identifying the cellular pathways inhibited by antibacterial molecules, overcoming a bottleneck in antibiotic discovery.

References

1. P. Nonejuie, M. Burkart, K. Pogliano, J. Pogliano, Bacterial cytological profiling rapidly identifies the cellular pathways targeted by antibacterial molecules, *Proc. Natl. Acad. Sci.* **110**, 16169–16174 (2013).

2. T. J. Mitchison, Small-molecule screening and profiling by using automated microscopy, *Chembiochem* **6**, 33–39 (2004).

3. T. U. Mayer, T. M. Kapoor, S. J. Haggarty, R. W. King, S. L. Schreiber, T. J. Mitchison, Small Molecule Inhibitor of Mitotic Spindle Bipolarity Identified in a Phenotype-Based Screen, *Science* **286**, 971–974 (1999).

4. L. L. Silver, Challenges of Antibacterial Discovery, *Clin. Microbiol. Rev.* **24**, 71–109 (2011).

5. K. Lewis, Platforms for antibiotic discovery, *Nat. Rev. Drug Discov.* **12**, 371–387 (2013).

6. D. J. Payne, M. N. Gwynn, D. J. Holmes, D. L. Pompliano, Drugs for bad bugs: confronting the challenges of antibacterial discovery, *Nat. Rev. Drug Discov.* **6**, 29–40 (2006).

7. M. A. Fischbach, C. T. Walsh, Antibiotics for Emerging Pathogens, *Science* **325**, 1089–1093 (2009).

8. R. Baltz, Renaissance in antibacterial discovery from actinomycetes, *Curr. Opin. Pharmacol.* **8**, 557–563 (2008).

9. J. W.-H. Li, J. C. Vederas, Drug Discovery and Natural Products: End of an Era or an Endless Frontier?, *Science* **325**, 161–165 (2009).

10. M. J. Claesson, I. B. Jeffery, S. Conde, S. E. Power, E. M. O'Connor, S. Cusack, H. M. B. Harris, M. Coakley, B. Lakshminarayanan, O. O'Sullivan, others, Gut microbiota composition correlates with diet and health in the elderly, *Nature* (2012).

11. L. V. Hooper, D. R. Littman, A. J. Macpherson, Interactions Between the Microbiota and the Immune System, *Science* **336**, 1268–1273 (2012).

12. V. Tremaroli, F. Bäckhed, Functional interactions between the gut microbiota and host metabolism, *Nature* **489**, 242–249 (2012).

13. N. V. Hud, K. H. Downing, Cryoelectron microscopy of λ phage DNA condensates in vitreous ice: the fine structure of DNA toroids, *Proc. Natl. Acad. Sci.* **98**, 14925–14930 (2001).

14. D. R. Zusman, A. Carbonell, J. Y. Haga, Nucleoid condensation and cell division in Escherichia coli MX74T2 ts52 after inhibition of protein synthesis, *J. Bacteriol.* **115**, 1167–1178 (1973).